Florida International University
FIU Digital Commons

FIU Electronic Theses and Dissertations | University Graduate School

3-6-2013

Glycogen Synthase Kinase 3 Influences Cell Motility and Chemotaxis by Regulating Phosphatidylinositol 3 Kinase Localization in Dictyostelium discoideum

Tong Sun
Florida International University, tsun001@fiu.edu

DOI: 10.25148/etd.FI13040103
Follow this and additional works at: https://digitalcommons.fiu.edu/etd

Recommended Citation
Sun, Tong, "Glycogen Synthase Kinase 3 Influences Cell Motility and Chemotaxis by Regulating Phosphatidylinositol 3 Kinase Localization in Dictyostelium discoideum" (2013). *FIU Electronic Theses and Dissertations*. 807.
https://digitalcommons.fiu.edu/etd/807

This work is brought to you for free and open access by the University Graduate School at FIU Digital Commons. It has been accepted for inclusion in FIU Electronic Theses and Dissertations by an authorized administrator of FIU Digital Commons. For more information, please contact dcc@fiu.edu.

FLORIDA INTERNATIONAL UNIVERSITY

Miami, Florida

GLYCOGEN SYNTHASE KINASE 3 INFLUENCES CELL MOTILITY AND CHEMOTAXIS BY REGULATING PHOSPHATIDYLINOSITOL 3 KINASE LOCALIZATION IN *DICTYOSTELIUM DISCOIDEUM*

A dissertation submitted in partial fulfillment of the

requirements for the degree of

DOCTOR OF PHILOSOPHY

in

BIOLOGY

by

Tong Sun

2013

To: Dean Kenneth Furton
College of Arts and Sciences

This dissertation, written by Tong Sun, and entitled Glycogen Synthase Kinase 3 Influences Cell Motility and Chemotaxis by Regulating Phosphatidylinositol 3 Kinase Localization in *Dictyostelium discoideum*, having been approved in respect to style and intellectual content, is referred to you for judgment.

We have read this dissertation and recommend that it be approved.

Lidia Kos

Ophelia Weeks

DeEtta Mills

Xiaotang Wang

Lou W. Kim, Major Professor

Date of Defense: March 06, 2013

The dissertation of Tong Sun is approved.

Dean Kenneth Furton
College of Arts and Sciences

Dean Lakshmi Reddi
University Graduate School

Florida International University, 2013

© Copyright 2013 by Tong Sun

All rights reserved

DEDICATION

This dissertation is dedicated to my parents, who always give me support both mentally and financially. I also dedicate this dissertation to my lovely wife who gave me encouragement, understanding, love and help in daily life. Without their various help, this work would not have been possible.

ACKNOWLEDGMENTS

Firstly, I would like to give my cordial thanks to my major professor Dr. Lou W. Kim. Dr. Kim accepted me as a volunteer researcher ten month before I was officially accepted as a graduate student here in FIU, during which time I learned numerous laboratory techniques. During my volunteer research, Dr. Kim also provided me a chance of taking his graduate-level course. I am very thankful for the enormous help, support and encouragement he has given me during my entire Ph.D training process. Without his intelligent guidance and help, this work would not have been accomplished.

I greatly appreciate all my committee members, Dr. Lidia Kos, Dr. Ophelia Weeks, Dr. DeEtta Mills, and Dr. Xiaotang Wang, for their diligent guidance, valuable time and precious advice. Special thanks to Dr. Kos, for her generosity in letting me take one of her class when I was a volunteer researcher. I would like to mention my colleagues who gave me valuable suggestions, discussions and help throughout my research, Bohye Kim, Marbelys Rodriguez, Dr. Nam-Sihk Lee, Dr. Seon-Hee Kim, Dr. Sudhakar Veeranki, Boris Castillo and Osmin Anis.

I would like to thank the people in Dr. Lidia Kos's lab, Dr. Alejandro Barbieri's lab and Dr. Fernando Noriega's lab, for their generosity in providing chemicals and equipment. I want to extend my thanks to the previous and current AHC building managers Wei Lin and Dr. Erasmo M. Perera, for their kindly and timely help on the equipment.

Finally, I would like to acknowledge the Department of Biological Sciences in Florida International University, through which I have been awarded a teaching assistantship as my financial support during my entire Ph.D training.

ABSTRACT OF THE DISSERTATION

GLYCOGEN SYNTHASE KINASE 3 INFLUENCES CELL MOTILITY AND CHEMOTAXIS BY REGULATING PHOSPHATIDYLINOSITOL 3 KINASE LOCALIZATION IN *DICTYOSTELIUM DISCOIDEUM*

by

Tong Sun

Florida International University, 2013

Miami, Florida

Professor Lou W. Kim, Major Professor

Glycogen Synthase Kinase 3 (GSK3), a serine/threonine kinase initially characterized in the context of glycogen metabolism, has been repeatedly realized as a multitasking protein that can regulate numerous cellular events in both metazoa and protozoa. I recently found GSK3 plays a role in regulating chemotaxis, a guided cell movement in response to an external chemical gradient, in one of the best studied model systems for chemotaxis - *Dictyostelium discoideum*.

It was initially found that comparing to wild type cells, *gsk3*$^-$ cells showed aberrant chemotaxis with a significant decrease in both speed and chemotactic indices. In *Dictyostelium*, phosphatidylinositol 3,4,5-triphosphate (PIP3) signaling is one of the best characterized pathways that regulate chemotaxis. Molecular analysis uncovered that *gsk3*$^-$ cells suffer from high basal level of PIP3, the product of PI3K. Upon chemoattractant cAMP stimulation, wild type cells displayed a transient increase in the level of PIP3. In contrast, *gsk3*$^-$ cells exhibited neither significant increase nor adaptation. On the other hand, no aberrant dynamic of phosphatase and tensin homolog (PTEN), which

antagonizes PI3K function, was observed. Upon membrane localization of PI3K, PI3K become activated by Ras, which will in turn further facilitate membrane localization of PI3K in an F-Actin dependent manner. The *gsk3*$^-$ cells treated with F-Actin inhibitor Latrunculin-A showed no significant difference in the PIP3 level.

I also showed GSK3 affected the phosphorylation level of the localization domain of PI3K1 (PI3K1-LD). PI3K1-LD proteins from *gsk3*$^-$ cells displayed less phosphorylation on serine residues compared to that from wild type cells. When the potential GSK3 phosphorylation sites of PI3K1-LD were substituted with aspartic acids (phosphomimetic substitution), its membrane localization was suppressed in *gsk3*$^-$ cells. When these serine residues of PI3K1-LD were substituted with alanine, aberrantly high level of membrane localization of the PI3K1-LD was monitored in wild type cells. Wild type, phosphomimetic, and alanine substitution of PI3K1-LD fused with GFP proteins also displayed identical localization behavior as suggested by the cell fraction studies. Lastly, I identified that all three potential GSK3 phosphorylation sites on PI3K1-LD could be phosphorylated *in vitro* by GSK3.

TABLE OF CONTENTS

CHAPTER PAGE

I. INTRODUCTION 1
1.1 *Dictyostelium discoideum* as a model system 1
1.2 Chemotaxis 3
1.2.1 Overview of chemotaxis 3
1.2.2 PIP3 signaling pathway in *Dictyostelium* 4
1.2.3 TORC2 signaling pathway in *Dictyostelium* 5
1.2.4 Other signaling pathways affecting *Dictyostelium* chemotaxis 6
1.3 Glycogen synthase kinase 3 7
1.3.1 Overview of GSK3 7
1.3.2 GSK3 in development and transcription factor regulation 11
1.3.3 GSK3 in mamamlian cell movement and polarity 13
1.3.4 GSK3 in *Dictyostelium* movement 15

II. CELLS LACKING GSK3 ARE DEFECTIVE IN MOTILITY 17
2.1 Materials and methods 17
2.1.1 *Dictyostelium* culture and pulsing 17
2.1.2 Chemotaxis assay and random motility assay 17
2.1.3 RT-PCR 18
2.1.4 Transfection by electroporation 18
2.1.5 Antibodies and western blotting 19
2.2 Results 20
2.2.1 The *gsk3*$^-$ cells showed aberrant movement in both chemotaxis and random movement 20
2.2.2 Re-introducing GFP fused GSK3 back to *gsk3*$^-$ cells rescued the chemotaxis defects 23
2.2.3 Expressing *sodC* in *gsk3*$^-$ cells could not rescue both chemotaxis and random movement defects 25
2.3 Discussion 29

III. ANALYSIS OF PI3K AND PTEN BEHAVIORS IN *gsk3*$^-$ CELLS 31
3.1 Materials and methods 31
3.1.1 GFP-fusion Proteins and Fluorescence Microscopy 31
3.1.2 cAMP stimulation 31
3.1.3 Latrunculin-A treatment 31
3.1.4 PI3K inhibition using LY294002 32
3.2 Results 32
3.2.1 PIP3 level along the plasma membrane, PI3K1-LD localization and PTEN localization in vegetative cells 32
3.2.2 Dynamics of PIP3 level along the plasma membrane upon cAMP stimulation 34
3.2.3 PI3K1-LD localization dynamics along the plasma membrane upon

cAMP stimulation 36
3.2.4 PTEN localization dynamics along the plasma membrane upon cAMP stimulation 38
3.2.5 Summary of the PHcrac, PI3K and PTEN dynamics 38
3.2.6 Latrunculin-A treatment 42
3.2.7 SPM-PI3K1-LD and SAS-PI3K1-LD localization dynamics along the plasma membrane upon cAMP stimulation 46
3.2.8 LY294002 treated *gsk3*$^-$ cells still showed aberrant chemotaxis 50
3.3 Discussion 52

IV. RAS ACTIVATION DYNAMICS 54
4.1 Materials and methods 54
4.1.1 Expression of GST-RBD protein in *E. coli* using IPTG-inducible stimulation 54
4.1.2 GST-RBD quantification using Coomassie Brilliant Blue staining 54
4.1.3 Ras binding assay 55
4.2 Results 55
4.2.1 GSK3 affected PI3K membrane localization independently from the Ras/PI3K/F-Actin feedback module 55
4.2.2 GSK3 regulated the Ras activation after cAMP stimulation 57
4.3 Discussion 58

V. GSK3 REGULATES PI3K1-LD PHOSPHORYLATION *IN VIVO* AND *IN VITRO* 61
5.1 Materials and methods 61
5.1.1 Generation of GST-PI3K1-LD expression construction 61
5.1.2 Antibodies 61
5.1.3 Subcellular fractionation of wild type and mutants GFP-PI3K1-LD proteins 62
5.1.4 IPTG inductions 62
5.1.5 GSK3 Kinase assay 62
5.1.6 *In vitro* peptide kinase assay 63
5.1.7 GST pull-down assay and lambda phosphatase treatment 64
5.2 Results 65
5.2.1 PI3K1-LD proteins were under-phosphorylated in *gsk3*$^-$ cells 65
5.2.2 Localization of PI3K1-LD, SPM-PI3K1-LD and SAS-PI3K1-LD 67
5.2.3 Unprimed PI3K1-LD was not a substrate of recombinant GSK3 71
5.2.4 Induced *Dictyostelium* GSK3 could not phosphorylate artificially synthesized peptides 73
5.2.5 Recombinant GSK3 could only phosphorylate one of the artificially synthesized peptides 75
5.2.6 Peptide Kinase assay using whole cell lysate of wild type cells indicated all artificially synthesized peptides are GSK3substrates 76
5.3 Discussion 77

VI. Conclusions and future directions 78

REFERENCES 82

APPENDICES 96

VITA 100

LIST OF FIGURES

FIGURE PAGE

1.1 Development of *Dictyostelium* 2

1.2 Mammalian GSK3β regulation via phosphorylation 10

1.3 The role of GSK3 in both PIP3 and TORC2 pathways in *Dictyostelium* 16

2.1 Chemotaxis assays using 10 μM cAMP point source..... 21

2.2 Chemotaxis assays using 2 μM cAMP point source..... 22

2.3 Random movement assays for both JH10 and *gsk3*$^-$ cells 23

2.4 Expression of GFP and GFP-GSK3 in *gsk3*$^-$ cells 24

2.5 Reintroducing GSK3 in *gsk3*$^-$ cells rescued their chemotaxis defect 24

2.6 RT-PCR experiment to determine the transcription level of sodC 25

2.7 Chemotaxis assays using cells expressing sodC 27

2.8 Random movement assay with cells expressing sodC..... 27

2.9 Summary of the chemotactic indices in chemotaxis assays..... 29

2.10 Summary of the speed in chemotaxis assays and random movement assays 30

3.1 GFP-PHcrac localization in vegetative cells..... 33

3.2 GFP-PI3K1-LD and GFP-PTEN in vegetative cells 35

3.3 GFP-PHcrac translocation after cAMP stimulation in pulsed cells..... 36

3.4 Quantification of the membrane fluorescence shown on figure 3.3 37

3.5 GFP-PI3K1-LD translocation after cAMP stimulation in pulsed cells 38

3.6 Quantification of the membrane fluorescence shown on figure 3.5 38

3.7 GFP-PTEN translocation after cAMP stimulation in pulsed cells..... 40

3.8 Quantification of the membrane fluorescence shown on figure 3.7 41

3.9 PHcrac, PI3K and PTEN localization pattern upon stimulation in wild type cells .. 42

3.10 PHcrac, PI3K and PTEN localization pattern upon stimulation in *gsk3*$^-$ cells 43

3.11 F-Actin polymerization induced positive feedback loop 44

3.12 GFP-PHcrac localization dynamics in Latrunculin-A treated vegetative cells 45

3.13 Quantification of the membrane fluorescence shown on figure 3.12 45

3.14 GFP-PHcrac localization dynamics in Latrunculin-A treated pulsed cells 46

3.15 Quantification of the membrane fluorescence shown on figure 3.14 47

3.16 Model of PIP3 signaling pathway under the regulation of GSK3 48

3.17 Three potential GSK3 phosphorylation sites on PI3K1-LD 48

3.18 Mutant PI3K1-LD-GFP tranlocation after cAMP stimulation in pulsed cells 50

3.19 Quantification of the membrane fluorescence shown on figure 3.18 51

3.20 Chemotaxis assays after LY294002 treatment 52

3.21 Control chemotaxis assays 53

4.1 Quantification Quantification of *E.coli* expressed GST-Raf1-RBD and GST-Byr2-RBD using Coomassie Brilliant Blue staining 57

4.2 Basal Ras activity in both wild type cells and *gsk3*$^-$ cells after pulsing..... 58

4.3 Ras activation patterns after stimulation using GST-Raf1-RBD 60

4.4 Long time Ras activation patterns after stimulation using GST-Raf1-RBD 61

4.5 Ras activation patterns after stimulation using GST-Byr2-RBD..... 61

5.1 GST-PI3K1-LD construct and full length PI3K1 66

5.2 (A) PI3K1-LD had less phosphorylation level in *gsk3*$^-$ cells compared to wild type cells. (B) Lambda phosphatase treatment was able to reverse the different phosphorylation level. 67

5.3 Quantifications of the relative band intensity for figure 5.2A 67

5.4 Quantifications of the relative band intensity for figure 5.2B 68

5.5 Localization of mutant PI3K1-LD in either wild type cells or *gsk3*$^{-}$ cells..... 69

5.6 Quantifications of the relative band intensity for figure 5.5 (top panel) 70

5.7 Quantifications of the relative band intensity for figure 5.5 (bottom panel) 71

5.8 Normalization of the total expression level 71

5.9 Quantifications of the relative band intensity for figure 5.8..... 72

5.10 Quantification of *E.coli* expressed GST-PI3K1-LD using Coomassie Brilliant Blue staining 73

5.11 GST could not be phosphorylated by recombinant GSK3..... 73

5.12 *In vitro* kinase assay using recombinant GSK3 73

5.13 Detection and quantifications of *E.coli* expressed GST-GSK3 74

5.14 Kinase activity of *E.coli* expressed GST-GSK3 75

5.15 *In vitro* peptide kinase assay using *E.coli* expressed GST-GSK3 75

5.16 *In vitro* peptide kinase assay using recombinant GSK3 76

5.17 *In vitro* peptide kinase assay using whole cell lysate 77

A1 DNA sequence of PI3K1-LD (1476 bp) 97

A2 Protein sequence of PI3K1-LD (492 amino acids) with potential GSK3 phosphorylation sites underlined 97

A3 Map of PGEX-4T-1 IPTG inducible vector..... 98

A4 Map of expression vector EXP-4 (+) 99

A5 Map of expression vector EXP-4 (+)-GST-PI3K1-LD..... 100

LIST OF ACRONYMS AND ABBREVIATIONS

AL	Activation loop
Ala	Alanine
APC	Adenomatous polyposis coli
AX3	*Dictyostelium* wild type strain
aPKC	Atypical protein kinase C
BSA	Bovine serum albumin
cAMP	3'-5'-cyclic adenosine monophosphate
CFP	Cyan fluorescent protein
CRAC	Cytosolic regulator of adenylyl cyclase
CREB	Cyclic AMP response element binding protein
CRMP-2	Collapsin response mediator protein- 2
Ci	Curie
DB	Developmental buffer
DNA	Deoxyribose nucleic acid
DTT	Dithiothreitol
EDTA	Ethylenediaminetetracetic acid
EGF	Epidermal growth factor
EGTA	Ethylene glycol tetraacetic acid
F-Actin	Filamentous actin
GAP	GTPase-activating protein
GEF	Guanine nucleotide exchange factor
GFP	Green fluorescent protein

GSK3	Glycogen synthase kinase 3
GST	Glutathion S-tansferase
GTT	Glutathion
HEPES	N-2-Hydroxyethylpiperazine-N'-2-ethanesulfonic acid
HM	Hydrophobic motif
Hr	Hour
HRP	Horse radish peroxidase
IGF	Insulin-like growth factor
IMPA	Inositol monophosphatase
IPTG	Isopropyl β-D-1-thiogalactopyranoside
JH10	*Dictyostelium* auxotrophic wild type strain
jgsk3^{-}	JH10 with disrupted *gsk3* gene
kD	Kilo Dalton
Kpa	Kilo Pascal
kV	Kilo Volt
L	Liter
LB	Luria broth
LD	Localization domain
Lef	Lymphoid enhancer factor
MAP1B	Microtubule associated protein 1B
Mb	Mega base pairs
MBP	Myelin basic protein
mg	Milligram

min	Minute
ml	Milliliter
mm	Millimeter
mM	Millimolar
ng	Nanogram
nm	Nanometer
nM	Nanomolar
OD	Optical density
p	Pico-
PCR	Polymerase chain reaction
PDGF	Platelet derived growth factor
PDK	Phosphoinositide-dependent kinases
PH	Pleckstrin homology
Phe	Phenylalanine
PI3K	Phosphatidylinositol-3-kinase
PI3K1-LD	Phosphatidylinositol-3-kinase 1 localization domain
PIP2	Phosphatidylinositol 4,5-bisphosphate
PIP3	Phosphatidylinositol 3,4,5-triphosphate
PIPES	Piperazine-1,4-bis[2-ethanesulfonic acid]
PLA2	Phospholipase A2
PLD	Phospholipase D
PKB	Protein kinase B
PKBR	Protein kinase BR

PKC	Protein kinase C
PP2A	Protein phosphatase 2A
PTEN	Phosphatase and tensin homolog
RBD	Ras binding domain
rpm	Round per minute
RNA	Ribonucleic acid
ROS	Reactive oxygen species
RTK	Receptor tyrosine kinases
RT-PCR	Reverse transcription polymerase chain reaction
SAS	Sextuple alanine substitution
SD	Standard deviation
s/sec	Second
Ser	Serine
sGC	Soluble guanylyl cyclase
SHIP	SH2 domain-containing inositol-polyphosphate 5'-phosphatase
SPM	Sextuple phospho-mimetic
Tcf	T-cell factor
TORC2	Target of rapamycin Complex 2
Tyr	Tyrosine
µF	MicroFarad
µg	Microgram
µl	Microliter

μm	Micrometer
μM	Micromolar
μ	Micro-
Wt	Wild type
Zak	Zaphod kinase

LIST OF SYMBOLS

SYMBOL	FULL NAME
^{o}C	Degree Celsius
%	Percentage
::	Over-expressing
/	is expressed in
~	Approximately
’	Minute
”	Second

CHAPTER I

INTRODUCTION

1.1 *Dictyostelium discoideum* as a model system

A unicellular social amoeba, *Dictyostelium discoideum,* has received a great deal of research attention and has become a model system to study development, survival, chemotaxis, and motility since the 1930s (Bonner, 1947; Bonner and Eldredge, 1945; Raper and Smith, 1939). It is one of the eight model systems chosen by the National Institutes of Health (NIH) for biomedical-related research. *Dictyostelium* lives in the soil and feeds on several species of bacteria. It can reproduce both sexually and asexually (Chang and Raper, 1981; Gerisch and Huesgen, 1976). In the asexual life cycle of *Dictyostelium*, deprivation of the food source triggers an important reversion in its life cycle. Around a hundred thousand cells aggregate together and form a multicellular organism. The aggregation process is organized by an autonomous secretion of 3'-5'-cyclic adenosine monophosphate (cAMP), which serves as a chemoattactant. The cAMP wave is sent out from the aggregation center in an oscillatory manner. Cells can sense each cAMP gradient wave and directionally migrate toward the aggregation center. Because of the direction sensing ability along the cAMP gradient, *Dictyostelium* has long been used as a model system for chemotaxis study (Gerisch, 1982; Konijn and Van Haastert, 1987; Newell et al., 1987). Upon aggregation, cells start to express cell type-specific genes and secrete extracellular matrix material to form an acellular covering named the sheath. Finally *Dictyostelium* develops into a fruiting body structure which is characterized by a ball of spores sitting on top of a long stalk and a basal disk (Figure 1.1). The spore head, which is fully encapsulated, is full of spores that are dispersed. One

entire round of aggregation and development process takes about 24 hours (Devreotes, 1989; Nagano, 2000).

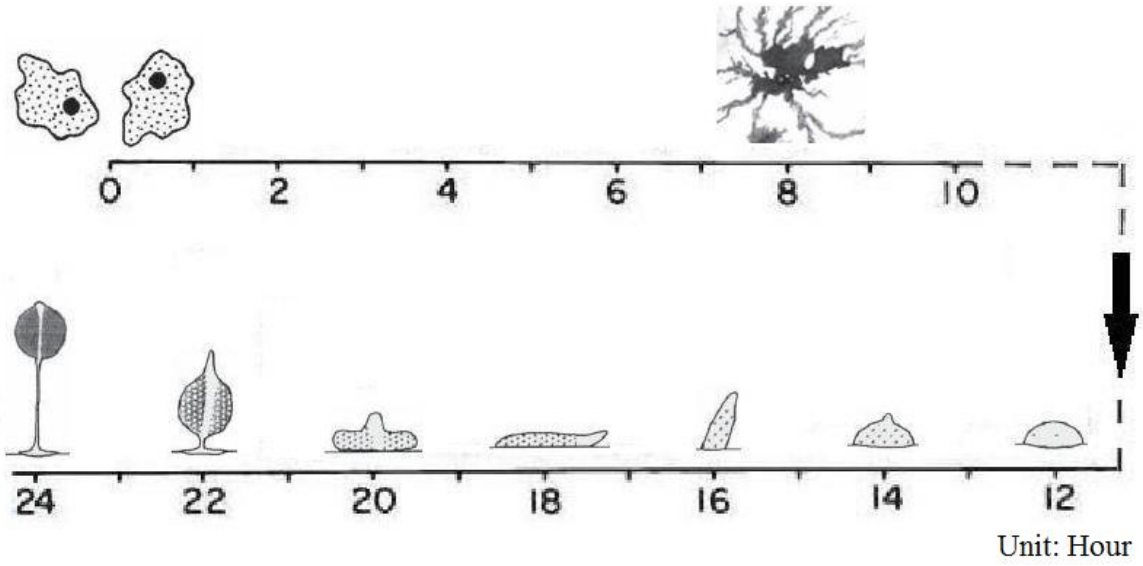

Fig 1.1 Development of *Dictyostelium*. Numbers in the figure represent time after cells are deprived of a food source (Modified from Figure 8.12, *Dictyostelium* - Evolution, Cell Biology and Development of Multicellularity, 2001).

In 2005, the genome of *Dictyostelium discoideum* was sequenced using the whole-chromosome shotgun (WCS) strategy, which greatly facilitated the research on the role of each individual gene (Eichinger et al., 2005). The 34 million base pair nuclear genome of *Dictyostelium* is distributed in six chromosomes. Systematically, it is relatively easy to study the regulatory strategies using *Dictyostelium*, through which one can predict the control networks in animals or plants. It is a haploid system which makes it a very powerful system for functional analysis of gene function. Out of the whole genome, the protein-coding genes are predicted to be at the range of 10,000-10,600. Among those genes, many of their encoded proteins are currently found to have homologs in higher eukaryotic cells and play a role in all kinds of cellular events such as development, chemotaxis, metabolism, signaling transduction, differentiation and endocytosis (Chen et

al., 2005; Davidoff, 1964; Eichinger et al., 2005; Kim et al., 2005; Lardy et al., 2005; Parent, 2004). What makes this model organism attractive is that the gene product information such as their function, their homologs in other organisms, signaling pathway they contribute to, the family they belong to and the protein they bind to can all be easily accessed at the *Dictyostelium* homepage (http://dictybase.org). A large number of *Dictyostelium* knockout and over-expression strains can be obtained from the *Dictyostelium* Stock Center.

1.2 Chemotaxis

1.2.1 Overview of chemotaxis

In one way or another, life is closely linked to motility. All cells are able to detect external stimuli in their living environment. In a broad point of view, chemotaxis is involved in numerous processes both at the cellular level and organism level. The way a butterfly finds a flower to the way sperm finds the ovum, and from how bacteria find their food and avoid enemies to how the germ cells know where to migrate during embryogenesis, the event of chemotaxis is almost ubiquitous and exerts crucial functions in numerous ways. Chemotaxis is defined as a guided cell movement in response to a chemical gradient of either chemoattractant or chemorepellent (Rappel and Loomis, 2009). In the long process of evolution, a chemosensory system would be one of the earliest systems to appear and is probably well conserved. Some of the well-studied examples include localization of optimal living environment, finding mating target and colonization coupled with differentiation or growth (Adler, 1987; Grebe and Stock, 1998; Palanivelu and Preuss, 2000; Rappel and Loomis, 2009; Schwartz et al., 1958). Because of the significant roles played by chemotaxis, its molecular mechanism has been one of

the foci of recent researches. Generally, across both prokaryotic and eukaryotic kingdoms, chemotaxis is triggered by external stimuli that bind to the cell surface-located receptor protein. The binding between the external stimuli and receptor protein further causes binding or dissociation of a molecule from the receptor protein, through which the external signal is transmitted from outside of the cell into inside of the cell. The downstream signaling cascades often involve remodeling of the cytoskeleton protein or stimulate the motor organ such as flagella (King and Insall, 2009; Sagi et al., 2003; Scharf et al., 1998; Spohn and Scarlato, 2001). In eukaryotic cells such as *Dictyostelium* and neutrophils, as low as a ~2% concentration difference of chemoattractant between the leading front and the back of the cell can be detected, underscoring that the gradient sensing mechanisms are impressively sensitive (Parent and Devreotes, 1999).

1.2.2 PIP3 signaling pathway in *Dictyostelium*

Early researches using green fluorescent protein (GFP) fused the cytosolic regulator of adenylyl cyclase (CRAC) showed that upon cAMP stimulation, CRAC transiently localized to the leading edge of a cell undergoing chemotaxis and the PH domain on CRAC seems to be mainly regulating this event (Parent et al., 1998). Later on, it was found that the second messenger phosphatidylinositol 3,4,5-triphosphate (PIP3) is the key product after cAMP stimulation which serves as a docking site for a number of PH domain containing proteins and further regulates the localized production of actin filament at the leading edge (Funamoto et al., 2002; Funamoto et al., 2001). In the *Dictyostelium* system, PIP3 is produced by five of the class I phosphatidylinositol 3-kinases, PI3K1-5, which phosphorylate phosphatidylinositol 4,5-bisphosphate (PIP2) to PIP3 in the inner leaflet of the plasma membrane. The N-terminal region preceding the

catalytic domain of PI3K is necessary and sufficient for its membrane localization. Ras GTPases, a group of membrane localized proteins, activate PI3K activity. At the same time, inhibition of PI3K activity blocks autonomous Ras activation indicating Ras and PI3K form a positive feedback loop (Funamoto et al., 2002; Sasaki et al., 2004; Sasaki and Firtel, 2005; Sasaki and Firtel, 2006; Sasaki et al., 2007). On the other hand, one of the known tumor suppressor-phosphatase and tensin homolog (PTEN) shuts down PIP3 signaling by switching PIP3 back to PIP2. The membrane localization of PTEN is dependent on its PIP2 binding domain and is independent of PIP3 and its localization dynamics in response to cAMP stimulation shows an opposite pattern from PI3Ks. Cyclic AMP triggers dissociation of PTEN from the leading edge and accumulation on the sides and rear of the cells. *pten*$^-$ cells have elevated basal PIP3 levels on the membrane and aberrant chemotaxis in the cAMP gradient (Iijima and Devreotes, 2002; Iijima et al., 2002; Iijima et al., 2004). In neutrophils, the SH2 domain-containing inositol-polyphosphate 5'-phosphatase (SHIP1 and SHIP2) are able to dephosphorylate PIP3 at the 5' position and produce phosphatidylinositol 3,4-bisphosphate. There are several of *Dictyostelium* SHIP homolog proteins that can catalyze similar reactions (Loovers et al., 2007; Mondal et al., 2012; Nishio et al., 2007; Vlahou and Rivero, 2006).

1.2.3 TORC2 signaling pathway in *Dictyostelium*

Parallel to PIP3 signaling, a signaling cascade which includes target of rapamycin complex 2 (TORC2), protein kinase B (PKB), protein kinase BR (PKBR) and Ras GTPase as main regulators, also significantly modulates chemotaxis of *Dictyostelium* (Cai et al., 2010; Kamimura et al., 2008; Lee et al., 2005; Liao et al., 2008). One of the dozen *Dictyostelium* Ras proteins, RasC, becomes activated in response to cAMP

stimulation, and subsequently turns on TORC2 complex, which is composed of TORC2, Lst8, RIP3 and Pia, at the leading edge. Then, PKB and PKBR are sequentially phosphorylated by TORC2 complex and phosphoinositide-dependent kinases (PDKs) on their C-terminal hydrophobic motif and activation loops respectively, which further modulates Filamentous Actin (F-Actin) polymerization. Intriguingly, RasC-TORC2 signaling is likely to crosstalk with PIP3 signaling through PKBA activation (Cai et al., 2010; Charest et al., 2010; Kamimura and Devreotes, 2010). Recently, it was reported that TORC2 signaling negatively regulates the activity of RasC in a feedback loop, which is independent of PIP3 signaling. The transient membrane localization of the RasC GEF (Aimless)/PP2A/Sca1 complex to the plasma membrane is responsible for the RasC activation after cAMP stimulation. Cells lacking either PKBR or both PKBR/PKB displayed strong and persistent RasC activation, indicating that PKB and PKBR antagonize RasC activation and form a negative feedback loop in response to chemoattractant stimulation (Charest et al., 2010).

1.2.4 Other signaling pathways affecting *Dictyostelium* chemotaxis

There are still other signaling pathways that contribute to the chemical gradient sensing ability in *Dictyostelium*. These pathways mainly include phospholipase A2 (PLA2) pathway and soluble guanylyl cyclase (sGC) pathway (Chen et al., 2007; Kortholt et al., 2011; van Haastert et al., 2007; Veltman et al., 2005). The PLA2 signaling acts independent of PIP3 signaling but deletion of both PLA2 homologs and two main PI3Ks almost completely obliterates chemotactic response of *Dictyostelium*. It was also suggested that the function of PLA2 is mediated through its catalytic product, arachidonic acid (Chen et al., 2007). In the cAMP gradient, similar to TORC2 and PI3K situation,

sGC was found to be located at the leading cortex of the cells as well. Virtually all the cGMP are produced by sGC and are essential in regulating chemotaxis via the accumulation of Myosin II near the plasma membrane at the rear of a cell doing chemotaxis (Veltman et al., 2005; Veltman and Van Haastert, 2006). Intriguingly, another phospholipase, Phospholipase D (PLD), was also reported to be an important player in actin-derived motility in *Dictyostelium*. Inhibition of PLD activity not only causes a completely mis-localization of F-Actin inside of the cells, but also results in a significant reduction of moving speed. And these defects were suggested to be the results of the role of PLD in supporting PIP2 synthesis (Zouwail et al., 2005).

The results indicated that all four pathways mentioned above contribute a significant portion of the total chemotactic ability in *Dictyostelium* in which some of them contribute more in the direction sensing and others contribute more on the remodeling of F-Actin (splitting of current pseudopods). What is more, when several signaling pathways are operating simultaneously, strong synergistic effects were observed which together induce the sensitivity to around 150 fold (Bosgraaf and Van Haastert, 2009; Kortholt et al., 2011).

1.3 Glycogen synthase kinase 3

1.3.1 Overview of GSK3

More than three decades ago, in the process of searching for an enzyme that could regulate the glycogen synthase activity using the rabbit skeleton muscle extract, an unique kinase was found to be able to phosphorylate glycogen synthase independent of either cAMP or calcium ion, the reaction mechanism of which is totally different from the previously discovered Glycogen Synthase Kinase 1 and Glycogen Synthase Kinase 2

(Embi et al., 1980). Thus, the name Glycogen Synthase Kinase 3 (GSK3) was given (Embi et al., 1980). The two homolog copies of GSK3 in mammalian system, GSK3α and GSK3β which are 52 kD and 46 kD respectively, were first cloned by Woodgett and was reported at the same time that both kinds of GSK3 are expressed in most tissue especially in the brain (Woodgett, 1990). Since its discovery, much of the initial work was concentrated on its purification, characterization and role in metabolism. An interesting characteristic of GSK3 is that in a number of cases, phosphorylation by GSK3 requires prior phosphorylation by a priming kinase such as casein kinase II in case of glycogen synthase on the consensus sequence of GSK3 to form the motif of –S-X-X-X-S-X-X-X-S(P)-, where 'X' represents any amino acid and 'P' represents phosphate group, an event known as 'priming' (DePaoli-Roach, 1984; Fiol et al., 1988; Fiol et al., 1990; Hemmings and Cohen, 1983; Hemmings et al., 1981; Woodgett and Cohen, 1984). In the metabolic pathway, besides its crucial inhibitory role on the glycogen synthase activity, it was also found to be able to phosphorylate the Type-II regulatory subunit of cAMP dependent protein kinase, inactive inhibitor-2, which inhibits protein phosphatase-1 by phosphorylation (Hemmings et al., 1982a; Hemmings et al., 1982b; Henry and Killilea, 1993). What is more, GSK3 can phosphorylate ATP citrate lyase (Hughes et al., 1992). In *Dictyostelium*, there is one GSK3 homolog, known as GskA, which was first cloned by Harwood and his colleagues. Earlier studies on *Dictyostelium* GSK3 was focused on its roles in multicellular development, while recently, it was reported that GSK3 play a role in movement as well (Harwood et al., 1995; Kim et al., 2011; Plyte et al., 1999; Teo et al., 2010).

Glycogen Synthase Kinase 3 itself is subjected to different regulatory mechanisms. Purified GSK3α and GSK3β were constitutively active and highly phosphorylated in tyrosine residues in their conserved region. Phosphorylation of the tyrosine 216 residue is essential for the activation of GSK3 (Figure 1.2). Mutation of Tyr216 to Phe led to a reduction of its activity by 10 fold (Hughes et al., 1993). In another study, treatment of GSK3 by a tyrosine phosphatase results in a decrease in its activity which further proved that tyrosine phosphorylation is necessary for the full activation of GSK3 (Wang et al., 1994). Furthermore, tyrosine phosphorylation of GSK3 was shown to be decreased in response to insulin treatment, which led to phosphorylation of GSK3 at serine residues at the amino terminal side, which was further underscored by the finding that GSK3 mutant lacking the first 9 amino acids containing the Akt target site still displayed diminished tyrosine phosphorylation in response to insulin treatment (Murai et al., 1996). Consistently, tyrosine kinases such as Fyn and Zak1/2 were shown to be able to activate GSK3 in human and *Dictyostelium* respectively (Kim and Kimmel, 2006; Kim et al., 1999; Lesort et al., 1999). Increasing the intracellular calcium level was initially found to have a positive role in the tyrosine phosphorylation of GSK3 and later it was found that protein tyrosine kinase 2 (PYK2), a calcium activated tyrosine kinase, is responsible for this event (Hartigan and Johnson, 1999). Intriguingly, the mitogen-activated protein kinase kinase (MEK1/2) was also found to be able to directly phosphorylate Tyr216 residue on GSK3 in skin fibroblast (Takahashi-Yanaga et al., 2004).

On the contrary, point mutation results showed that the phosphorylation on the either Ser21 residue of GSK3α or Ser9 residue of GSK3β exerts an inhibitory role on the activity of GSK3 (Figure 1.2). Pioneer researches indicated that p90rsk-1 kinase and p70

ribosomal S6 kinase could phosphorylate Ser9 on GSK3β thus inhibit GSK3 activity *in vitro*, a phenomenon which can be reversed by protein phosphatase 2A (Sutherland et al., 1993). In the insulin-induced signaling cascade, Akt is activated in a phosphatidyl inositol 3-kinase and 3-phosphinositide-dependent kinase 1 dependent manner (Cross et al., 1995; Delcommenne et al., 1998). The activated Akt phosphorylates the Ser9 on GSK3β and inhibits GSK3β (Cross et al., 1995; Cross et al., 1997). Later on, some other stimuli were discovered which initiate signaling pathways that merge with insulin triggered signaling at the point of Akt in both PI3K dependent and independent ways, all of which consequently inhibit the activity of GSK3 resembling the action of insulin. These stimuli include growth factor in PC12 cells (Pap and Cooper, 1998), insulin-like growth factor I (IGF-I) in mouse cerebellar granule cells (Cui et al., 1998), epidermal growth factor (EGF) in human myoblasts (Halse et al., 1999), isoproterenol in rat epididymal fat cells (Moule et al., 1997), and isoproterenol in myocytes (Morisco et al., 2000). Distinct from the insulin mediated GSK3 inhibition, Wnt ligands were also shown to suppress GSK3 activity via protein kinase C (PKC) activation. GSK3 can be inactivated by protein kinase C delta fragment in apoptosis as well (Cook et al., 1996; Tsujio et al., 2000).

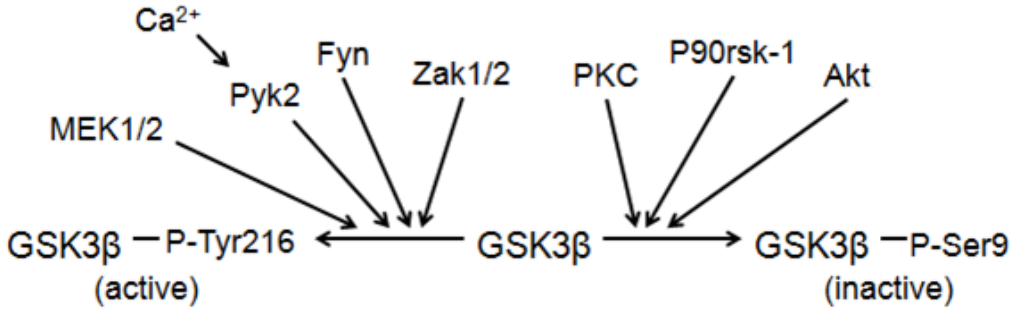

Fig 1.2 Mammalian GSK3β regulation via phosphorylation. 'P' indicates phosphate group.

Besides direct phosphorylation mediated regulation, GSK3 was later found to be regulated by certain GSK3 binding proteins which can form protein complexes with GSK3. Similar to the insulin signaling pathway, activation of Wnt signaling pathway also decreased GSK3 activity. However, it was reported in different systems that the phosphorylation status of Ser9 residue on GSK3β is not affected (Ding et al., 2000; Ruel et al., 1999). It was found that a family of GSK3-binding proteins (GBP) is able to suppress the activity of GSK3 by forming protein complexes. In *Xenopus*, expression of GBP decreased GSK3β activity and reduced GSK3 facilitated β-catenin degradation (Yost et al., 1998). Given the fact that GBP bound GSK3β can still phosphorylate a peptide substrate, GBP inhibits GSK3 activity by steric hindrance effect, which discourages large substrate protein from approaching the kinase catalytic domain of GSK3, without affecting the kinase activity of GSK3 (Farr et al., 2000). On the contrary, forming a protein complex with Axin stimulates the activity of GSK3. Phosphorylated by GSK3β, Axin is stabilized which was proved by the fact that inhibition of GSK3β by lithium decrease Axin level. Axin, together with adenomatous polyposis coli (APC) and β-catenin, all bind to GSK3β and facilitate the phosphorylation and degradation of β-catenin (Behrens et al., 1998; Hedgepeth et al., 1999; Kishida et al., 1998; Rubinfeld et al., 1996; Yamamoto et al., 1999).

1.3.2 GSK3 in development and transcription factor regulation

Thirty years after discovery, the cellular events orchestrated by GSK3 have greatly exceeded what its name implies. In the field of development, GSK3 was found to be one of the key regulators of early embryogenesis in *Drosophila*. In the embryonic epidermis,

non-functional mutant of GSK3 disrupts denticle belts development while non-functional β-catenin mutant, results in the loss of naked cuticle (Kim and Kimmel, 2000; Peifer et al., 1994). In *Xenopus,* binding with GSK3, axin inhibits axial development. Injecting catalytically inactive GSK3β into embryos resulted in the ectopic formation of another set of dorsal and anterior structures (Dominguez et al., 1995; Itoh et al., 1998). In *C. elegans*, during the asymmetrical division of four-cell-stage blastomere, GSK3 promotes endoderm specification and mitotic spindle orientation (Schlesinger et al., 1999; Walston and Hardin, 2006). Similarly, GSK3 also plays a significant role in the development of *Dictyostelium*. *Dictyostelium* cells lacking GSK3 displays an abnormally enlarged basal disk and a greatly reduced spore head. At the molecular level, compared to wild type cells, *gsk3*$^-$ cells showed a precocious and elevated expression of prestalk/stalk-specific gene while prespore marker genes reduce dramatically compare to those in wild type cells (Harwood et al., 1995; Insall, 1995). In the area of transcription factor regulation, a number of transcription factors have been found to be targets of GSK3. Upon stabilization in response to Wnt signaling, β-catenin forms a bipartite transcription factor T-cell factor (Tcf)/Lymphoid enhancer factor (Lef), and regulates target genes. Wnt signaling is known to be able to inhibit GSK3 mediated phosphorylation of β-catenin. Mutant β-catenin lacking the GSK3 phosphorylation site is more stable than the wild type β-catenin (Hart et al., 1998; Papkoff and Aikawa, 1998; Yost et al., 1996). Another transcription factor AP1, which is a heterodimer of *jun* and *fos* gene products, is also a substrate of GSK3, of which phosphorylation by GSK3 decreases its DNA binding capability (Boyle et al., 1991; de Groot et al., 1993; Nikolakaki et al., 1993). Cyclic AMP response element binding protein (CREB) is yet another example of transcription factor

which is under the control of GSK3. It seems that GSK3 can modulate CREB activity in a cell type or tissue specific manner (Fiol et al., 1994; Grimes and Jope, 2001a; Tullai et al., 2007). Besides what is mentioned above, there are other transcription factors that are either positively or negatively regulated by GSK3, such as Heat shock factor-1 (Bijur and Jope, 2000; Xavier et al., 2000), Nuclear factor of activated T cells (Neal and Clipstone, 2001; Sheridan et al., 2002; van der Velden et al., 2008), Myc (Galletti et al., 2009; Gregory et al., 2003) and C/EBP (Grimes and Jope, 2001b; Ross et al., 1999). In this dissertation, the function of GSK3 in eukaryotic cell migration is the primary study focus.

1.3.3 GSK3 in mammalian cell movement and polarity

In neuronal development, early neurites which are indistinguishable between dendrites and the axons are formed by the extension of neurons. One of the neurites will develop into an axon with a longer shape than the dendritic neurites. It was found that a requirement for neuronal polymerization is to decrease GSK3β activity. On the contrary, expressing a constitutively active form of GSK3β suppresses the formation of axon. Glycogen Synthase Kinase 3β plays a central role in both establishing and maintaining neuronal polarity. There is high GSK3β activity and low Akt activity in the dendrites, but the opposite is displayed in axons (Jiang et al., 2005). Downstream of GSK3β, collapsin response mediator protein- 2 (CRMP-2) was found to be a direct substrate of GSK3β (Yoshimura et al., 2005a). The role of CRMP-2 is to bind to tubulin heterodimers and thus establish and promote neuronal polarity. Phosphorylation of CRMP-2 by GSK3β decreases its tubulin binding affinity thus suppresses the neuronal cell polarization (Yoshimura et al., 2005a; Yoshimura et al., 2005b).

Rho GTPases has long been established as a key regulator of F-Actin cytoskeleton. GTPase-activating proteins (GAPs) inactivate Rho GTPase, while guanine nucleotide exchange factors (GEFs) activate it. Two of the RhoGAPs, p190A and p190B were demonstrated to have essential roles in mouse embryonic tissue morphogenesis (Brouns et al., 2000; Brouns et al., 2001). Recently, p190A was found to be under the direct regulation of GSK3β. After phosphorylation by a priming kinase, GSK3β directly phosphorylates p190A at the C-terminal region and inhibits the RhoGAP activity of p190A. Consistent with the Brouns and others (2000), a phosphorylation-defective mutant of p190A showed a greatly increased cell motility, which is reminiscent of those seen in the Rho GTPase inhibited cells (Jiang et al., 2008).

On another occasion, small GTPase Cdc42 regulates atypical protein kinase C (aPKC) complex, which further regulates directed cell migration. Using rat primary astrocytes, Par6-PKCζ complex was shown to directly contact with GSK3β and phosphorylates the Ser9 residue on GSK3β at the leading front of migrating cells, which inhibits GSK3β. The inhibition of GSK3β is essential for the binding of adenomatous polyposis coli (APC) with the plus ends of microtubules, which is important for cell polymerization. Expression of a nonphosphorylatable GSK3β mutant and a kinase dead mutant of GSK3β block centrosome reorientation and induce aberrant cell polarization (Baluch and Capco, 2008; Etienne-Manneville and Hall, 2003).

Besides APC mentioned above, GSK3 regulates the microtubule stability in other ways. GSK3β destabilizes microtubule by phosphorylating microtubule-associated protein 1B (MAP1B), which contributes to the dynamics in growing axon. Introducing MAP1B with mutated GSK3β sites partially rescues the microtubule destabilization. The

microtubule binding protein tau can also be phosphorylated by GSK3β at multiple serine residues. Co-transfection of tau together with GSK3β induces microtubule destabilization and phosphorylation on tau. Inhibition of GSK3β by lithium ion stimulates microtubule assembly and the binding of tau to microtubules (Cho and Johnson, 2003; Cho and Johnson, 2004; Ciani et al., 2004; Sun et al., 2009; Sun et al., 2002; Trivedi et al., 2005).

1.3.4 GSK3 in *Dictyostelium* movement

Several recent studies demonstrated that GSK3 modulates cell polarization and chemotaxis in *Dictyostelium* (Kim et al., 2011; Kolsch et al., 2012; Teo et al., 2010). The *gsk3*$^-$ cells display not only aberrant differentiation, but also greatly reduced migration speed and direction sensing ability. A GSK3 activator, ZAK1 is shown to be essential for proper chemotaxis of *Dictyostelium* cells (Kim et al., 2011). Transient increase in the level of PIP3 on the plasma membrane is generally observed from wild type cells. In contrast, *gsk3*$^-$ cells exhibit high basal level of PIP3 uniformly through the entire plasma membrane, which does not further increase in response to chemoattractant stimulation. The lack of chemoattractant dependent generation of PIP3 in *gsk3*$^-$ cells seems to be the central defect, given that *gsk3*$^-$ cells were able to undergo chemotaxis when proper PIP3 response was restored upon increasing the level of PI3K substrate PIP2 by over-expressing PIP2 producing enzyme inositol monophosphatase (IMPA). Furthermore, *gsk3*$^-$ cells over-expressing IMPA displays normal activation of PKBA, but not PKBR, indicating that the operation of chemoattractant mediated PIP3/PKBA signaling can effectively restore *gsk3*$^-$ cell chemotaxis in the absence of proper PKBR signaling (Teo et al., 2010). In contrast to the study by Teo and colleagues (2010), a recent study by Kolsch and colleagues (2012) showed that *gsk3*$^-$ cells display greatly extended activation of both

PKBA and PKBR. A recently found Ras activator-Daydreamer (DydA), which was revealed to be another important regulator of chemotaxis, was reported to be a direct target of GSK3. Re-introducing Daydreamer with non-phosphorylatable GSK3 recognition sites back into *dydA*$^-$ cells could neither rescue the chemotaxis defects nor fully suppress the extended phosphorylation of the activation loop (AL) and hydrophobic motif (HM) of Akt/PKB and PKBR1 exhibited in *dydA*$^-$ cells, which indicate that the function of DydA requires GSK3 phosphorylation (Figure 1.3). In this dissertation, a novel finding that GSK3 affects chemotaxis through regulating PI3K membrane localization is described.

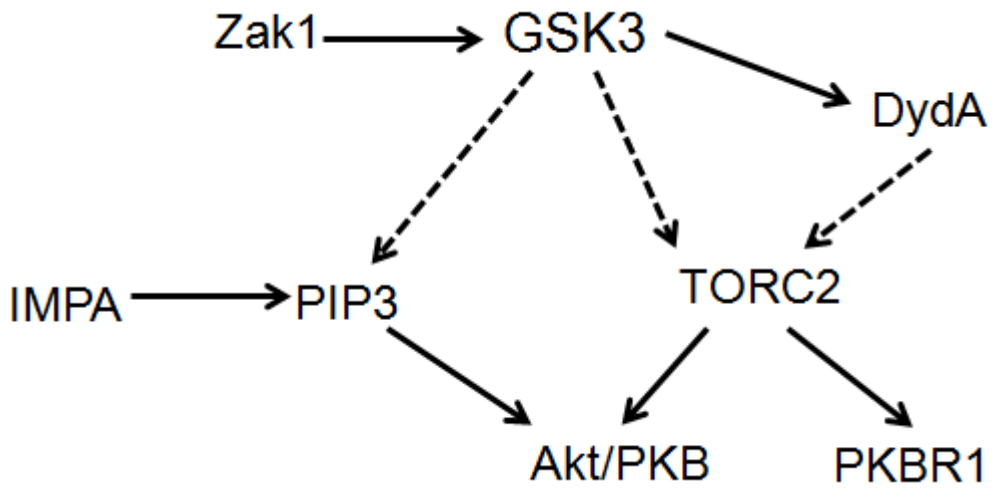

Fig 1.3 The role of GSK3 in both PIP3 and TORC2 pathways in *Dictyostelium*. Arrows with solid line represent directly regulate, arrows with dotted line represent indirect regulation.

CHAPTER II

CELLS LACKING GSK3 ARE DEFECTIVE IN MOTILITY

2.1 Materials and methods

2.1.1 *Dictyostelium* culture and pulsing

Dictyostelium discoideum thymidine auxotrophic strain JH10 and *gsk3*$^-$ cells generated from JH10 were cultured axenically in D-3T media (14.3 g/l Bacto peptone #3, 15.4 g/l glucose, 7.15 mg/l yeast extract, 0.525 g/l Na_2HPO_4, 0.48 g/l KH_2PO_4,) with 0.5 mg/ml thymidine at 20°C (Kim et al., 2002; Louis et al., 1994). Cells with selection markers were grown with D-3T supplemented with either 20 μg/ml of Neomycin (G418) or 5 μg/ml of Blasticidin as needed. For the chemotaxis assay, cells were inoculated and cultured in a sterilized culture flask with a shaking speed of 150 rpm at 20°C. After reaching log phase (exponential growth phase), 100 million cells were spun down, washed once with ice-cold developmental buffer (DB) (2 mM $MgCl_2$, 0.2 mM $CaCl_2$, 7.4 mM NaH_2PO_4•H_2O and 4 mM Na_2HPO_4•$7H_2O$) and re-suspended in 5 ml of DB. Cells were then shaken at room temperature for 1 hr and pulsed with 50 nM of cAMP every 6 min for a total period of 4 hr (cells after pulsing are referred to as 'pulsed cells' henceforth).

2.1.2 Chemotaxis assay and random motility assay

After pulsing, aggregation competent cells were placed in a 35 x 10 mm tissue culture dish coverslip (Becton Dickinson Labware) filled with DB at a density of $6x10^4$ cells/cm^2. Five minutes were allowed for cells to adhere to the bottom of the coverslip. A micromanipulator (Narishige) controls the positioning of the micropipette (Femtotip, Eppendorf) filled with either 2 μM or 10 μM cAMP solution. The tissue culture dish

coverslip was placed on the inverted microscope (Leica DM IRB). A pressure of 20 Kpa was provided by a FemtoJet pump (Eppendorf) to generate a cAMP gradient. Images were taken at 100X total magnification every 6 min using Openlab software (PerKinElmer) and a CoolSNAP digital camera. For the random movement assay, the procedures were the same as the chemotaxis assay, except that no cAMP gradient was provided when recording the cell movement. The recorded images were later analyzed using Openlab (PerKinElmer) and Microsoft Office. Chemotactic indices, which is defined as the distance moved in the direction of the pipette divided by the total distance moved, were obtained from the centroid positions of the cells, which is described previously, and the position of the micropipette (Loovers et al., 2006). Speed is defined as the total distance moved divided by the total time elapsed.

2.1.3 RT-PCR

After reaching log phase, 10^7 cells were harvested. Total RNA were isolated using Trizol reagent. The RNA concentrations were adjusted to 1 µg/µl which is confirmed by using spectrophotometry and one step RT-PCR reaction was performed by using Masterscript RT PCR kit (5 PRIME) and 0.3 g of total RNA. Levels of *sodC* messages were assessed by RT-PCR using forward primer 5'-ATGAGACTTTTATCTGTATTAG-3' and reverse primer 5'-TTAAAGCAAAGCAAAGATAATT-3'. *IG7* messages were detected by using forward primer 5'-GGTGAGCGAAAGCCGAGGAGAG-3' and reverse primer 5'-GCAACAGTTACGGGTTCCGCC-3'.

2.1.4 Transfection by electroporation

Five hundred thousand log phase cells were centrifuged and washed twice with ice-cold H-50 buffer (20 mM HEPES, 50 mM KCl, 10 mM NaCl, 1 mM $MgSO_4$, 5 mM

$NaHCO_3$, 1 mM $NaHPO_4$) and re-suspended in 100 µl H-50 buffer. Around 10 µg of DNA were then mixed with the cells and the whole suspension was transferred into 1 mm gap electroporation cuvette (Fisherbrand). The cells were electroporated at 0.85 kV and 3 µF twice with 5 sec break using Gene Pulser Xcell (Bio-Rad). After 10 min incubation on ice, the cells were plated in a 100 x 20 mm tissue culture plate (BD Falcon). Proper antibiotics were added the next day.

2.1.5 Antibodies and western blotting

Anti-GFP antibodies were purchased from Covance (1:1000 dilution in 2% BSA).

For western blotting, protein samples were run on 10% SDS - polyacrylamide gel and later on transferred to a nitrocellulose membrane (Immobilon) using western system purchased from Biorad. Membranes were then blocked 30 min in 2% bovine serum albumin (BSA) solution, and incubated in corresponding primary antibody for 2 hr at room temperature. Membranes were washed three times at 10 min intervals using TBST (0.2% Tween 20, 10 mM Tris HCl at pH7.7, 0.12 M NaCl, 1 mM EDTA) and incubated using proper HRP-conjugated secondary antibody for 1 hr at room temperature. Membranes were subsequently washed three times at 10 min intervals using TBST with an additional final wash with TBS (10 mM Tris HCl at pH7.7, 0.12 M NaCl, 1 mM EDTA) for 5 min and incubated with ECL reagent (GE Health care) to obtain the final images.

2.2 Results

2.2.1 The *gsk3*$^-$ cells showed aberrant movement in both chemotaxis and random movement

Aggregation competent cells of both wild type and *gsk3*$^-$ cells were either challenged in different cAMP gradients or were subjected to random movement assay. The *gsk3*$^-$ cells showed significant defects in both chemotactic indices and speed compared to wild type cells. The chemotactic indices of *gsk3*$^-$ cells were around 14% of wild type cells. Also, the speed of *gsk3*$^-$ cells was only about 20% of the wild type level (Figure 2.1). The severe abnormalities for *gsk3*$^-$ cells in both chemotactic indices and speed were shown not only during the first 20 min after challenged with 10 μM cAMP point source, but also during the second 20 min (Table 2.1). Similar defects of chemotactic indices and speed for *gsk3*$^-$ cells were observed under a shallow cAMP gradient. The chemotactic indices in *gsk3*$^-$ cells using a 2 μM cAMP point source dropped below zero indicating that the cells completely lost their direction sensing ability. In the meantime, the speed of *gsk3*$^-$ cells dropped to around 50% of the wild type level (Figure 2.2).

Furthermore, *gsk3*$^-$ cells displayed 5.1 μm/min of random movement, whereas wild type cells moved at the speed of 8.93 μm/min (Figure 2.3). It is worth to mention here that the relatively large standard deviation in the random movement assays were because of the cells were not challenged with any cAMP gradient.

The *gsk3*$^-$ cells displayed severe chemotaxis and random movement defects under both weak and steep cAMP gradient and showed compromised polarization during the period of assays.

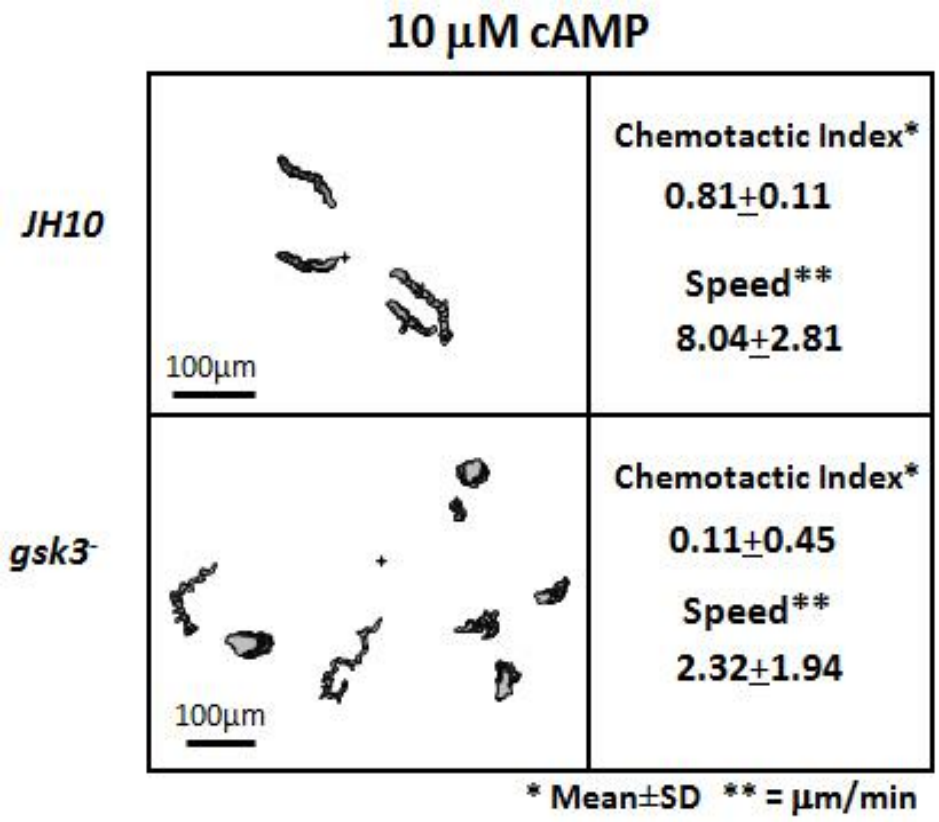

Fig 2.1 Chemotaxis assays using 10 µM cAMP point source. Both JH10 cells and *gsk3*$^-$ cells were challenged with a point source of 10 µM cAMP. Superimposed tracing images were grouped. For JH10 cells, a total time period of 20 min were recorded and 40 min were recorded for *gsk3*$^-$ cells. Numbers are shown as mean ± standard deviation (SD). Data are representative of at least three independent experiments.

Time period	CI	speed
0-40′	0.11±0.38	2.68±2.36
0-20′	0.11±0.45	2.32±1.94
20-40′	0.09±0.48	3.04±2.93

Table 2.1 Summary of chemotactic indices and speed of *gsk3*$^-$ cells in different time frames. The unit for the speed is µm/min.

2 μM cAMP	Cell type	Chemotaxis Index Mean ± SD	Speed (μm/min) Mean ± SD
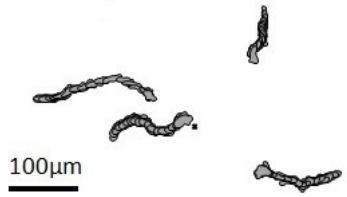	*JH10*	**0.85±0.11**	**7.11±1.87**
	gsk3⁻	**-0.06±0.39**	**3.71±2.12**

Fig 2.2 Chemotaxis assays using 2 μM cAMP point source. Both JH10 cells and *gsk3*$^-$ cells were challenged with a point source of 2 μM cAMP. Superimposed tracing images were grouped. For JH10 cells, a total time period of 20 min were recorded and 35 min were recorded for *gsk3*$^-$ cells. Numbers are shown as mean ± standard deviation (SD). Data are representative of at least three independent experiments. Scale bars represent 100 μm.

random movement	Cell type	Speed (μm/min) Mean ± SD
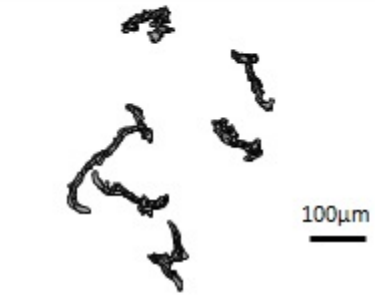	*JH10*	8.93±3.74
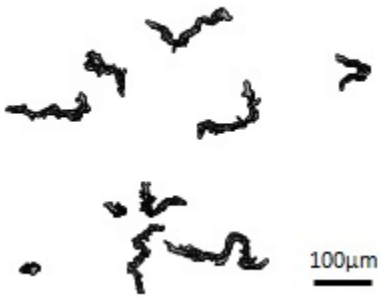	*gsk3⁻*	5.10±2.65

Fig 2.3 Random movement assays for both JH10 and *gsk3⁻* cells. Both assays were recorded for 40 min. Superimposed tracing images were grouped. Numbers are shown as mean ± standard deviation (SD). Data are representative of at least three independent experiments. Scale bars represent 100 μm.

2.2.2 Re-introducing GFP fused GSK3 back to *gsk3⁻* cells rescued the chemotaxis defects

The GFP and GFP-GSK3 fusion proteins were introduced into *gsk3⁻* cells separately. Expression was confirmed by western blotting (Figure 2.4). The *gsk3⁻* cells expressing GFP served as a negative control. As shown in Figure 2.5, GFP alone could not improve either chemotactic indices or speed in *gsk3⁻* cells. However, expressing GFP-GSK3 in *gsk3⁻* cells was able to partially restore wild type like chemotactic indices and speed

compared to those in wild type situations indicating GSK3 indeed played a crucial role in *Dictyostelium* chemotaxis.

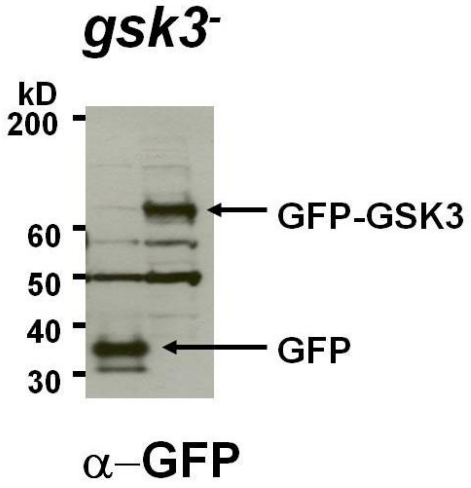

Fig 2.4 Expression of GFP (left lane) and GFP-GSK3 (right lane) in *gsk3*$^-$ cells.

0.1 μM cAMP	Cell type	Chemotaxis Index Mean ± SD	Speed (μm/min) Mean ± SD
	Wt	0.87± 0.06	9.75 ± 3.09
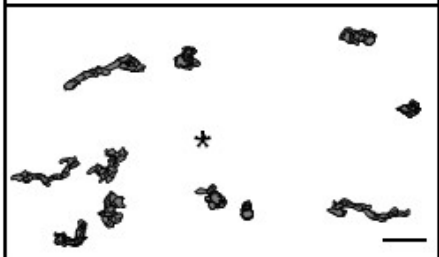	*GFP/ gsk3*$^-$	0.21 ± 0.43	2.89 ± 4.38
	GFP-GSK3/ gsk3$^-$	0.68 ± 0.19	7.34 ± 2.00

Fig 2.5 Reintroducing GSK3 in *gsk3*$^-$ cells rescued their chemotaxis defect. *gsk3*$^-$ cells expressing either GFP alone or GFP-GSK3 were challenged with a point source of 0.1 μM cAMP. Forty minutes were recorded in each assay. Superimposed tracing images were grouped. Numbers are shown as mean ± standard deviation (SD). Data are representative of at least three independent experiments. Scale bars represent 100 μm.

2.2.3 Expressing *sodC* in *gsk3*$^-$ cells could not rescue both chemotaxis and random movement defects

It was previously shown by microarray and proteomics studies that in the early development stage, *sodC* gene is under-expressed in *gsk3*$^-$ cells, which was further confirmed by my RT-PCR data (Figure 2.8). Since a GPI-anchored outer membrane superoxide dismutase (encoded by *sodC*) has been proven to be another key regulator of chemotaxis, we expressed *sodC* into both wild type and *gsk3*$^-$ cells (designated Wt::*sodC* or *sodC*/Wt, *gsk3*$^-$::*sodC* or *sodC*/*gsk3*$^-$. '::' referred to as 'expressing' while '/' referred to as 'is expressed in' henceforth), while Wt::*sodC* served as a control here. The expression levels after pulsing were confirmed by RT-PCR experiments (Figure 2.6).

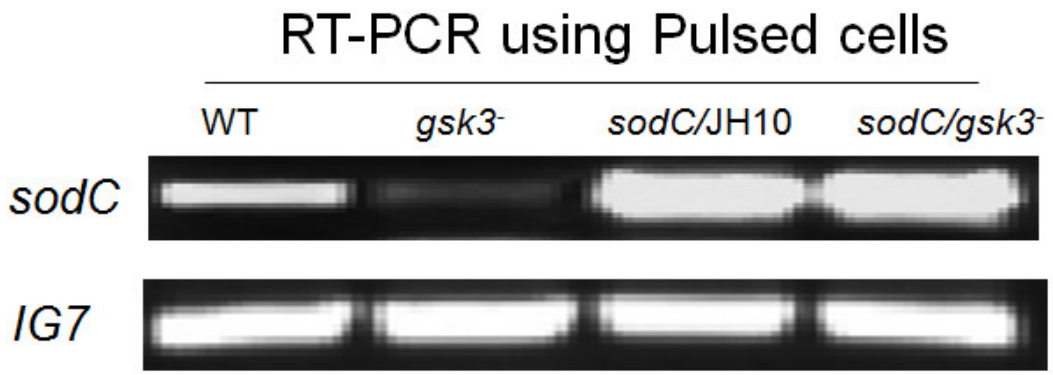

Fig 2.6 RT-PCR experiment to determine transcription level of *sodC*. *IG 7* transcript serves as a control. The *sodC* was under-expressed in *gsk3*$^-$ cells compared with wild type cells (first two lanes). The *sodC* was over-expressed in both wild type cells and *gsk3*$^-$ cells by using transfection (lane three and lane four).

The level of *sodC* messages in wild type cells and *gsk3*$^-$ cells expressing *sodC* under constitutively active Actin-15 promoter were higher than that of wild type cells. Wt::*sodC* showed modestly reduced chemotactic indices and significant reduction in the speed compared to those of wild type cells. *gsk3*$^-$::*sodC* also failed to show any statistically meaningful improvement in terms of both chemotactic indices and speed (Figure 2.7). Wt::*sodC* cells displayed 40-50% reduction in random motility speed compared to that of wild type cells while *gsk3*$^-$::*sodC* showed no significant change from *gsk3*$^-$ cells (Figure 2.8). *sodC*$^-$ cells with reintroduced *sodC* under Actin-15 promoter also showed *sodC* messages were higher than the endogenous ones, and displayed significantly improved chemotactic indices (from 0.0 to 0.7), but not the speed (5.2 to 3.5 μm/min) (Veeranki et al., 2008), which is reminiscent of Wt::*sodC* cells. These data together suggest that the level of *sodC* needs to be tightly controlled for optimal speed of chemotaxing cells, and SodC is not likely to function at upstream of GSK3 in the context of cell motility regulation.

10 μM cAMP	Cell type	Chemotactic Index Mean ± SD	Speed (μm/min) Mean ± SD
	sodC/JH10	0.70±0.23	3.91±2.15
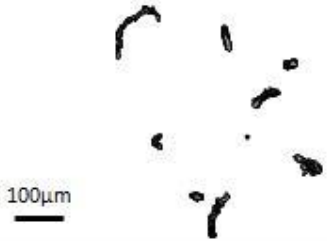	*sodC/ gsk3⁻*	0.18±0.57	2.50±1.94

Fig 2.7 Chemotaxis assays using cells expressing *sodC*. Both JH10 cells and *gsk3⁻* cells expressing *sodC* were challenged with a point source of 10 μM cAMP after pulsing. Superimposed tracing images were grouped. A total time period of 30 min were recorded. Numbers are shown as mean ± standard deviation (SD). Data are representative of at least three independent experiments. Scale bars represent 100 μm.

10 μM cAMP	Cell type	Chemotactic Index Mean ± SD	Speed (μm/min) Mean ± SD
	sodC/JH10	0.70±0.23	3.91±2.15
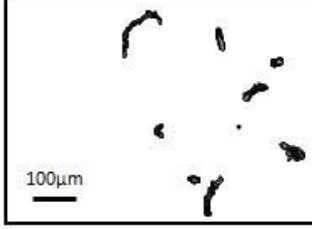	*sodC/ gsk3⁻*	0.18±0.57	2.50±1.94

Fig 2.8 Random movement assay with cells expressing *sodC*. Both assays were recorded for 30 min. Superimposed tracing images were grouped. Numbers are shown as mean ± standard deviation (SD). Data are representative of at least three independent experiments. Scale bars represent 100 μm.

Summary of all the chemotactic indices and speed obtained from either the chemotaxis assay or the random movement assay described above were shown as bar charts (Figure 2.9 and 2.10). In short, under the same treatment used in wild type cells, *gsk3*$^-$ cells exhibited severe defects in both directional sensing ability (chemotactic index) and moving speed. Under the same experimental condition, *gsk3*$^-$ cells displayed compromised speed and almost no sense of direction under all assay conditions tested. What is more, these defects could not be rescued by increasing the level of *sodC*, which was shown to be under-expressed in *gsk3*$^-$ cells during the developmental aggregation stage. In the following chapters, the molecular basis of GSK3 mediated regulation of chemotaxis and regulation of motility speed will be described.

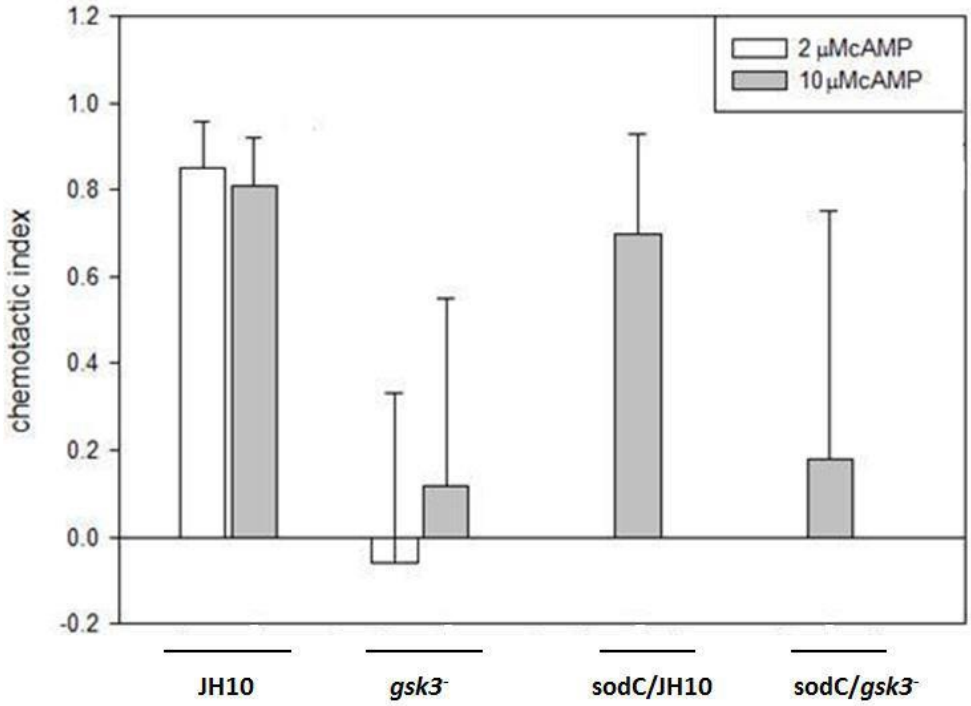

Fig 2.9 Summary of the chemotactic indices in chemotaxis assays. White bars represent 2 μM cAMP point sources were used and grey bars represent 10 μM cAMP point sources were used. Averages and standard deviations were calculated out of at least three independent experiments.

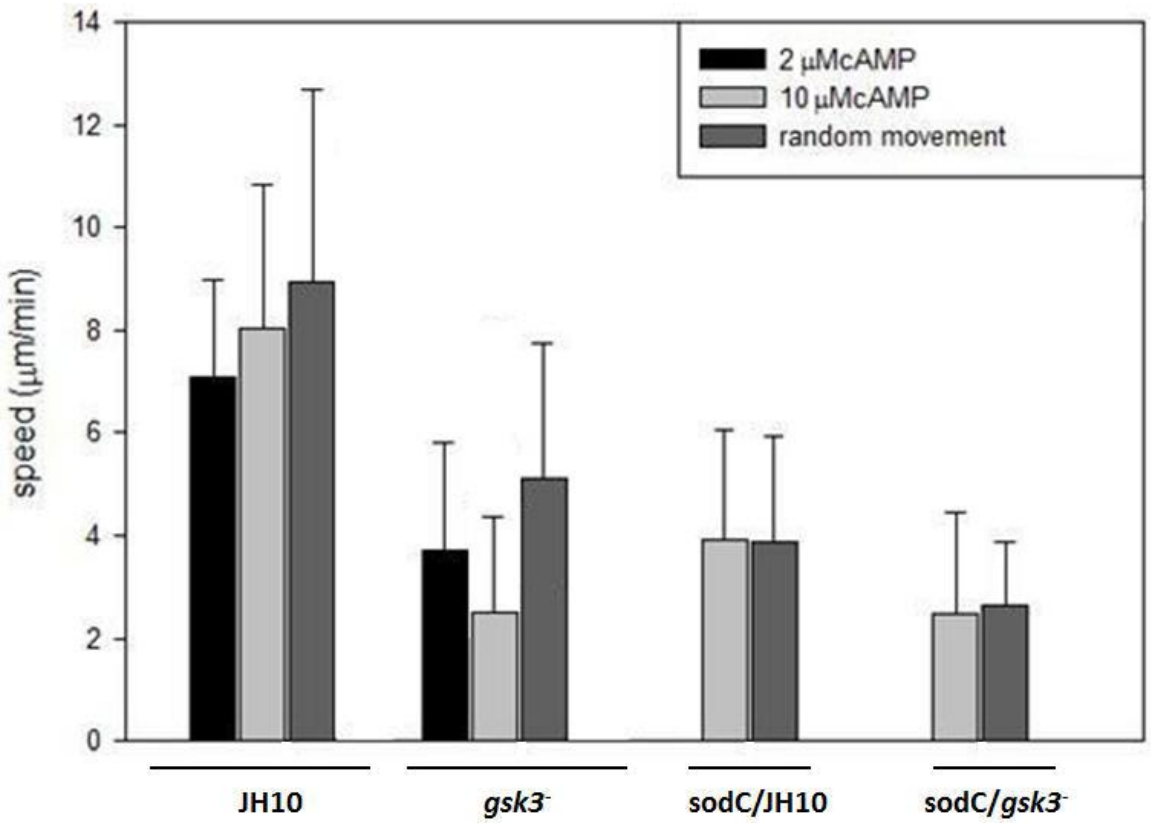

Fig 2.10 Summary of the speed in either chemotaxis assays or random movement assays. Black bars represent 2 μM cAMP point sources were used, light grey bars represent 10 μM cAMP point sources were used and dark grey bars represent random movement assay. Averages and standard deviations were calculated out of at least three independent experiments.

2.3 Discussion

In *Dictyostelium discoideum* system, it has been established that GSK3 plays a crucial role in regulating cell fate choice (Harwood et al., 1995). The GSK3 stimulates prespore cell fate while it inhibits prestalk cell fate (Harwood et al., 1995; Kim et al., 2002). Here, I discovered that *gsk3*$^-$ cells in aggregation competent stage exhibited severe movement abnormality in terms of both direction sensing and speed, which indicating GSK3 is also a key player in regulating cell motility and chemotaxis. The facts that *gsk3*$^-$ cells failed to undergo chemotaxis under both relatively steep and relatively shallow chemoattractant

gradient as well as that the chemotactic deficiency of *gsk3*$^-$ cells persisted in both of the 20 minutes time frames in chemotaxis assays suggest that GSK3 may influence multiple parallel signaling pathways which regulate chemotaxis in *Dictyostelium*. What is more, since GSK3 is found to be able to suppress the transcription levels of some of the key chemotactic regulatory proteins (Strmecki et al., 2007; Teo et al., 2010), I tested one of them, SodC, by over-expressing *sodC* in *gsk3*$^-$ cells. The result that *gsk3*$^-$ cells over-expressing *sodC* showed no improvement in both chemotactic indices and speed together with the finding that wild type cells over-expressing *sodC* displayed compromised speed and slightly reduced chemotactic indices, suggested that either under-expression of *sodC* in *gsk3*$^-$ cells has minor role for the chemotactic defects or the expression level of *sodC* need to be tuned to a level which is comparable to the *sodC* level in wild type cells in order to fully or partially rescue the chemotactic defects in *gsk3*$^-$ cells. It would be interesting in the future to express *sodC* in gsk3- cells to a similar level to wild type cells and see how the cells behave under a cAMP gradient.

It is worth to mention here that Teo and others (2010) was able to rescue the defective chemotaxis in *gsk3*$^-$ cells in both chemotactic indices and speed by over-expressing inositol monophosphatase gene IMPA. The *gsk3*$^-$ cells over-expressing IMPA showed partial rescue in both PIP3 signaling and TORC2 signaling, which may have synergistic effects and partially rescue the chemotactic defects in *gsk3*$^-$ cells.

CHAPTER III

ANALYSIS OF PI3K AND PTEN BEHAVIORS IN *gsk3*$^-$ CELLS

3.1 Materials and methods

3.1.1 GFP-fusion Proteins and Fluorescence Microscopy

The GFP-RBD, PI3K1-LD-GFP, SPM-PI3K1-LD-GFP and SAS-PI3K1-LD-GFP constructs were either described as previously (Sasaki et al., 2004; Veeranki et al., 2008) or have been generated via site-directed mutagenesis. All constructs were introduced into either wild type cells or *gsk3*$^-$ cells via electroporation. Fluorescent images were obtained from Leica DM IRB inverted epifluorescence microscope using 100X oil-immersion lens and recorded using CoolSNAP digital camera with Openlab software (PerKinElmer). Fluorescence intensities were quantified using Image J software (NIH). At least three independent assays were performed for each assay.

3.1.2 cAMP stimulation

After pulsing, cells were spun down and washed once with ice cold DB. Then, the cells were re-suspended in DB and plated in eight-well chambers (Nalge Nunc International, 155409) at a density of $6x10^4$ cells/cm^2. Five minutes were allowed for the cells to settle down at the bottom of the chamber before cells were challenged with a final concentration of 10 μM cAMP. Right before and at different time points after cAMP stimulation, images were recorded as mentioned earlier (3.1.1).

3.1.3 Latrunculin-A treatment

Aggregation competent (cAMP pulsed) cells were spun down and washed once with ice cold DB buffer, re-suspended in DB and plated in eight-well chambers at a density of $6x10^4$ cells/cm^2. Five minutes were allowed for the cells to settle down at the bottom of

the chamber before 0.5 μM Latrunculin-A was added. Images were taken before and at different specific time points after Latrunculin-A treatment.

3.1.4 PI3K inhibition using LY294002

After pulsing (described in chapter II), cells were plated in a 35 x 10 mm tissue culture dish coverslip filled with DB containing 15 μM LY294002 which is a PI3K inhibitor. Cells were treated for 20 min before subjected to chemotaxis assay.

3.2 Results

3.2.1 PIP3 level along the plasma membrane, PI3K1-LD localization and PTEN localization in vegetative cells

GFP-PHcrac was expressed both in wild type cells and *gsk3*$^-$ cells. PHcrac is the Pleckstrin Homology domain of the cytosolic regulator of adenylyl cyclase, which binds to PIP3 along the plasma membrane, and served as an indirect indicator of the PIP3 level on the plasma membrane (Veeranki et al., 2008). In vegetative state, *gsk3*$^-$ cells showed an increased membrane PIP3 level compared to wild type cells (Figure 3.1).

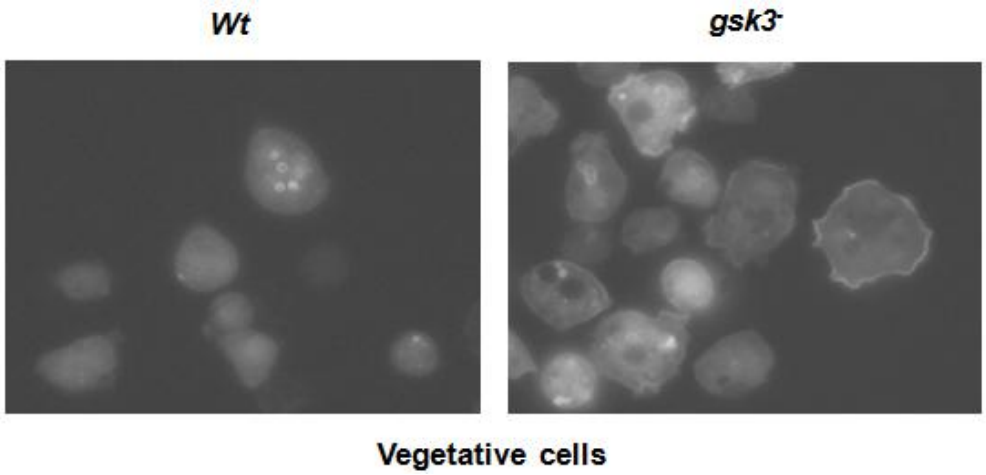

Fig 3.1 GFP-PHcrac localization in vegetative cells. Images were taken from cells at vegetative stage. *gsk3*$^-$ cells showed higher basal membrane localization of GFP-PHcrac

compared to wild-type cells. Data are representative of at least three independent experiments.

I then determined the chemoattractant induced regulation of PI3K and PTEN, which are two main regulators of PIP3 (Figure 3.2). In *Dictyostelium*, PI3K1 and PI3K2 are largely responsible for generating PIP3 from PI(4,5)P2. Cells lacking *pi3k1* and *pi3k2* displayed greatly reduced polarity, aberrant directional sensing, and speed (Funamoto et al., 2002; Funamoto et al., 2001). Upon cAMP stimulation, PI3K1 and PI3K2 translocate to the plasma membrane, which is dependent on the amino terminal membrane localization domain (LD). The membrane localization domain is composed of 1-492 amino acids of PI3K1 (Picture A1 and A2). Although it was reported that under certain laboratory conditions, complete blocking PIP3 signaling by eliminating all class I PI3Ks in *Dictyostelium* does not affect orientation of the cells doing chemotaxis but impairs the moving velocity, it was reported later on that PI3K mediated PIP3 signaling influences the direction sensing ability of the cells especially in shallow cAMP gradient. What is more, the synergistic effect performed by PI3K together with other parallel signaling pathways can further amplify cAMP gradient sensing (Hoeller and Kay, 2007; Kortholt et al., 2011). On the other hand, PTEN, which dephosphorylates PIP3 at 3' position on the inositol ring thus change PIP3 back into PIP2, is located on the plasma membrane mainly through its N-terminal PIP2 binding motif. In response to cAMP stimulation, PTEN transiently dissociates from the plasma membrane, an event independent of intracellular PIP3 level and the actin cytoskeleton (Iijima et al., 2004). The phosphatase activity of PTEN, although not essential for its localization, is critical for chemotaxis. Knocking out *pten* or introducing phosphatase inactive PTEN caused a great reduction in the direction

sensing and moving velocity of the cells (Funamoto et al., 2002; Iijima et al., 2004). Wild type and *gsk3*$^-$ cells expressing either GFP-PI3K1-LD or GFP-PTEN were analyzed using fluorescent microscopy. PI3K1-LD proteins were aberrantly enriched at the plasma membrane of *gsk3*$^-$ cells, whereas no such misregulation was observed for PTEN (Figure 3.2).

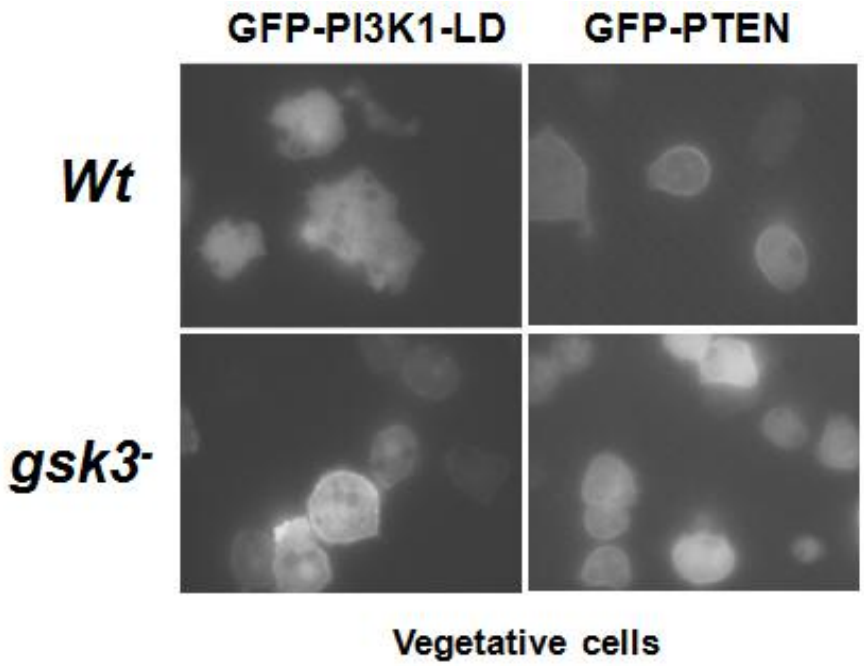

Fig 3.2 GFP-PI3K1-LD and GFP-PTEN in vegetative cells. Images were taken from cells at vegetative stage. *gsk3*$^-$ cells showed higher basal membrane localization of GFP-PI3K1-LD compared to wild-type cells. Membrane levels of GFP-PTEN in both cell types were similar. Data are representative of at least three independent experiments.

3.2.2 Dynamics of PIP3 level along the plasma membrane upon cAMP stimulation

Funamoto and colleagues (2002) showed that there is a transient increase of PIP3 on the plasma membrane in response to cAMP stimulation, using GFP fused PH domain-containing protein PhdA as an indirect PIP3 indicator. Here, I used GFP-PHcrac as used in the previous study to test the dynamics of membrane PIP3 level after cAMP

stimulation in *gsk3*$^-$ cells (Sasaki et al., 2004). Wild type cells expressing GFP-PHcrac served as a control. After pulsed cells were treated with 10 μM cAMP, the PIP3 level along the plasma membrane in wild type cells increased 30% at 10 sec, then the amount of PIP3 gradually went down to basal level after 30 sec. In *gsk3*$^-$ cells, however, there was a higher basal amount of PIP3 on the plasma membrane compared to wild type cells and this level stayed flat without any significant changes during the whole 30 sec period of time (Figure 3.3 and 3.4).

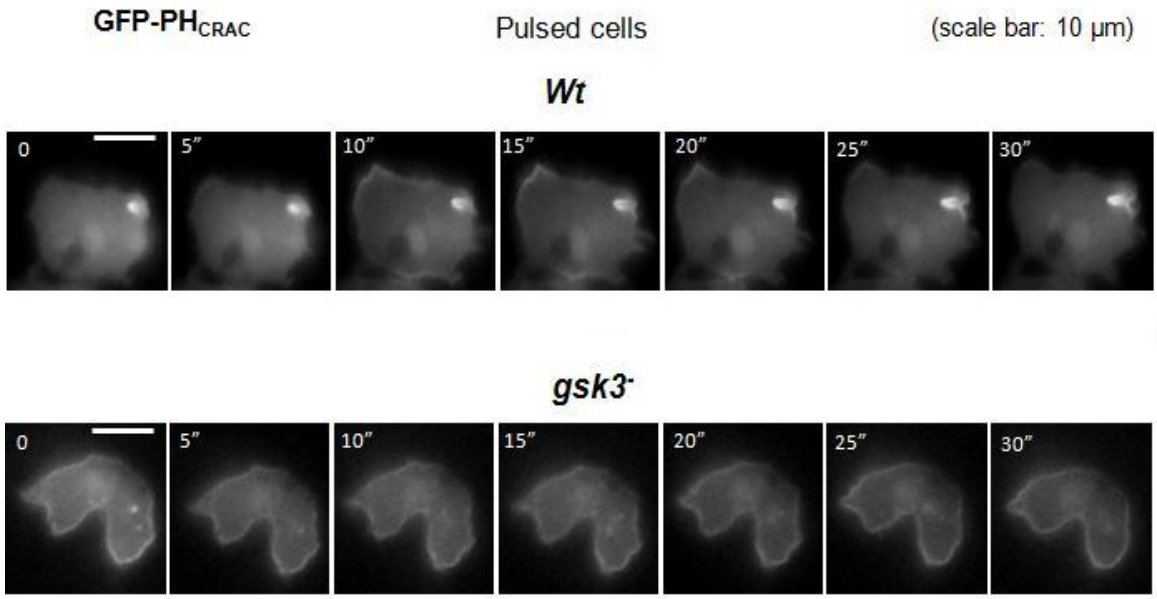

Fig 3.3 GFP-PHcrac translocation after cAMP stimulation in pulsed cells. Images were taken at the indicated time points. Data are representative of at least three independent experiments. Scale bars represent 10 μm. Double apostrophe indicates second.

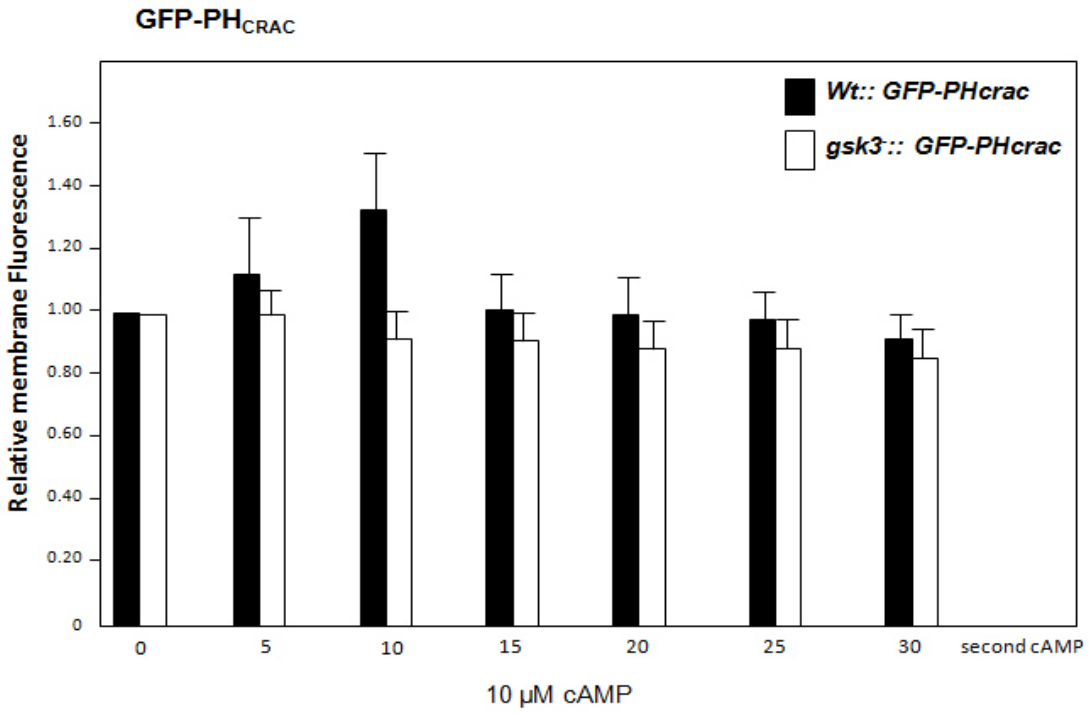

Fig 3.4 Quantification of the membrane fluorescence shown on figure 3.3. Horizontal axis represents the time that passed after cAMP stimulation in seconds. Vertical axis represents the relative membrane fluorescence ratio compared to the fluorescence at time zero. Error bars represent standard deviations. Numbers were obtained from at least three independent experiments. For each cell at different time points, at least three random position along the plasma membrane were picked, fluorescence intensity were obtained using Image J software. Black bars indicate Wt::GFP-PHcrac, white bars indicate *gsk3*$^-$ ::GFP-PHcrac.

3.2.3 PI3K1-LD localization dynamics along the plasma membrane upon cAMP stimulation

Previous study of PI3K localization using GFP fused PI3K1 and CFP fused PI3K2 showed that after challenged with cAMP, there was a transient localization of PI3K to the plasma membrane in wild type cells (Funamoto et al., 2002). I thus globally stimulated both aggregation competent wild type cells and *gsk3*$^-$ cells expressing GFP-PI3K1-LD. Consistent with the previous reports, wild type cells displayed maximal membrane re-localization of PI3K around 10 sec which subsided to the basal level after 30 sec. In

contrast, *gsk3*⁻ cells exhibited constitutive membrane localization of PI3K1-LD in a cAMP insensitive manner (Figure 3.5 and 3.6).

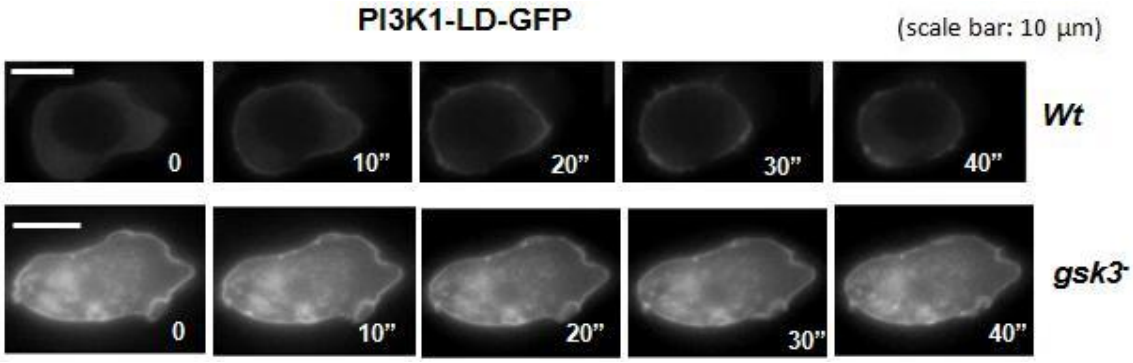

Fig 3.5 GFP-PI3K1-LD translocation after cAMP stimulation in pulsed cells. Images were taken at the indicated time points. Data are representative of at least three independent experiments. Scale bars represent 10 µm. Double apostrophe indicates second.

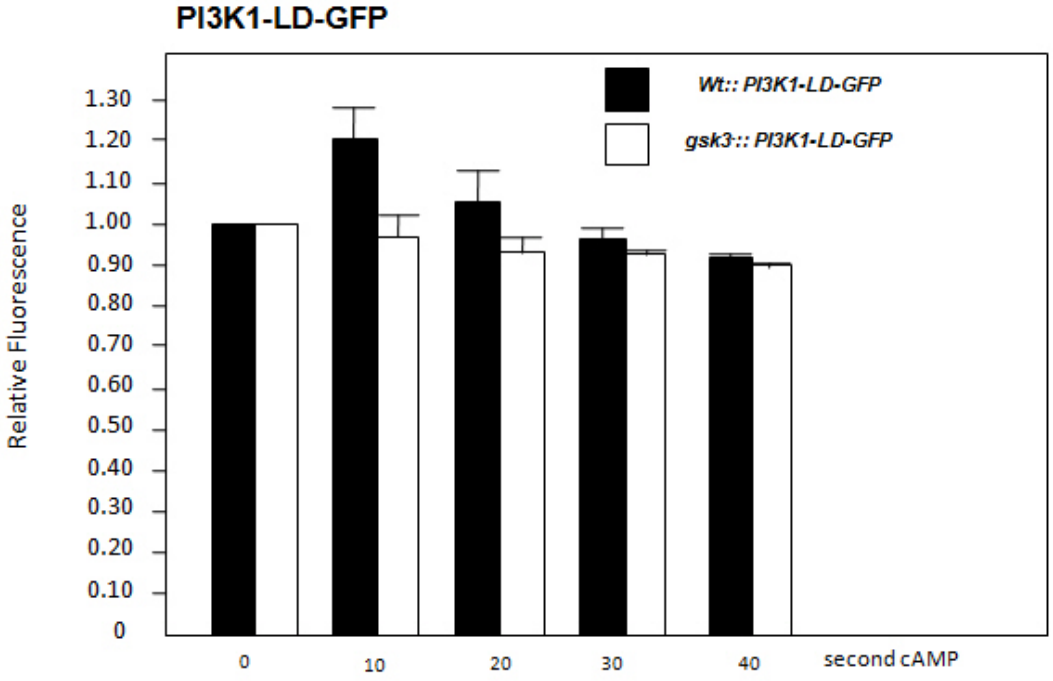

Fig 3.6 Quantification of the membrane fluorescence shown on figure 3.5. Horizontal axis represents the time that passed after cAMP stimulation in seconds. Vertical axis represents the relative membrane fluorescence ratio compared to the fluorescence at time

zero. Error bars represent standard deviations. Numbers were obtained from at least three independent experiments. For each cell at different time points, at least three random position along the plasma membrane were picked, fluorescence intensity were obtained using Image J software. Black bars indicate Wt::PI3K1-LD-GFP, white bars indicate *gsk3*$^-$::PI3K1-LD-GFP.

3.2.4 PTEN localization dynamics along the plasma membrane upon cAMP stimulation

As previously mentioned, the pre-stimulus PTEN subcellular localization in *gsk3*$^-$ cells did not seem to be aberrant. In response to cAMP stimulation, GFP-PTEN translocalized to the cytoplasm in both wild type and *gsk3*$^-$ cells, maximally around 10 sec. Around 30 sec post-stimulation, GFP-PTEN re-localized to the plasma membrane in both wild type and *gsk3*$^-$ cells (Figure 3.7 and 3.8). These findings are consistent with a recent study by Teo and colleagues (2010).

3.2.5 Summary of the PHcrac, PI3K and PTEN membrane localization dynamics

Membrane localization patterns of PI3K and PTEN were mutually exclusive in wild type cells and there was a transient increase of PIP3 level on the plasma membrane upon cAMP stimulation as detected by GFP-PHcrac. I also noticed that the membrane localized PHcrac protein went back down to the basal level slightly faster than PI3K did after cAMP stimulation (Figure 3.9). In contrast, *gsk3*$^-$ cells displayed constitutive high level of PIP3 on the plasma membrane and constitutive PI3K membrane localization whereas PTEN was normally regulated (Figure 3.10), which indicated that either the kinase activity of PI3K could not be stimulated by cAMP signaling cascade or that *gsk3*$^-$ cells were deficient of PI3K substrate PIP2.

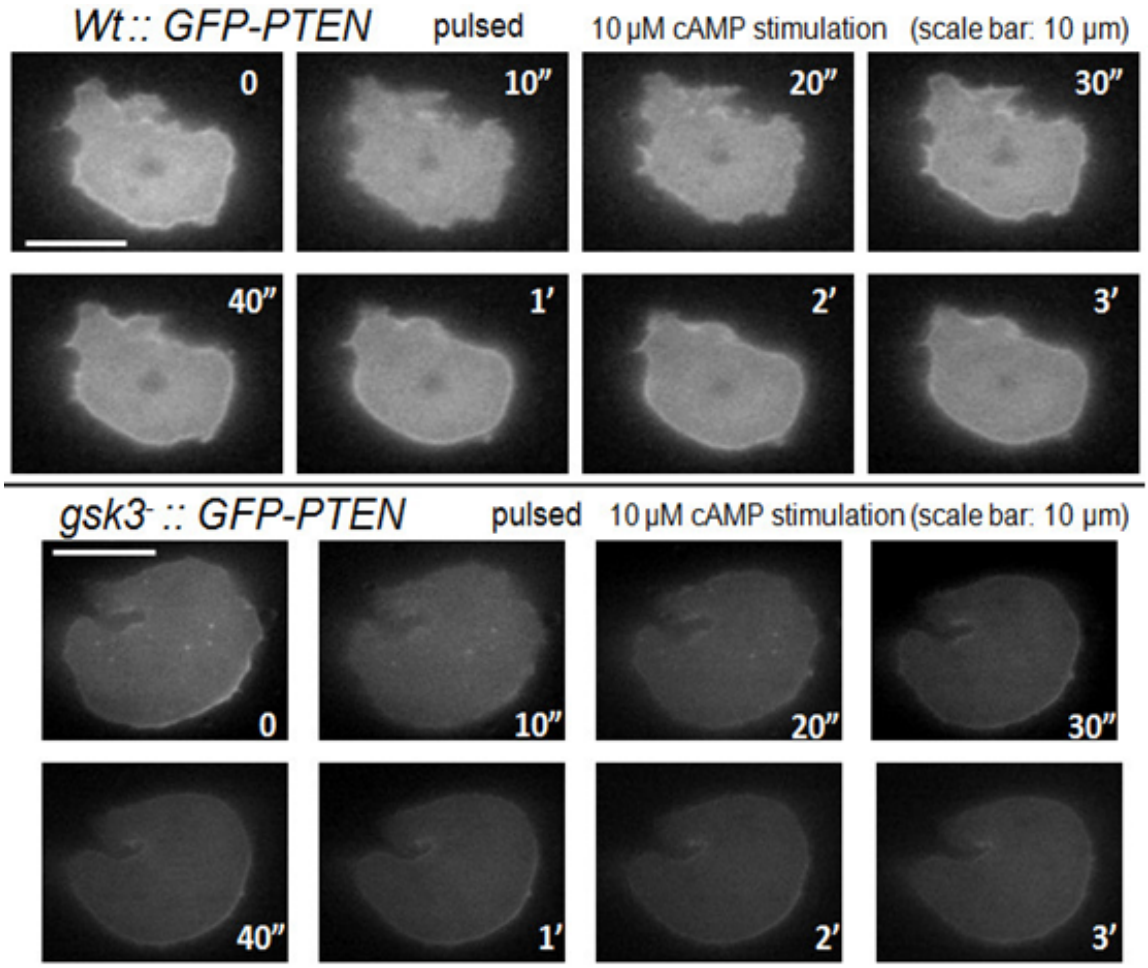

Fig 3.7 GFP-PTEN translocation after cAMP stimulation in pulsed cells. Images were taken at the indicated time points. Data are representative of at least three independent experiments. Scale bars represent 10 μm. Double apostrophe indicates second and single apostrophe indicates minute.

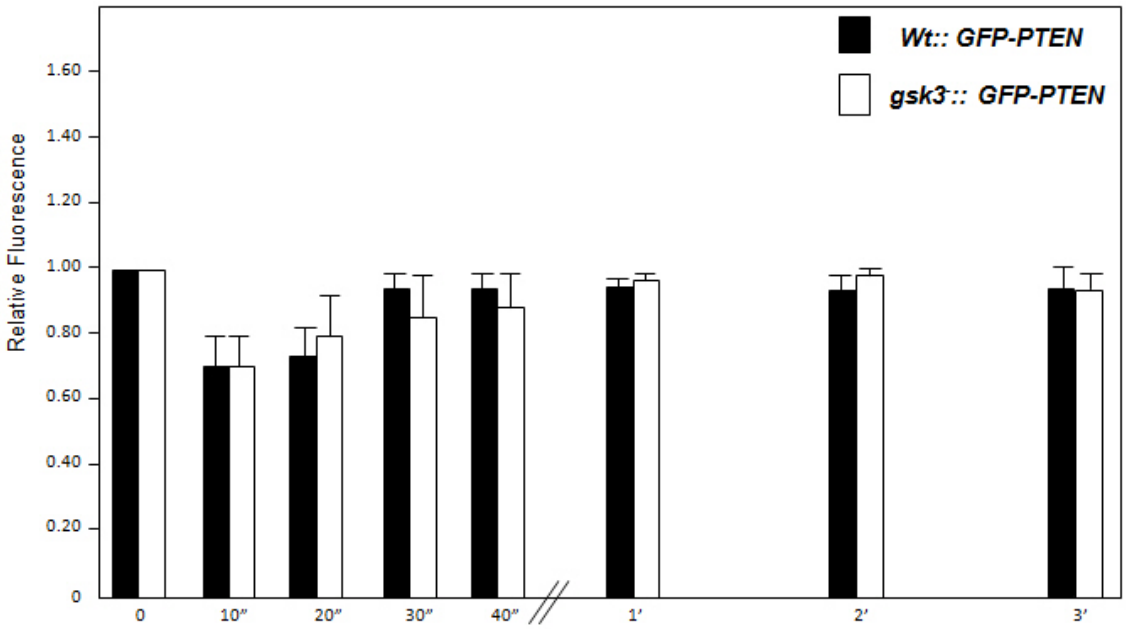

Fig 3.8 Quantification of the membrane fluorescence shown on figure 3.7. Horizontal axis represents the time that passed after cAMP stimulation. Vertical axis represents the relative membrane fluorescence ratio compared to the fluorescence at time zero. Error bars represent standard deviations. Numbers were obtained from at least three independent experiments. For each cell at different time points, at least three random position along the plasma membrane were picked, fluorescence intensity were obtained using Image J software. Black bars indicate Wt::GFP-PTEN, white bars indicate *gsk3*$^-$ ::GFP-PTEN. Double apostrophe indicates second and single apostrophe indicates minute.

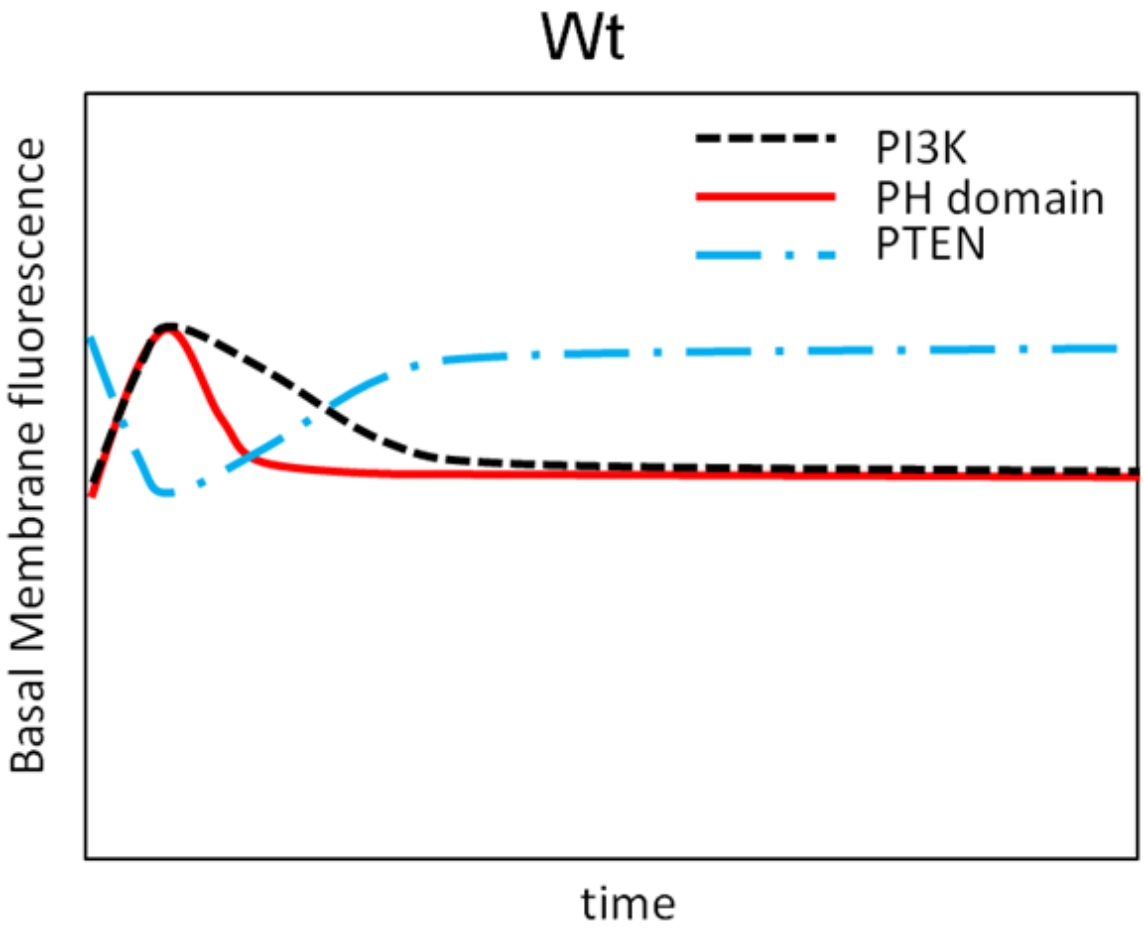

Fig 3.9 PHcrac, PI3K and PTEN localization pattern upon stimulation in wild type cells. X-axis represents time after cAMP stimulation. Y-axis represents the relative membrane fluorescence. Dotted line indicates the localization of PI3K on the plasma membrane, solid line indicates the localization of PHcrac on the plasma membrane, and dot-dash-dot line represents localization of PTEN on the plasma membrane

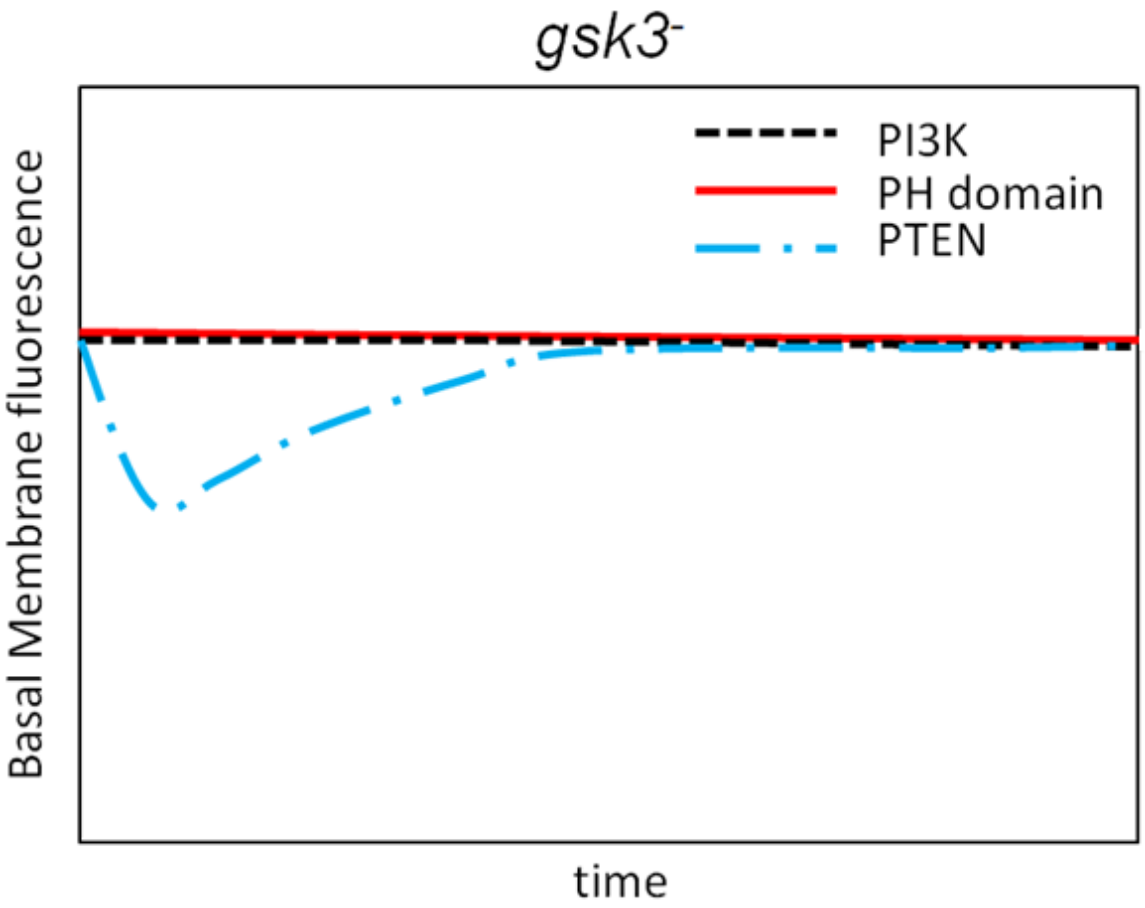

Fig 3.10 PHcrac, PI3K and PTEN localization pattern upon stimulation in *gsk3*$^-$ cells. X-axis represents time after cAMP stimulation. Y-axis represents the relative membrane fluorescence. Dotted line indicates the localization of PI3K on the plasma membrane, solid line indicates the localization of PHcrac on the plasma membrane, and dot-dash-dot line represents localization of PTEN on the plasma membrane

3.2.6 Latrunculin-A treatment

Sasaki and colleagues (2004) proposed previously that stochastic Ras activation depends on the PI3K activity and F-Actin synthesis, the three of which form a positive feedback loop in cells moving at random directions (Figure 3.11). To determine whether GSK3 interacts with the F-Actin mediated feedback loop, wild type and *gsk3*$^-$ cells were treated with Latrunculin-A (Figure 3.12 through and 3.15). Five minutes after 0.5 μM Latrunculin-A treatment, cells lost their pseudopods and became circular indicating

significantly reduced level of F-Actin synthesis in the presence of Latrunculin-A. In contrast, GFP-PHcrac signals on the plasma membrane of *gsk3*$^{-}$ cells persisted during the course of Latrunculin-A treatment indicating that the high basal level of PIP3 in *gsk3*$^{-}$ cells is not induced through the F-Actin feedback loop.

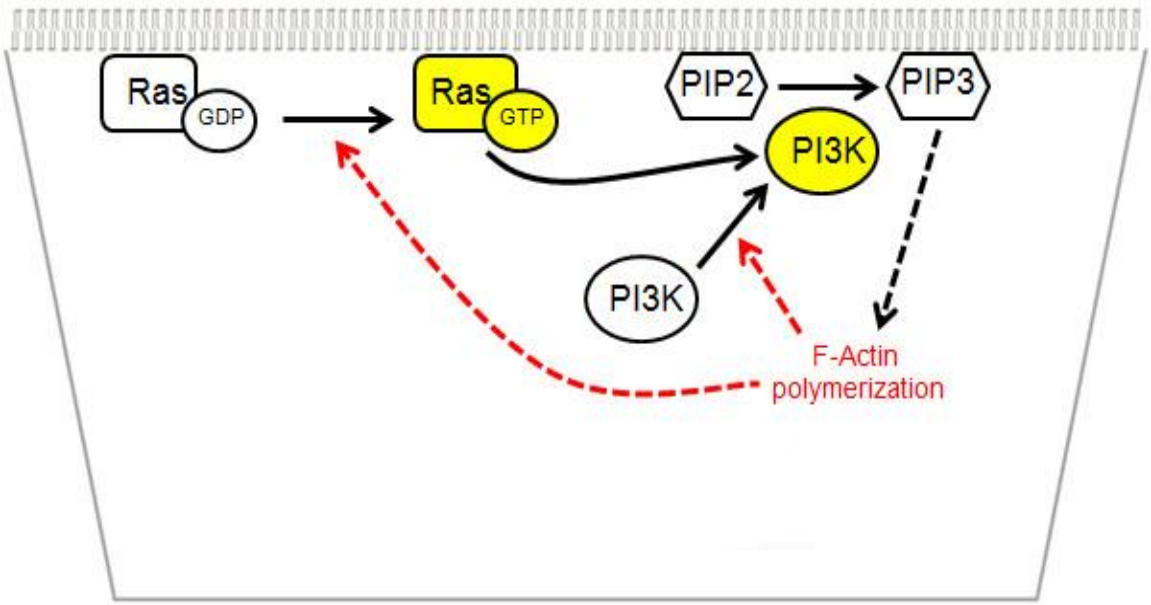

Fig 3.11 F-Actin polymerization induced positive feedback loop. Localized F-Actin polymerization can stimulate PIP3 signaling through a positive feedback loop by recruiting more PI3K to the plasma membrane.

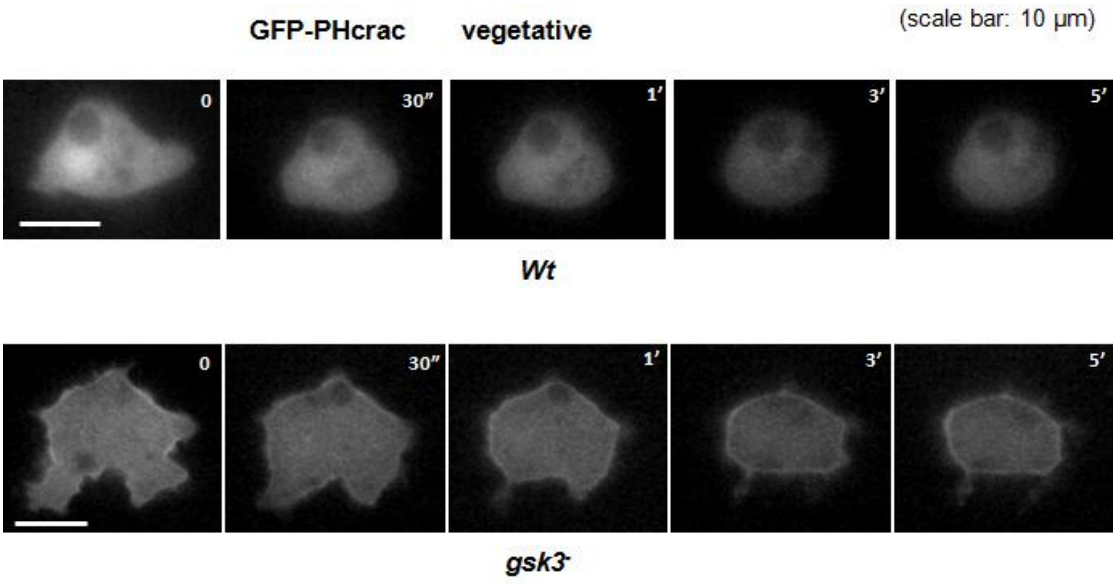

Fig 3.12 GFP-PHcrac localization dynamics in Latrunculin-A treated vegetative cells. Cells at vegetative stage were treated with 0.5 µM Latrunculin-A. Images were taken at the indicated time points. Data are representative of at least three independent experiments. Scale bars represent 10 µm. Double apostrophe indicates second and single apostrophe indicates minute.

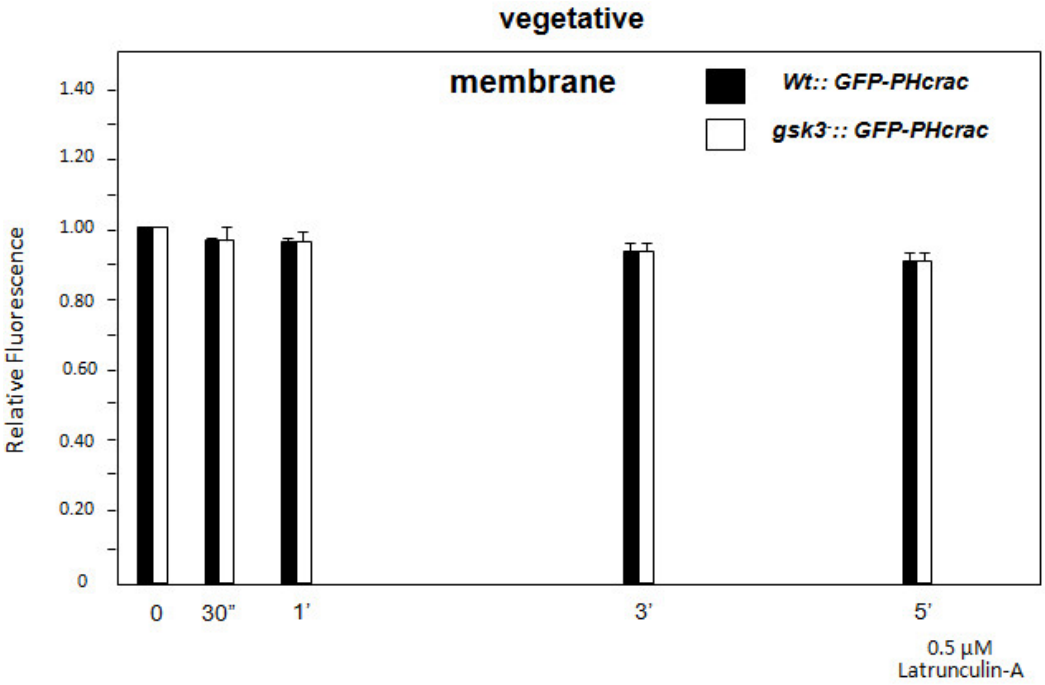

Fig 3.13 Quantification of the membrane fluorescence shown on figure 3.12. Horizontal axis represents the time that passed after 0.5 µM Latrunculin-A was added. Vertical axis represents the relative membrane fluorescence ratio compared to the fluorescence at time

zero. Error bars represent standard deviations. Numbers were obtained from at least three independent experiments. For each cell at different time points, at least three random position along the plasma membrane were picked, fluorescence intensity were obtained using Image J software. Black bars indicate Wt::GFP-PHcrac, white bars indicate *gsk3*$^{-}$ ::GFP-PHcrac. Double apostrophe indicates second and single apostrophe indicates minute.

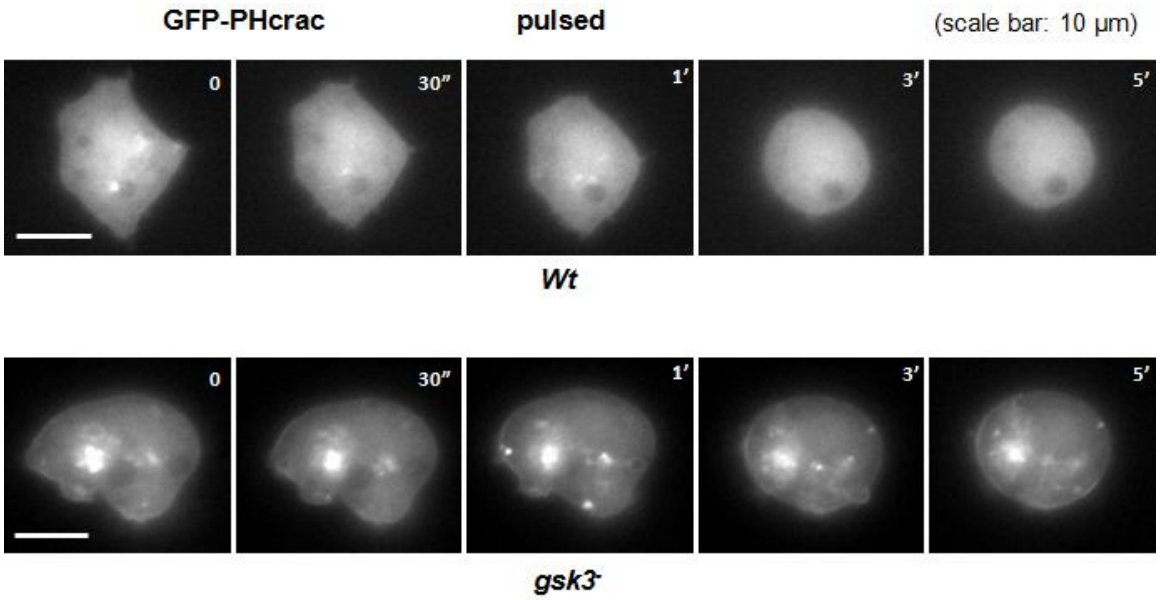

Fig 3.14 GFP-PHcrac localization dynamics in Latrunculin-A treated pulsed cells. Aggregation competent cells were treated with 0.5 μM Latrunculin-A. Images were taken at the indicated time points. Data are representative of at least three independent experiments. Scale bars represent 10 μm. Double apostrophe indicates second and single apostrophe indicates minute.

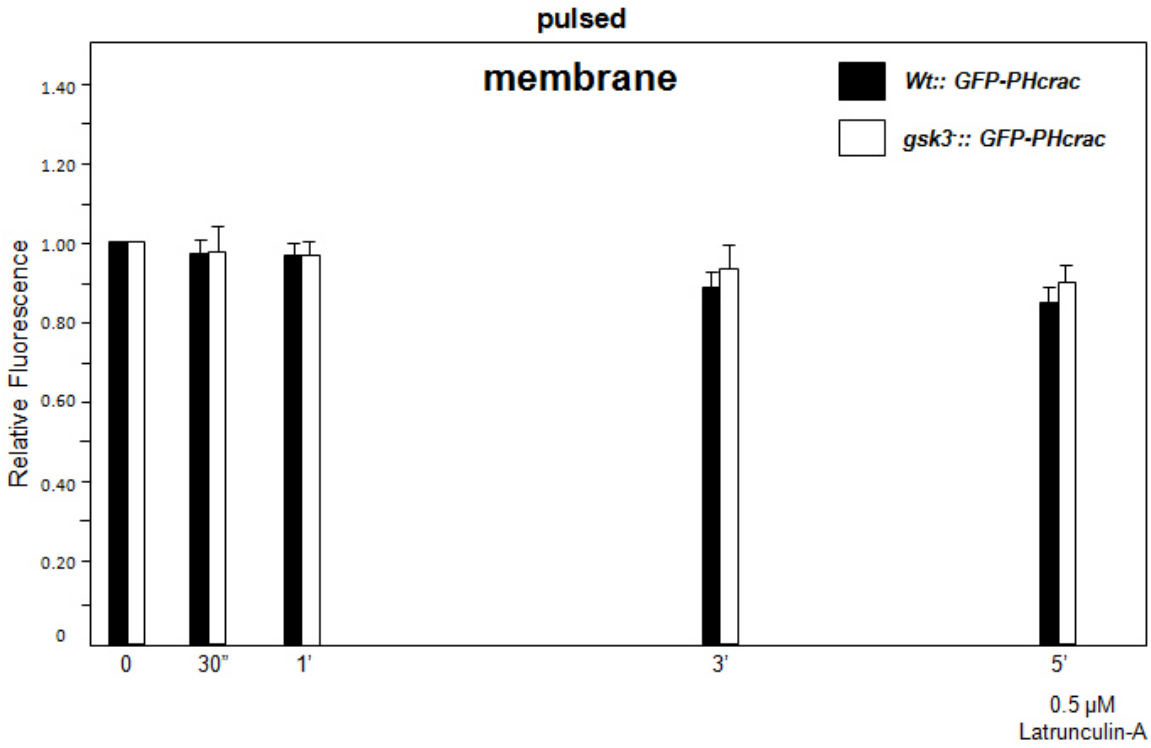

Fig 3.15 Quantification of the membrane fluorescence shown on figure 3.14. Horizontal axis represents the time that passed after 0.5 µM Latrunculin-A was added. Vertical axis represents the relative membrane fluorescence ratio compared to the fluorescence at time zero. Error bars represent standard deviations. Numbers were obtained from at least three independent experiments. For each cell at different time points, at least three random position along the plasma membrane were picked, fluorescence intensity were obtained using Image J software. Black bars indicate Wt::GFP-PHcrac, white bars indicate *gsk3*$^-$ ::GFP-PHcrac. Double apostrophe indicates second and single apostrophe indicates minute.

3.2.7 SPM-PI3K1-LD and SAS-PI3K1-LD localization dynamics along the plasma membrane upon cAMP stimulation

In the light of the fluorescent microscopic data described above, I hypothesized that in *Dictyostelium*, GSK3 affects PIP3 signaling pathway by negative control of the plasma membrane localization of PI3K (Figure 3.16).

I recognized that PI3K1 contains three potential GSK3 phosphorylation sites in the localization domain (Figure 3.17 and A2). In order to determine whether the

phosphorylation on these sites affects the subcellular localization of PI3K, I generated serial substitution mutants of PI3K1 (Table 3.1). The sextuple phosphor-mimetic PI3K1-LD (SPM-PI3K1-LD) mimics constitutively phosphorylated PI3K1-LD, whereas the sextuple alanine substitution mutant (SAS-PI3K1-LD) represents non-phosphorylatable PI3K1-LD (Table 3.1). I then introduced GFP fused SPM-PI3K1-LD into both wild type cells and *gsk3*$^{-}$ cells and GFP fused SAS-PI3K1-LD into wild type cells. These cells at pulsed stage were stimulated with cAMP and GFP images were recorded at time points described in Figure 3.18.

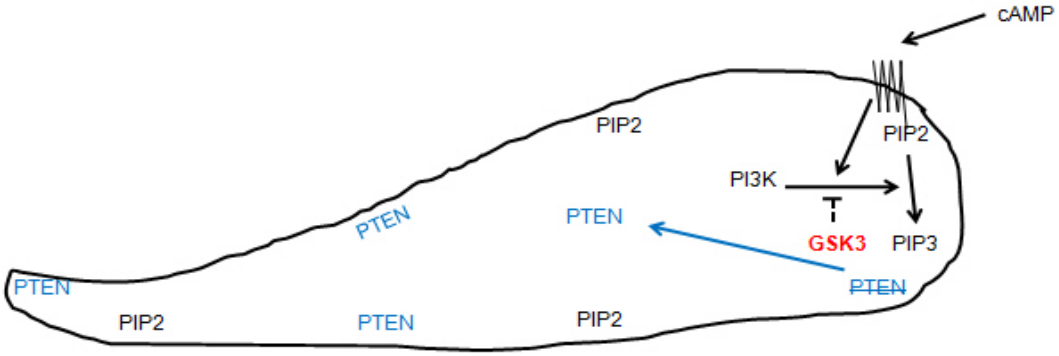

Fig 3.16 Model of PIP3 signaling pathway under the regulation of GSK3. A single aggregation competent cell was challenged with cAMP gradient with cAMP point source coming from the right side. The leading edge of the cells is on the right and its rear region is on the left. See the test for the details.

```
1   MNSIESS7SNDS11NEINKNSNKNNTHLNSNYNNIYKNNSTSSNNNNNHNNIEIIGIDNNKNNNKNNNDNNNN
71  NNNIDKKRKDSKNKQNQEINQEMSENKKIYNSNDSNCSS109GSSS113GGHVNNGHHILIEENERLEHENQEIQE
141 IYKQKGMEFQKKDLRFGYDVNSNNNNNNGGGSSSGSS177SGGS181DESASNQPIIRTRNREGSILNLKKQGLVK
211 EISQRFQTPDTASYTRPNANNISIKDKISILKKEQERRKQDSEVQQREKVIVLSADSSNIQIYHPSVLIE
281 KMNSKLDTEEKPATTTTTTTTTSTSISTSTPTTTTTTTTNTSTTNDITIKPKTSPTKNNEERSQSPITTP
351 KQPVEEIVKKVSTPKSNNTSKKTSSDTTPTGKTTKKDKKDKKDKSRDSGNLVIVNNTNNTSSNNNNNNNN
421 NNNNETIIKRRGRVLVTPSSDLKKNIQIYFTIPINPPVNKTNKPNQLLSNTSQQFLKTLISNEIPIDCKI
491 ND
```

Fig 3.17 Three potential GSK3 phosphorylation sites on PI3K1-LD. The localization domain of PI3K1 (amino acids 1-492) was shown. Three potential GSK3 phosphorylation sites were boxed. Among the numbered Serine residues, Ser11, Ser113 and Ser181 are predictive phosphorylation sites of priming kinase. Ser7, Ser109 and Ser177 are predictive phosphorylation sites of GSK3.

PI3K1-LD-GFP	SPM-PI3K1-LD-GFP Sextuple Phospho-Mimetic Mutant	SAS-PI3K1-LD-GFP Sextuple Alanine Substitution Mutant
SIESS^{7}SNDS^{11} SNCSS^{109}GSSS^{113} SSGSS^{177}SGGS^{181}	SIESD^{7}SNDD^{11} SNCSD^{109}GSSD^{113} SSGSD^{177}SGGD^{181}	SIESA^{7}SNDA^{11} SNCSA^{109}GSSA^{113} SSGSA^{177}SGGA^{181}

Table 3.1 GFP fused sextuple phosphor-mimetic mutant and sextuple alanine substitution mutants of PI3K1-LD.

The phosphomimetic mutant SPM-PI3K1-LD suppressed the aberrant basal plasma membrane localization of PI3K1-LD in *gsk3*$^{-}$ cells. Similar to the membrane localization dynamic pattern of Wt::PI3K1-LD, SPM-PI3K1-LD translocalized to the plasma membrane upon cAMP stimulation in both wild type cells and *gsk3*$^{-}$ cells which reached the peak level at 15 sec. On the other hand, the sextuple serine to alanine substitution mutant SAS-PI3K1-LD exhibited high basal plasma membrane localization and this membrane SAS-PI3K1-LD level persisted in response to cAMP stimulation in wild type cells, which is reminiscent of the situation of PI3K in *gsk3*$^{-}$ cells (Figure 3.18 and 3.19).

The time-lapse fluorescent microscope assays using PI3K1-LD mutant suggested that phosphorylation is important for the membrane recruitment of PI3K.

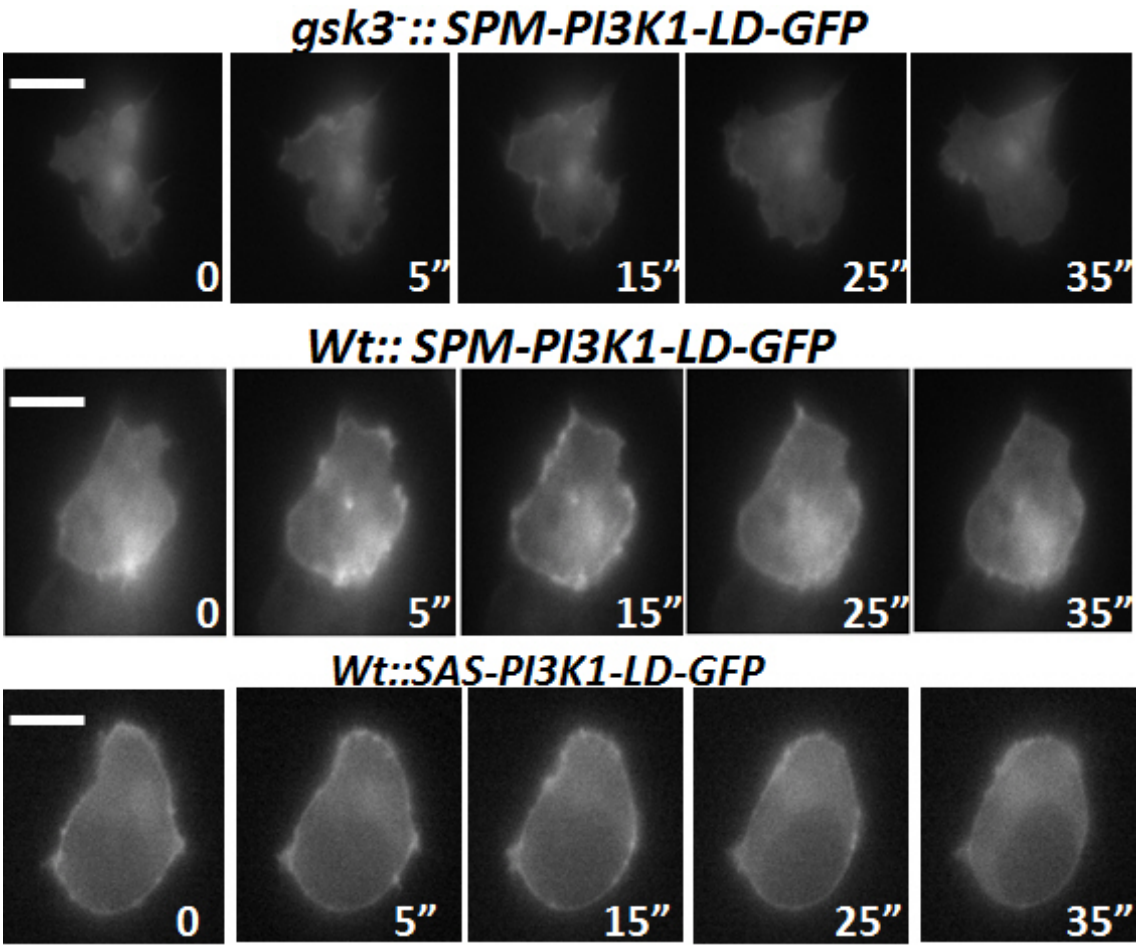

Fig 3.18 Mutant PI3K1-LD-GFP translocation after cAMP stimulation in pulsed cells. Images were taken at the indicated time points. Data are representative of at least three independent experiments. Scale bars represent 10 μm. Double apostrophe indicates second.

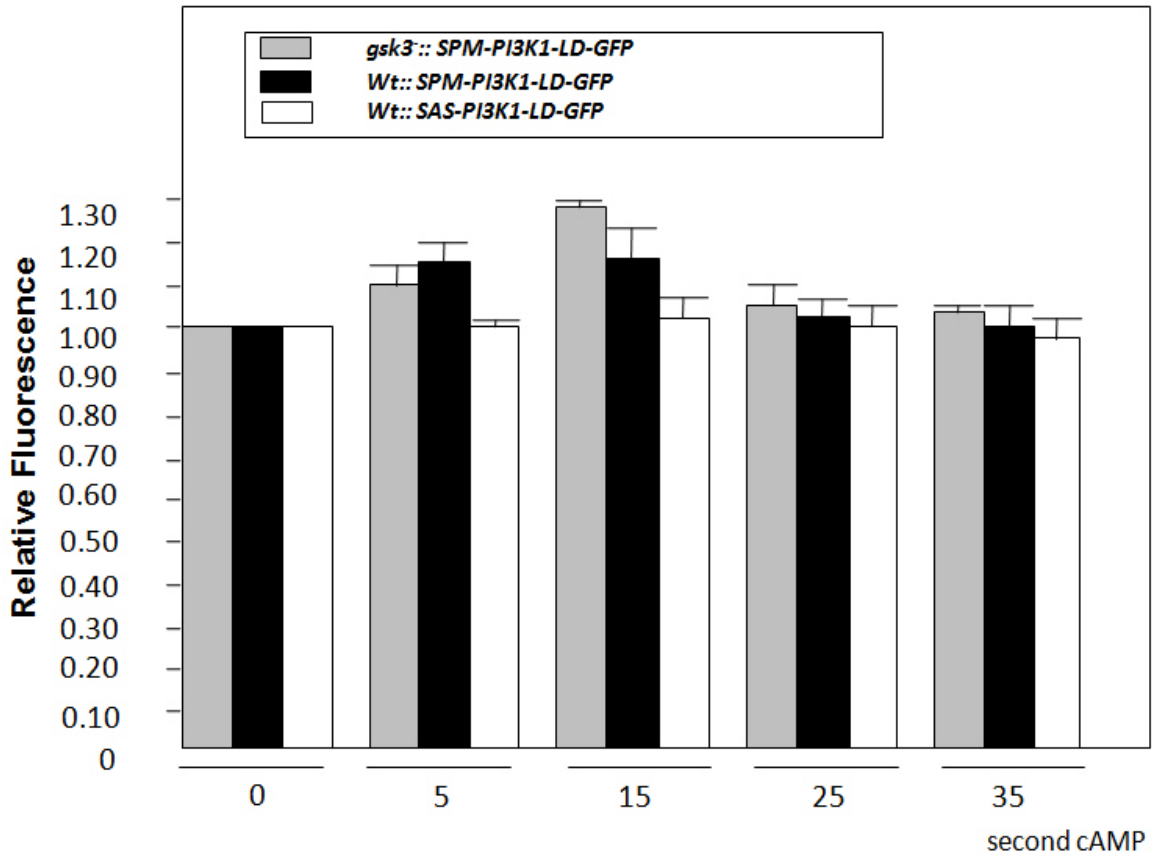

Fig 3.19 Quantification of the membrane fluorescence shown on figure 3.18. Horizontal axis represents the time that passed after cAMP stimulation. Vertical axis represents the relative membrane fluorescence ratio compared to the fluorescence at time zero. Error bars represent standard deviations. Numbers were obtained from at least three independent experiments. For each cell at different time points, at least three random position along the plasma membrane were picked, fluorescence intensity were obtained using Image J software. Gray bars indicate *gsk3*⁻::SPM-PI3K1-LD-GFP, black bars indicate Wt::SPM-PI3K1-LD-GFP and white bars indicate Wt::SAS-PI3K1-LD-GFP.

3.2.8 LY294002 treated *gsk3*⁻ cells still showed aberrant chemotaxis

If the chemotaxis defects of *gsk3*⁻ cells were mainly caused by the elevated localization level of PI3K along the plasma membrane, inhibition of PI3K would at least partially rescue this defect. Previous study in my laboratory demonstrated that inhibition of PI3K in cells exhibiting high basal PIP3 level (*sodC*⁻ cells) significantly improved chemotaxis. In contrast to *sodC*⁻ cells which served as a positive control (Figure 3.21),

inhibition of PI3K in *gsk3*$^-$ cells displayed no such attenuation even with extended time periods tested (Figure 3.20 and Table 3.2).

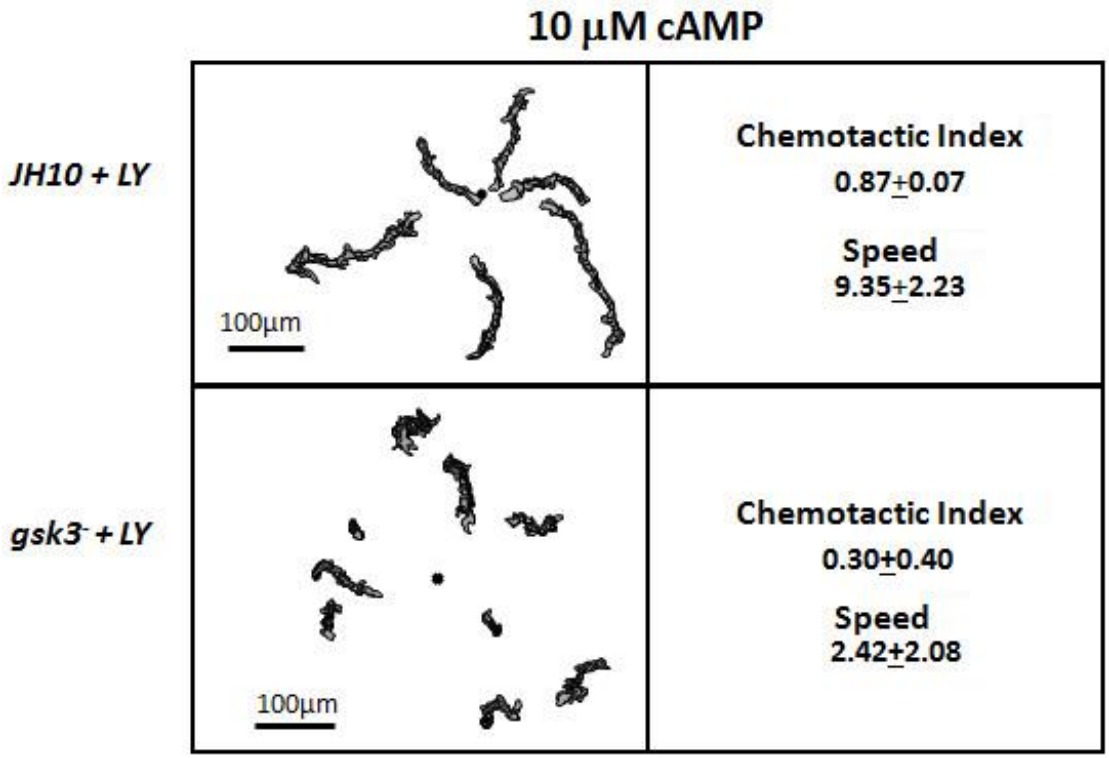

Fig 3.20 Chemotaxis assays after LY294002 treatment. Both JH10 cells and *gsk3*$^-$ cells were treated with 15 µM LY294002 after pulsing and then challenged with a point source of 10 µM cAMP. Superimposed tracing images were grouped. For JH10 cells, a total time period of 20 min were recorded and 40 min were recorded for *gsk3*$^-$ cells. Numbers are shown as mean ± standard deviation (SD). Data are representative of at least three independent experiments. Scale bars represent 100 µm.

gsk3⁻ + LY

Time period	CI	speed
0-40′	0.30±0.40	2.42±2.08
0-20′	0.26±0.43	2.07±1.98
20-40′	0.33±0.48	2.77±2.37

Table 3.2 Summary of chemotactic indices and speed of *gsk3*$^-$ cells treated with 15 µM LY294002 for 15 min in different time frames. Single apostrophe indicates minute.

10 µM cAMP	Cell type	Chemotactic Index Mean±SD	Speed (µm/min) Mean±SD
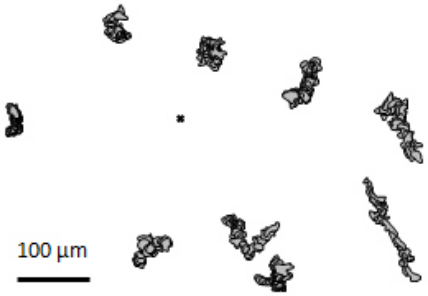	*sodC*⁻	0.19±0.45	4.08±2.54
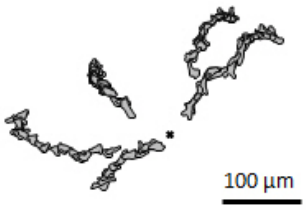	*sodC*⁻ + LY294002	0.73±0.15	8.50±2.27

Fig 3.21 Control chemotaxis assays. *sodC*⁻ cells were challenged with a point source of 10 µM cAMP with or without 15 µM LY294002 treatment for 20 min. Superimposed tracing images were grouped. A total time period of 20 min was recorded Numbers are shown as mean ± standard deviation (SD). Data are representative of at least three independent experiments. Scale bars represent 100 µm.

3.3 Discussion

In response to cAMP stimulation, *gsk3*⁻ cells exhibited wild type like PTEN localization dynamics while there were no detectable changes in PIP3 and PI3K level along the plasma membrane. Iijima and others (2002) reproted before that PTEN localization along the plasma membrane is dependent on PIP2 but not PIP3 level on the plasma membrane, which suggested that in *gsk3*⁻ cells there should be a transient switch of PIP2 into PIP3. The reason that the PIP3 pattern here in *gsk3*⁻ cells showed flat upon cAMP stimulation could be because of the relatively high basal level of PIP3 on the plasma membrane in *gsk3*⁻ cells is much more than the dynamic pool of PIP3, thus

masked the PIP3 level change upon cAMP stimulation. Teo and others (2010) reported that *gsk3*$^-$ cells shows normal PIP2 level on the plasma membrane compared to wild type cells, and the reason I did not detect any significant PIP3 level change in *gsk3*$^-$ cells upon cAMP stimulation could also be that GSK3 is able to stimulate the phosphatase activities of certain inositol 5-phosphatases so that the transiently produced PIP3 is quickly switched back to PIP2. The use of Latrunculin-A ruled out the possibility that GSK3 contributes to the high basal membrane level of PIP3 and high basal membrane localization of PI3K through pre-stimulation of F-Actin positive feedback loop. On the other hand, fluorescence assays using PI3K mutants supported the idea that phosphorylation of the potential GSK3 recognition sites on PI3K1-LD is important for the localization of PI3K between plasma membrane and cytosol and given that SAS-PI3K1LD mutant stayed persistently on the plasma membrane, the phosphorylations on those potential GSK3 recognition sites by both GSK3 and other priming kinase(s) are important prerequisites for the PI3K1 subcellular localization. Upon been phosphorylated by GSK3 and other priming kinase(s), PI3K1 membrane trans-localization in response to cAMP stimulation is independent of any de-phosphorylation events. Finally, chemotaxis assays followed by LY294002 treatment indicated that GSK3 affects chemotaxis through multiple ways. Not only through the PIP3 signaling pathway, by also likely through other pathways and factors such as TORC2 pathway and SodC (Teo et al., 2010; Veeranki et al., 2008).

CHAPTER IV

RAS ACTIVATION DYNAMICS

4.1 Materials and methods

4.1.1 Expression of GST-RBD protein in *E. coli* using IPTG-inducible stimulation

GST-Raf1-RBD and GST-Byr2-RBD in PGEX constructs were described previously (Kae et al., 2004; Sasaki et al., 2004). For the Isopropyl β-D-1-thiogalactopyranoside (IPTG) induction, *E. coli* containing either GST-Raf1-RBD or GST-Byr2-RBD in PGEX-4T vector were inoculated into 50 ml of Luria broth (LB) containing 50 μg/ml ampicillin and incubated overnight at 37°C until the cells reached log phase. The OD value at 600 nm ($OD_{600\ nm}$) was measured and then the cells were diluted with LB containing 50 μg/ml ampicillin to reach a final $OD_{600\ nm}$ value of 0.1. The cells were further incubated at 37°C to reach an $OD_{600\ nm}$ value of 0.4-0.6 before IPTG was added to a final concentration of 0.1 mM. After another incubation of 3-4 hr at 37°C, cells were lysed with complete *E. coli* lysis buffer [20 mM TrisCl (pH7.7), 5% glycerol, 1% Triton X-100, 150 mM NaCl, 2 mM EDTA, 0.1% β-mercaptoethanol and 1 x Roche Protease Inhibitor mix] and further sonicated on ice until the cell suspension became clear.

4.1.2 GST-RBD protein quantification using Coomassie Brilliant Blue staining

Different volume of *E. coli* lysate obtained from 4.1.1, together with the known amount of BSA, were loaded on a 10% SDS-polyacrylamide gel. After running, the gel was stained with Coomassie Brilliant Blue R-250 followed by de-staining and gel-drying. The amount of IPTG induced GST-RBD were estimated by comparing with the band intensity of BSA control.

4.1.3 Ras binding assay

Aggregation competent cells were lysed with cell lysis buffer [20 mM TrisCl (pH7.7), 5% glycerol, 1% Triton X-100, 150 mM NaCl, 1 mM EDTA, 1 mM Na_3VO_4, 40 μM sodium molybdate, 0.1% beta-mercaptoethanol, and 1 x protease inhibitor cocktail (Roche)]. *E. coli* lysate including about 10 μg of GST-RBD (Ras Binding Domain) was mixed with 50 μl of 50% slurry of glutathione (GTT) Sepharose beads (GE Healthcare) and incubated 1.5 hr at 4^oC with agitation. The beads were then spun down and washed three times with cell lysis buffer containing 10 mM $MgCl_2$. The whole cell lysates were mixed with the beads and further incubated for 1.5 hr at 4^oC. The glutathione Sepharose beads bound with GST-RBD and active Ras were washed three times with cell lysis buffer containing 10 mM $MgCl_2$. The active Ras proteins bound with GST-RBD were visualized by western blotting using anti-Pan-Ras antibody (Calbiochem, Ab-3).

4.2 Results

4.2.1 GSK3 affected PI3K membrane localization independently from the Ras/PI3K/F-Actin feedback module.

Randomly moving cells exhibit spontaneous activation of Ras proteins which spatiotemporally coincide with PI3K activation and F-Actin synthesis (Sasaki et al., 2007). Detailed biochemical and imaging analysis demonstrated that this stochastic activation of Ras depends on the functional PI3K and F-Actin synthesis, and thus it was proposed that the three components form a self-organizing feedback loop (Sasaki et al., 2007). To determine whether the PI3K mis-localization was caused by aberrant high Ras activity in *gsk3*$^-$ cells, I measured Ras activities in wild type and *gsk3*$^-$ cells.

Ras binding domains (RBD) from either Raf1 or Byr2 were tagged with GST and induced in the *E.coli* system. According to the quantification by using Coomassie Brilliant Blue staining that around 10 µg of GST-RBD were used for each binding (Figure 4.1).

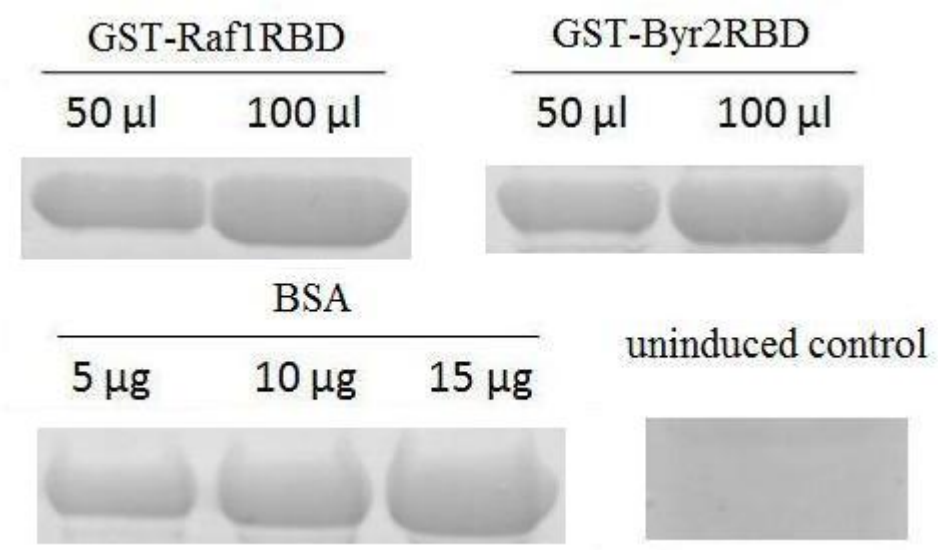

Fig 4.1 Quantification of *E.coli* expressed GST-Raf1-RBD and GST-Byr2-RBD using Coomassie Brilliant Blue staining. Compared with the bands using specific amount of BSA, approximately 10 µg of either GST-Raf1-RBD or GST-Byr2-RBD were used for each binding.

GFP-RBD assays using either GST-Raf1-RBD or GST-Byr2-RBD showed that there were no obvious difference of basal active Ras level in between wild type cells and *gsk3*$^{-}$ cells indicating that GSK3 affects PI3K membrane localization independently from the Ras/PI3K/F-Actin feedback module (Figure 4.2).

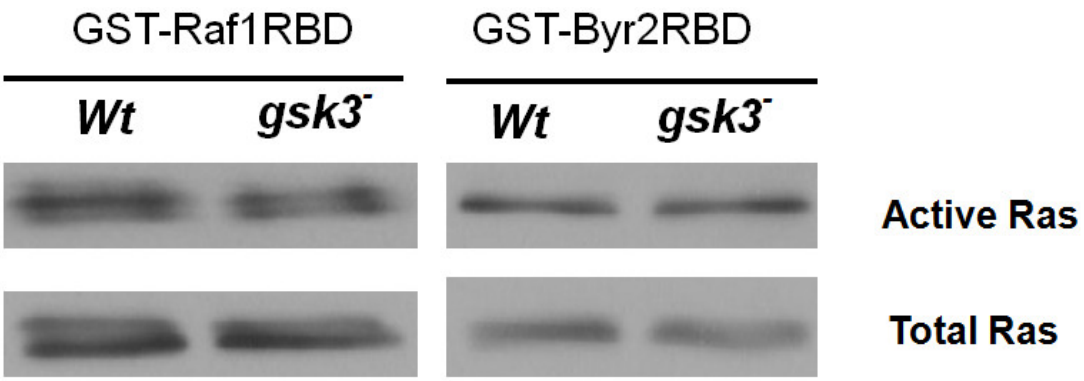

Fig 4.2 Basal Ras activity in both wild type cells and *gsk3*$^-$ cells after pulsing. Amount of total Ras proteins were first normalized by total amount of Ras. Amount of active Ras proteins was detected by GST-RBD assays.

4.2.2 GSK3 regulated the Ras activation pattern after cAMP stimulation.

As previously described, *gsk3*$^-$ cells generated no further PIP3 in response to cAMP stimulation (Figure 3.3 and 3.4). It was shown that RasG is an upstream regulator of PI3K activation (Sasaki and Firtel, 2006). Furthermore, a specific PI3K mutant (K736E), which is unable to bind to active Ras, displays normal cAMP mediated membrane translocation but fail to activate its downstream effector Akt (Funamoto et al., 2002). I thus hypothesized that *gsk3*$^-$ cells may have compromised cAMP induced Ras activation.

cAMP induced regulation of Ras in wild type and *gsk3*$^-$ cells were determined using GST-RBD pull down assay (Kae et al., 2004; Sasaki et al., 2004). Briefly, the active Ras which bind to GST tagged RBD protein is separated using GTT Sepharose beads through centrifugation, and the amount of active Ras is further detected through western blot. Wild type cells exhibited a transient activation of Ras proteins, which peaked at 5 sec after cAMP stimulation and subsequently decreased to the basal level after 1 min. In contrast, persistent Ras activation was observed in *gsk3*$^-$ cells in response to cAMP

stimulation. Active Ras proteins persisted and showed no sign of adaptation even at 90 sec after stimulation (Figure 4.3).

I thus analyzed Ras activation pattern in *gsk3*$^-$ cells beyond the normal activation/adaptation time frame. Wild type cells displayed usual transient Ras activation around 5 sec post-stimulation with additional activations, which were likely caused by paracrine Ras activation by autonomous secretion of cAMP. In contrast, *gsk3*$^-$ cells displayed persistent Ras activation up to 12 min. In addition, no additional Ras activation peak was observed from *gsk3*$^-$ cells. Previous study demonstrated that *gsk3*$^-$ cells are unable to produce extracellular cAMP (Teo et al., 2010), and thus it is likely that no paracrine Ras activation pathway was operating in *gsk3*$^-$ cells (Figure 4.4).

To determine if other Ras proteins, such as RasC, which does not efficiently associate with Raf1-RBD, were misregulated in *gsk3*$^-$ cells, Byr2 from *Schizosaccharomyces pombe* was used. Ras binding domain of Byr2 was shown to have good affinity to both active RasC and RasG (Kae et al., 2004). Pull-down assay using Byr2 demonstrated that a subset of Ras proteins that bind to Byr2 were normally and transiently activated in response to cAMP stimulation *gsk3*$^-$ cells compared to wild type cells (Figure 4.5).

4.3 Discussion

The data above suggested that certain Ras species, likely RasD and RasB, were persistently activated by cAMP in *gsk3*$^-$ cells, whereas RasC and RasG were normally regulated. Both groups of Ras proteins showed normal basal activity in *gsk3*$^-$ cells. It is thus likely that misregulation of RasD may interfere with cell differentiation, but not chemotaxis of *gsk3*$^-$ cells (Louis et al., 1997). It could also be that GSK3 regulate some other yet to be defined Ras species which are able to interact with Raf1-RBD proteins.

Unlike *sodC*$^{-}$ cells situation reported by Veeranki and others (2008), GSK3 is able to stimulate persistent activation of certain Ras species while leaving the basal Ras activity unaffected. How GSK3 achieve this kind of Ras activation dynamics still needs further investigation. It is likely that GSK3 is able to regulate certain specific GEF or GAP proteins. It would be interesting in the future to firstly find out which specific type of Ras is misregulated upon cAMP stimulation by using specific Ras antibidies before further investigate the potential role of GSK3 on certain GEF or GAP proteins.

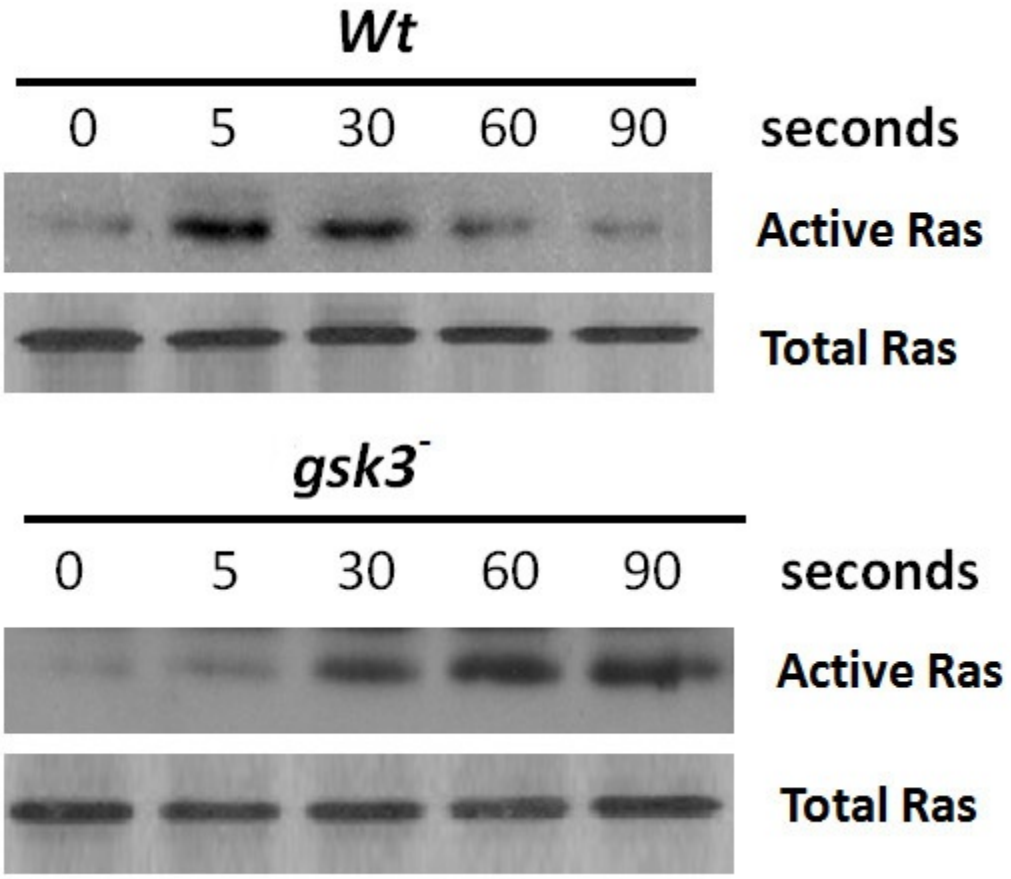

Fig 4.3 Ras activation patterns after stimulation using GST-Raf1-RBD. Aggregation competent cells were stimulated with 10 μM cAMP as indicated. Amount of total Ras proteins were first normalized by total Ras level. Amount of active Ras proteins were detected by GST-Raf1-RBD. Data are representative of at least three independent experiments.

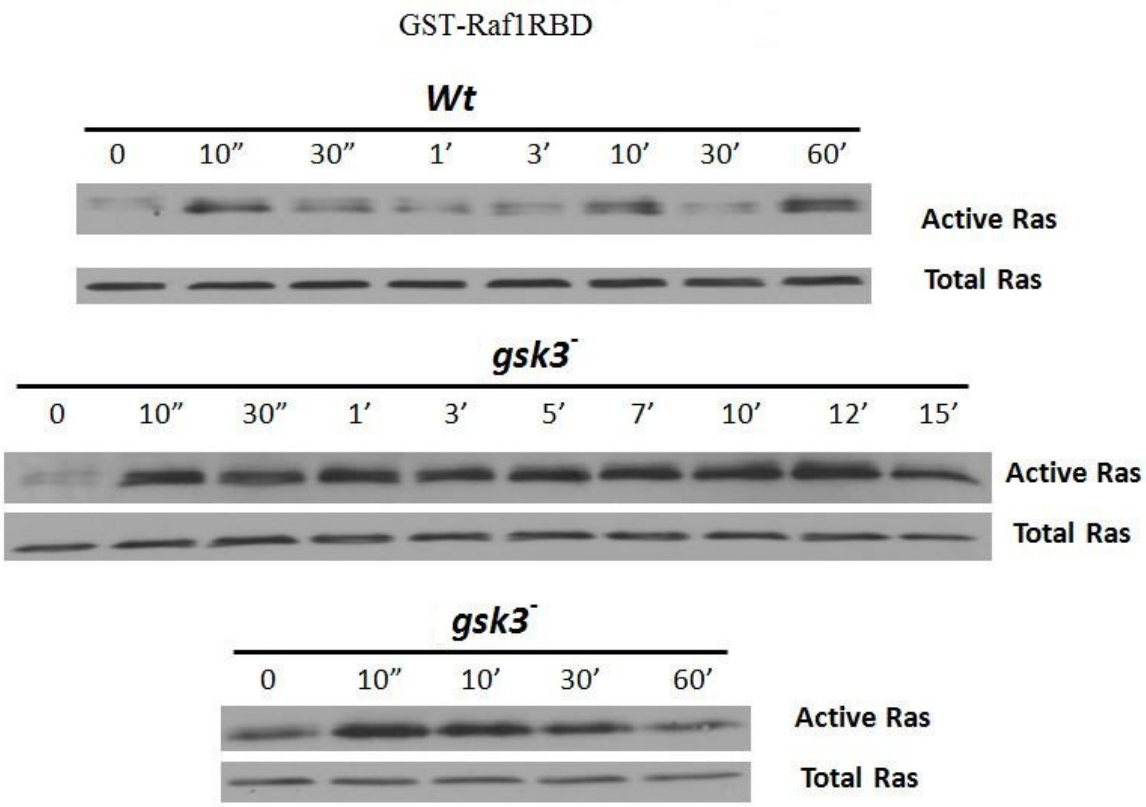

Fig 4.4 Long time Ras activation patterns after stimulation using GST-Raf1-RBD. Aggregation competent cells were stimulated with 10 μM cAMP as indicated. Amount of total Ras proteins were first normalized by total Ras level. Amount of active Ras proteins were detected by GST-Raf1-RBD. Double apostrophe indicates second and single apostrophe indicates minute.

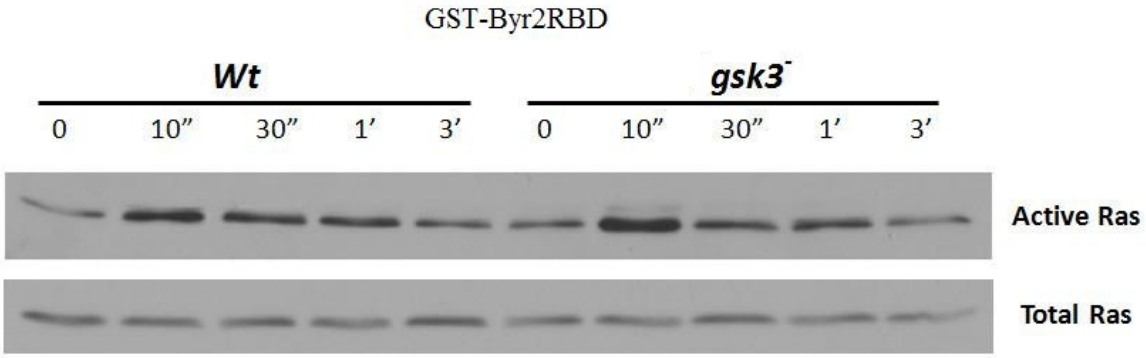

Fig 4.5 Ras activation patterns after stimulation using GST-Byr2-RBD. Aggregation competent cells were stimulated with 10 μM cAMP as indicated. Amount of total Ras proteins were firstly normalized by western blotting using anti-Pan-Ras antibody. Amount of active Ras proteins were detected by GST-Byr2-RBD. Double apostrophe indicates second and single apostrophe indicates minute.

CHAPTER V

GSK3 REGULATES PI3K1-LD PHOSPHORYLATION *IN VIVO* AND *IN VITRO*

5.1 Materials and methods

5.1.1 Generation of GST-PI3K1-LD expression construction

A coding sequence of GST with 5' *BamHI* and 3' *EcoRI* sites were generated by PCR using pGEX-4T-1 as a template and a primer set 5'- GAAGATCTATGTCCCCTATAC TAGGTTATTGG-3' and 5'-GAAGATCTGAATTCCGGGGATCCACG-3' (Figure A3). The EXP-4(+)-PI3K1-LD-GFP expression construct was a generous gift from Dr. Firtel (Funamoto et al., 2002). *GFP* was first excised from pEXP-4(+)-PI3K1-LD-GFP by *KpnI* digestion, and *GST* was subcloned to the upstream of PI3K1-LD by utilizing a *BglII* site. A stop codon immediate downstream of PI3K1-LD (open reading frame of 1476 bp) was added by annealing two oligo nucleotides 5'-CGATTGTAAAATCAATGATTAAGG TAC-3' and 5'-CTTAATCATTGATTTTACAAT-3' and utilizing both *ClaI* and *KpnI* sites (Figure A4 and A5). All constructs were confirmed by sequencing.

5.1.2 Antibodies

Western blot analysis was performed as described in chapter II. Anti-phospho-serine antibody was purchased from Introgen and 250 X dilution was made for each western blot to achieve a final concentration of 1 μg Ab/ml. Anti-GST antibodies were purchased from Santa Cruz Biotech (1:1000 dilution). Anti-GFP antibodies were purchased from Covance (1:1000 dilution). Anti-Pan-Ras antibodies were purchased from Calbiochem (Ab-3). Anti-GSK3 (4G-1E) antibodies were from Millipore. Intensities of the bands were quantified by using UN-SCAN-IT program (Silk Scientific Corporation).

5.1.3 Subcellular fractionation of wild type and mutants GFP-PI3K1-LD proteins

Cell fractionation assay were performed as described previously with minor modifications (Han et al., 2006). Twenty five million aggregation competent cells were spun down and washed once with ice-cold PBS (137 mM NaCl, 2.7 mM KCl, 10 mM Na_2HPO_4, 1.8 mM KH_2PO_4) and the cell pellets were treated with 400 µl of 0.02% TritonX-100 and incubated 10 min at 4°C with agitation. All solutions contained protease inhibitors (Roche, Complete Mini). Mixtures were centrifuged at 12,000 x g for 5 min at 4°C. The supernatants were then mixed with 4 x SDS protein loading dye and the pellet were mixed with 100 µl of 1 x SDS protein loading dye. Forty microliters of cytosolic fractions and 1 µl of membranous fractions were loaded onto SDS-PAGE and analyzed by western blotting using anti-GFP antibody. Ras proteins were used as a marker enriched at the pellet fraction.

5.1.4 IPTG inductions

IPTG mediated GST-GSK3 induction was performed similar to the GST-RBD induction described in chapter IV except that the fusion proteins were induced at room temperature. The induction levels were checked by western blotting using either anti-GST antibodies or anti-GSK3 antibodies.

IPTG Induction and quantitative analysis of GST-PI3K1-LD by Coomassie Brilliant Blue staining were as described in chapter IV.

5.1.5 GSK3 kinase assay

Twenty units of recombinant GSK3β (New England Biolabs) and ~10 µg of recombinant GST-PI3K1-LD were mixed in the kinase assay buffer (50 mM HEPES, pH 7.5, 4 mM $MgCl_2$, 0.5 mM EGTA, 2 mM DTT, 100 µM ATP, [γ-^{32}P]ATP to 500-1000

counts/minute per pmol). The same amount of MBP protein was used as positive control. The reaction mixtures were resolved by SDS-PAGE, exposed to an X-ray film, and autoradiographs were obtained.

5.1.6 *In vitro* peptide kinase assay

Three types of GSK3 were used for *in vitro* peptide kinase assay. Twenty units of recombinant mammalian GSK3β (New England Biolabs) or 1 μg of recombinant *Dictyostelium* GST-GSK3 were used for each assay. Alternatively, whole cell lysates were used as a GSK3 source: ten million cells were lysed using ice-cold GS lysis buffer (0.5% NP40, 10 mM NaCl, 20 mM PIPES, pH 7.0, 5 mM EDTA, 50 mM NaF, 0.1 mM Na_3VO_4, 0.05% 2-mercaptoethanol, 5 μg/ml aprotinin, 5 μg/ml benzamidine) and insoluble fractions were removed by centrifuging at 10,000 x g. Five microliters of whole cell lysate was used for each assay.

The GSK3 peptide kinase assay was performed as described previously (Plyte et al., 1999). The sequences of primed peptide substrates are as follows: GSM peptide - RRRPASVPPSPSLSRHSS^{-P}HQRR, P1 peptide - RRRMNSIESS$_7$SNDS$_{11}$$^{-P}$NRR, P2 peptide - RRRNDSNCSS$_{109}$GSSS$_{113}$$^{-P}$GRR, and P3 peptide - RRRGSSSGSS$_{177}$SGGS$_{181}$$^{-P}$DRR. For each assay, 20 μg of each peptide, together with a source of GSK3 mentioned above, were mixed in the assay buffer (50 mM HEPES, pH 7.5, 4 mM $MgCl_2$, 0.5 mM EGTA, 2 mM DTT, 100 μM ATP, [γ-^{32}P]ATP to 500-1000 counts/minute per pmol) at room temperature in a final volume of 20 μl. The same amount of GSM peptide was used as a positive control (Plyte et al., 1999). Eight minutes were allowed for the reaction before stopped by an equal volume of 15 mM phosphoric acid. Incorporation of [γ-^{32}P]ATP was detected by binding to P81 phosphocellulose paper (Whatman), washed

extensively for three times with 7.5 mM phosphoric acid and were counted with scintillation counter. Control samples were assayed in the presence of 50 mM LiCl, a GSK3 inhibitor, and lithium sensitive specific activities were calculated by subtracting the counts in control samples from the total counts. Specific activity was expressed as picomole of phosphate transferred per assay. Each experiment was repeated three times.

5.1.7 GST pull-down assay and lambda phosphatase treatment

Twenty five million of either wild type cells or *gsk3*$^-$ cells expressing GST-PI3K1-LD were lysed with 1 ml of cell lysis buffer [20 mM TrisCl (pH7.7), 5% glycerol, 1% Triton X-100, 150 mM NaCl, 1 mM EDTA, 1 mM Na_3VO_4, 40 μM sodium molybdate, 0.1% beta-mercaptoethanol, and 1x protease inhibitor cocktail (Roche)]. Two hundred and fifty microliters of cell lysate was mixed with 50% slurry of glutathione (GTT) Sepharose beads (GE Healthcare) and incubated 1.5 hr at 4°C with agitation. The beads were then spun down and washed three times with cell lysis buffer. GST-PI3K1-LD proteins on the glutathione Sepharose beads were detected by western blotting using anti-GST antibody (Santa Cruz Biotech). PI3K1-LD phosphorylation levels were detected by western blotting using anti-phospho-serine antibody (Introgen).

Lambda phosphatase was purchased from New England Biolab and lambda phosphatase treatment of GST-PI3K1-LD, which was purified from *Dictyostelium* cell lysate was performed as suggested by the provider. In short, the reactions were carried out at 30°C for 20 min and stopped by heating to 65°C for 1 hr before the mixture was subjected to SDS-PAGE.

5.2 Results

5.2.1 PI3K1-LD proteins were under-phosphorylated in *gsk3*$^-$ cells

Full length PI3K1 consists of several domains (Figure 5.1), among which the localization domain resides at the amino terminus. To determine whether PI3K1-LD is phosphorylated in a GSK3 dependent manner *in vivo*, a GST tagged PI3K1-LD construct was generated and expressed in both wild type and *gsk3*$^-$ cells (Figure 5.1).

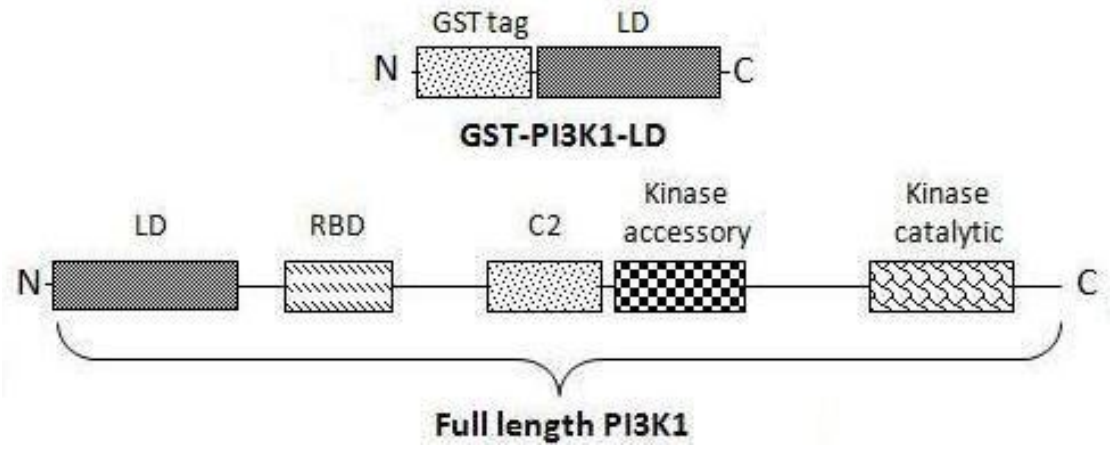

Fig 5.1 GST-PI3K1-LD construct and full length PI3K1. Full-length PI3K1 is characterized by a localization domain, a Ras binding domain, a C2 domain, a kinase accessory domain and a kinase catalytic domain. The localization domain of PI3K1 is fused with a GST tag and expressed in both wild type cells and *gsk3*$^-$ cells.

The expression levels in both wild type cells and *gsk3*$^-$ cells were firstly normalized using both whole cell lysate and purified GST-PI3K1-LD. The phosphorylation level on serine residues of PI3K1-LD in *gsk3*$^-$ cells revealed a ~60% decrease compared to that in wild type cells. Consistent with this, I noticed a slight increase in GST-PI3K1-LD motility purified from *gsk3*$^-$ cells on SDS gels compared to that from wild type cells (Figure 5.2A and 5.3). Upon treatment of the samples with lambda phosphatase, the levels of phosphorylation on serine residues of PI3K1-LD declined significantly.

Furthermore, there were no more mobility shift differences between GST-PI3K1-LD proteins purified from wild type and *gsk3*$^-$ cells (Figure 5.2B and 5.4).

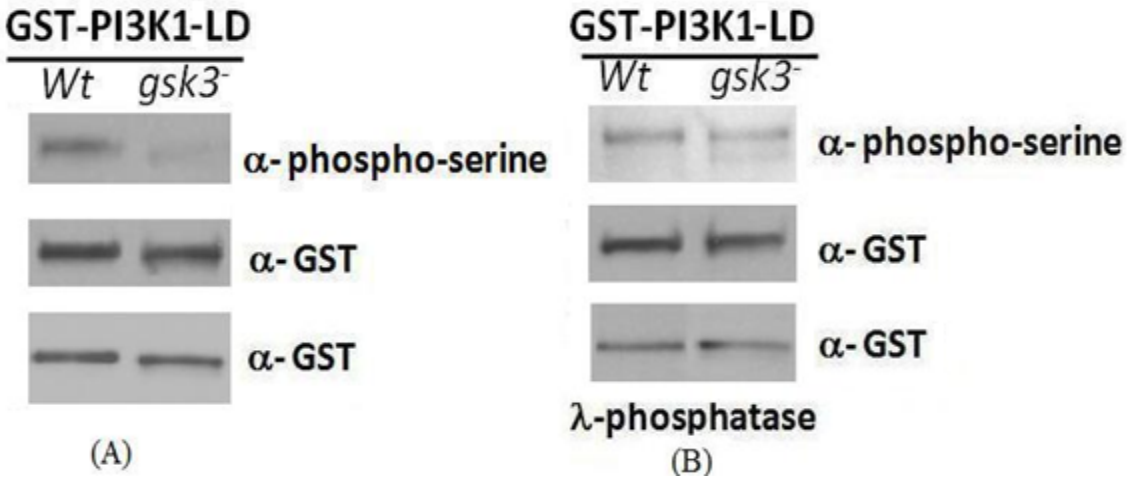

Fig 5.2 (A) PI3K1-LD had less phosphorylation level in *gsk3*$^-$ cells compared to wild type cells. (B) Lambda phosphatase treatment was able to reverse the different phosphorylation level. Data are representative of at least three independent experiments.

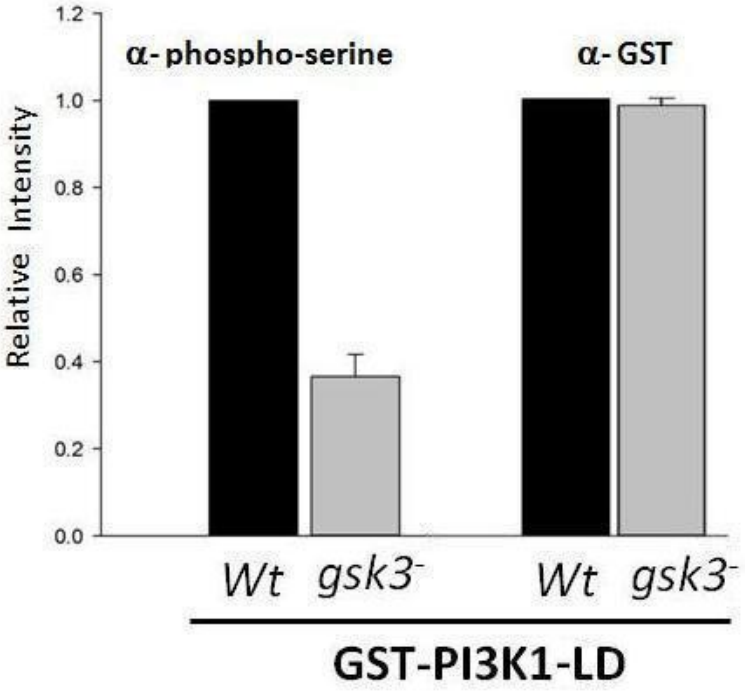

Fig 5.3 Quantifications of the relative band intensity for figure 5.2A (top and middle panel). *gsk3*$^-$ bands were compared with wild type bands. Data are representative of at least three independent experiments. Error bars represent standard deviations.

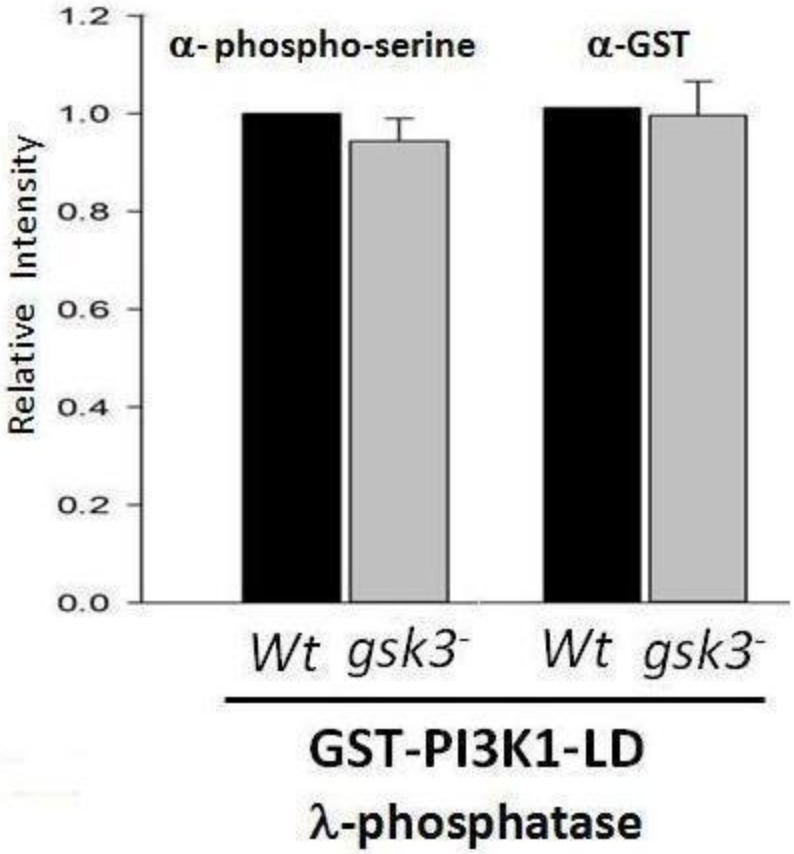

Fig 5.4 Quantifications of the relative band intensity for figure 5.2B (top and middle panel). The *gsk3*$^-$ bands were compared with wild type bands. Data are representative of at least three independent experiments. Error bars represent standard deviations.

5.2.2 Localization of PI3K1-LD, SPM-PI3K1-LD and SAS-PI3K1-LD

To further determine the role of phosphorylation on PI3K1-LD for its localization at molecular level, I used the GFP-PI3K1-LD mutants mentioned in chapter III (Table 3.1) and performed cell fractionation assay. Consistent with the fluorescent imaging data, GFP-PI3K1-LD localized almost two-fold more on the plasma membrane than in the cytosol of *gsk3*$^-$ cells. In wild type cells, GFP-PI3K1-LD showed ~40% more PI3K1-LD localization in the cytosol than on the plasma membrane. In contrast, phosphomimetic mutant (SPM-PI3K1-LD) of GFP-PI3K1-LD in *gsk3*$^-$ cells displayed more cytosolic

localization resembling PI3K1-LD in wild type cells. On the other hand, sextuple serine to alanine substitution mutant (SAS-PI3K1-LD) showed more membrane localization in wild type cells, which was reminiscent of PI3K1-LD subcellular localization in *gsk3*$^{-}$ cells (Figure 5.5 and 5.6). Two controls were performed in this assay. In all cell types, Ras proteins displayed consistent membrane enrichment. The ratios between Ras proteins localized to the membrane (the pellet fraction) and cytosol (the supernatant fraction) were all around 2:1, indicating that all fractionations were of equivalent quality (Figure 5.5 and 5.7). Also, the total expression levels of PI3K1-LD and PI3K1-LD mutants were comparable (Figure 5.8 and 5.9).

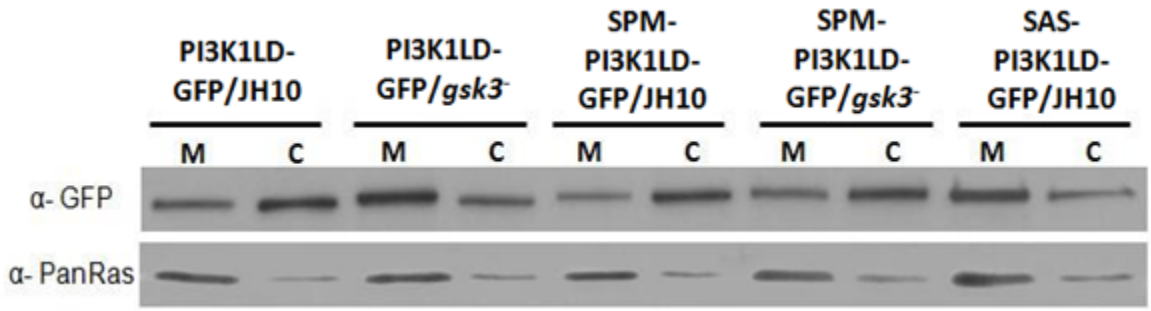

Fig 5.5 Localization of mutant PI3K1-LD in either wild type cells or *gsk3*$^{-}$ cells. Ras, which is a membrane localized protein, served as a control. The ratios between Ras proteins localized to the membrane and cytosol were all around 2:1 (Figure 5.6) suggesting all types of cells were fractionated to the similar extent. Data are representative of at least three independent experiments. 'M' stands for membraous fraction, while 'C' stands for cytosolic fraction.

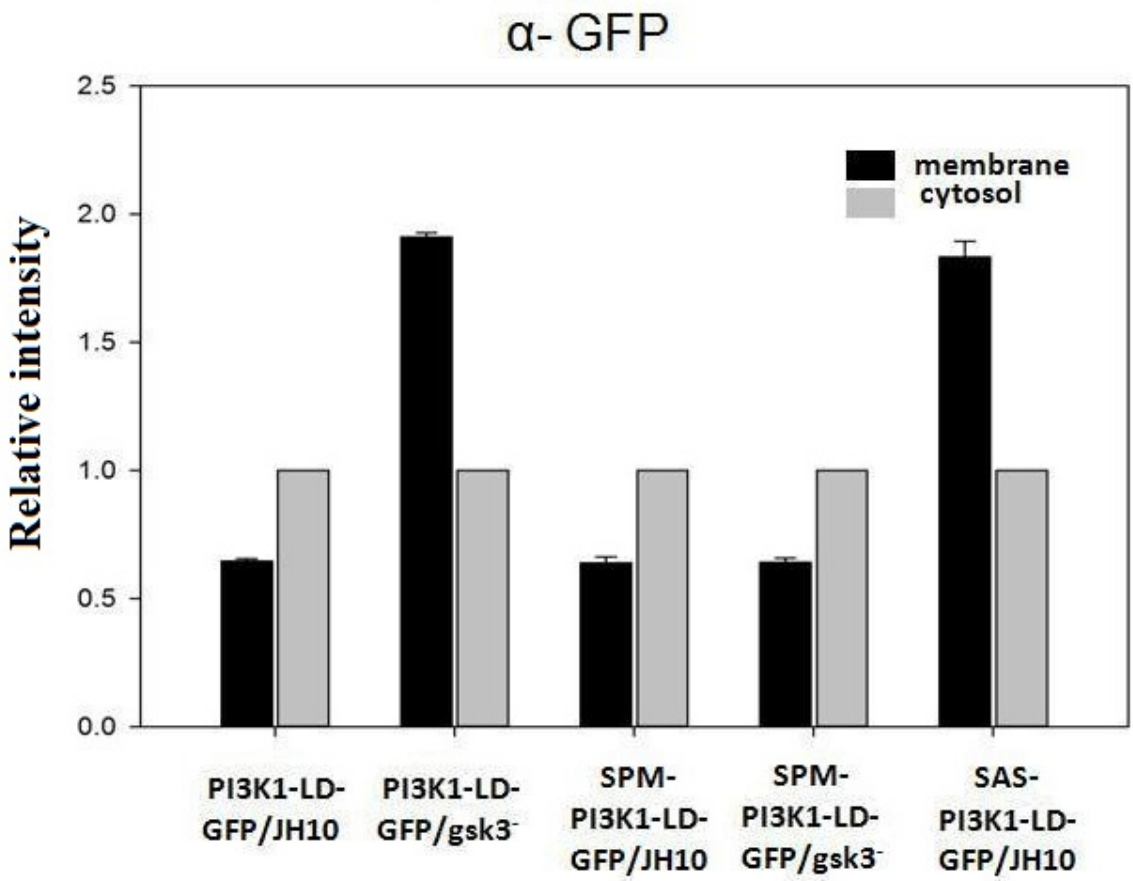

Fig 5.6 Quantifications of the relative band intensity for Figure 5.5 (top panel). Black bars indicate membranous fractions and grey bars indicate cytosolic fractions. Band intensities for membranous fractions were compared with those for cytosolic fractions. Data are representative of at least three independent experiments. Error bars represent standard deviations.

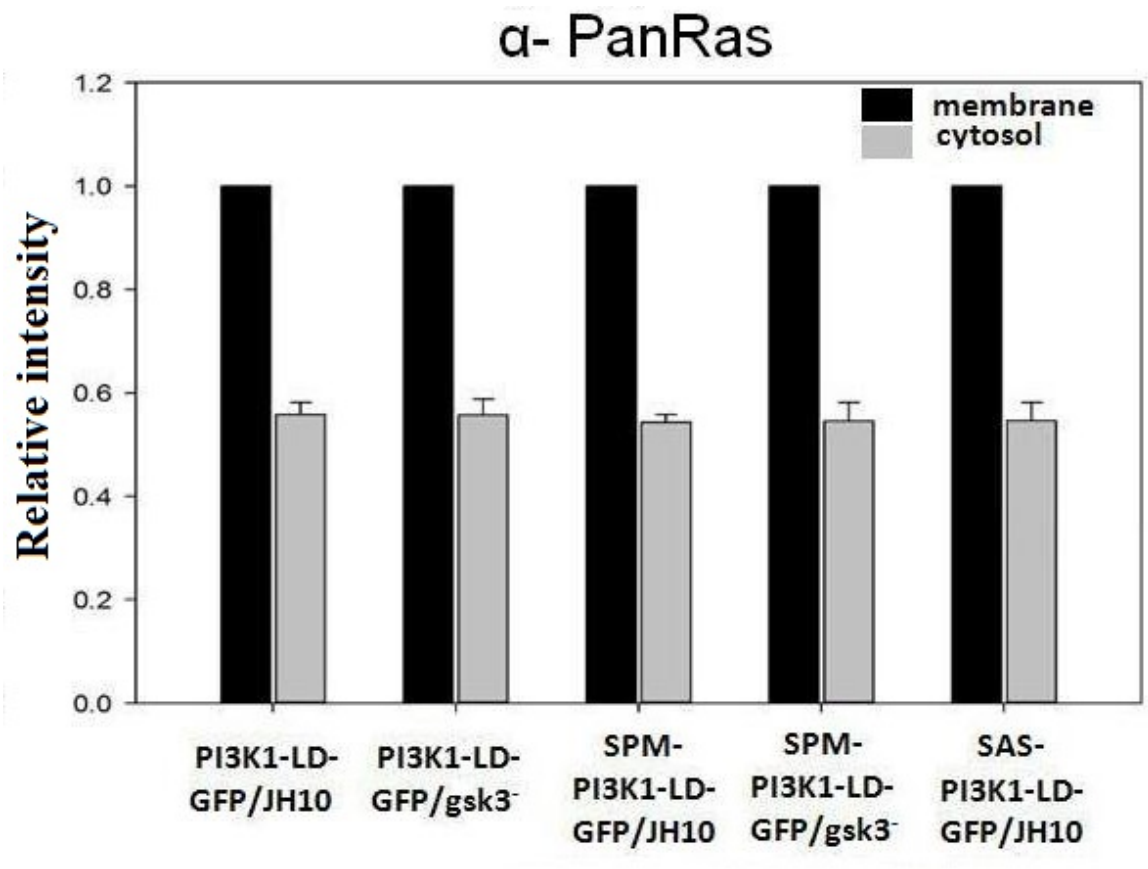

Fig 5.7 Quantifications of the relative band intensity for Figure 5.5 (bottom panel). Black bars indicate membranous fractions and grey bars indicate cytosolic fractions. Band intensities for cytosolic fractions were compared with those for membranous fractions. Data are representative of at least three independent experiments. Error bars represent standard deviations.

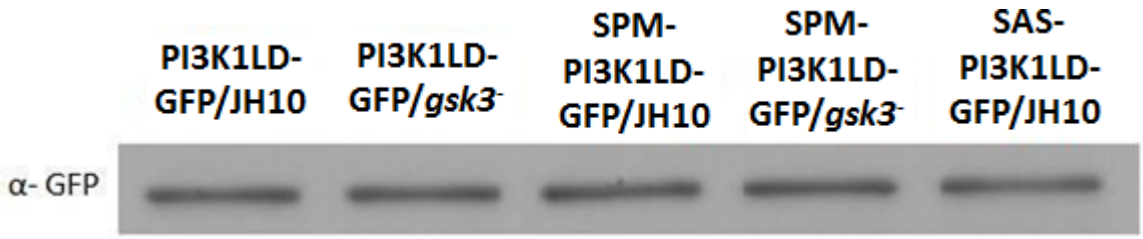

Fig 5.8 Normalization of the total expression level. For each cell type, same amount of membranous fraction and cytosolic fraction, which were used in Figure 5.5, were combined before subjected to SDS-PAGE. The expression level of either GFP fused PI3K1LD or GFP fused mutated PI3K1LD are similar in all cell types. Data are representative of at least three independent experiments.

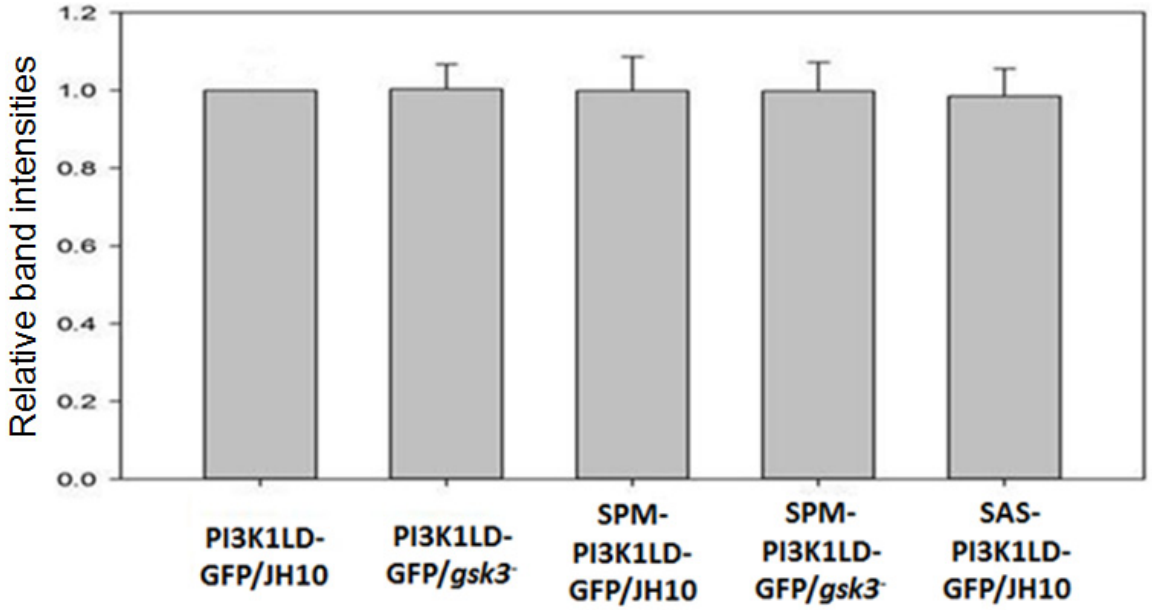

Fig 5.9 Quantifications of the relative band intensity for Figure 5.8. The band intensities were all compared to those for JH10 cells expressing PI3K1-LD. Data are representative of at least three independent experiments. Error bars represent standard deviations.

5.2.3 Unprimed PI3K1-LD was not a substrate of recombinant GSK3

To determine whether PI3K1-LD can be directly phosphorylated by recombinant GSK3 without being pre-phosphorylated by another kinase, GST-PI3K1-LD were express in *E.coli* and *in vitro* kinase assays were performed (Figure 5.10). First, GST was not a substrate of recombinant GSK3 compared to the positive control myelin basic protein (MBP), which is a known GSK3 substrate (Figure 5.11). However, GST-PI3K1-LD was not utilized by recombinant GSK3 indicating that without pre-phosphorylation by another kinase, PI3K1-LD could not be phosphorylated by GSK3 (Figure 5.12).

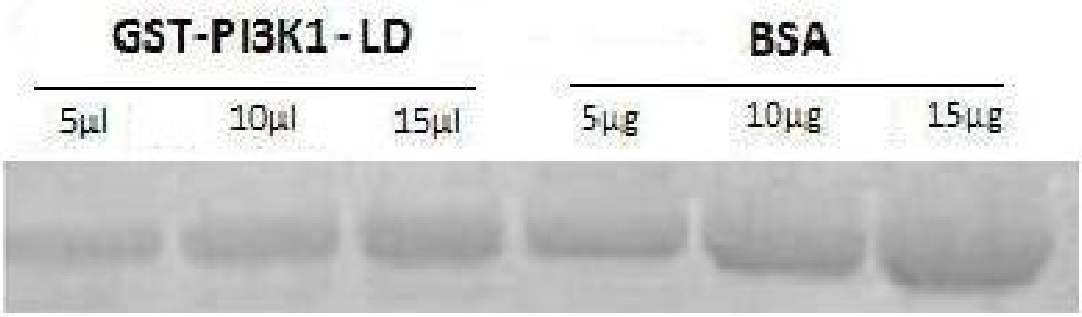

Fig 5.10 Quantification of *E.coli* expressed GST-PI3K1-LD using Coomassie Brilliant Blue staining.

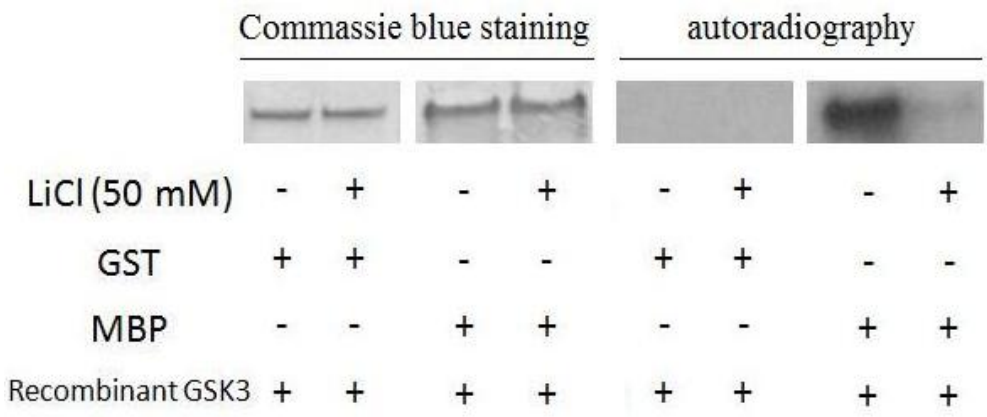

Fig 5.11 GST could not be phosphorylated by recombinant GSK3. Commassie blue stained gel showed there was comparable input amount of with GST protein or MBP protein. The autoradiography images after kinase assay showed that GST was not a GSK3 substrate while the positive control (MBP), as well as the GSK3 inhibitor LiCl, worked fine.

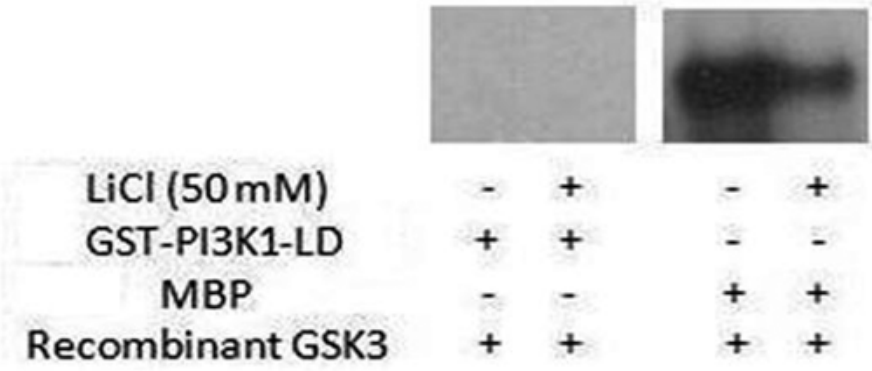

Fig 5.12 *In vitro* kinase assay using recombinant GSK3. Around 10 μg of GST-PI3K1-LD was used for each reaction. IPTG induced GST-PI3K1-LD could not be phosphorylated by recombinant GSK3 (left panel) while the positive control worked fine (right panel). Data are representative of at least three independent experiments.

5.2.4 Induced *Dictyostelium* GSK3 could not phosphorylate artificially synthesized peptides

According to the data above, I reasoned that GSK3 may phosphorylate only the primed PI3K1-LD. To pursue that, the pre-phosphorylated peptides P1, P2, and P3 (phosphoserine at position 11, 113, and 181) containing three potential GSK3 sites of PI3K1-LD were synthesized. GST-GSK3 construct and *E.coli* expression were described previously (Kim et al., 2002). *Dictyostelium* recombinant GST-GSK3 was quantified and proved to be able to phosphorylate MBP as mammalian recombinant GSK3 does (Figure 5.13 and 5.14). However, all three pre-phosphorylated peptides (referred to as P1, P2 and P3 henceforth) could not be phosphorylated by GST-GSK3 compared to GSM positive control (Figure 5.15). I also cut off the GST tag from GST-GSK3 after purification and repeated the same experiment, and similar results were obtained (data not shown).

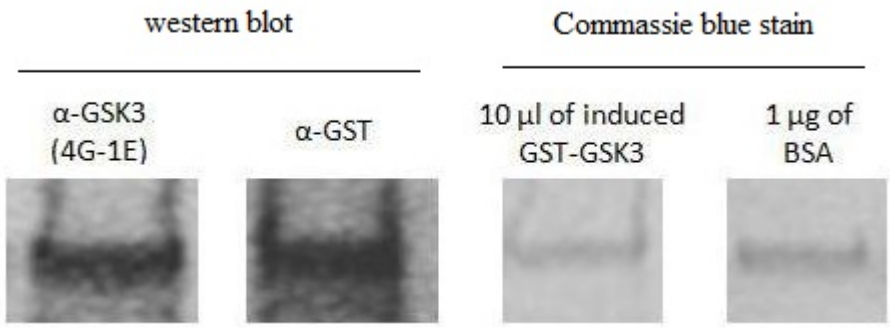

Fig 5.13 Detection and quantifications of *E.coli* expressed GST-GSK3. *E.coli* expressed GST-GSK3 was clearly detected by western blot using either anti-GSK3 or anti-GST antibodies. Commassie blue stained gel showed that the input amount of GST-GSK3 for each assay was around 1 µg.

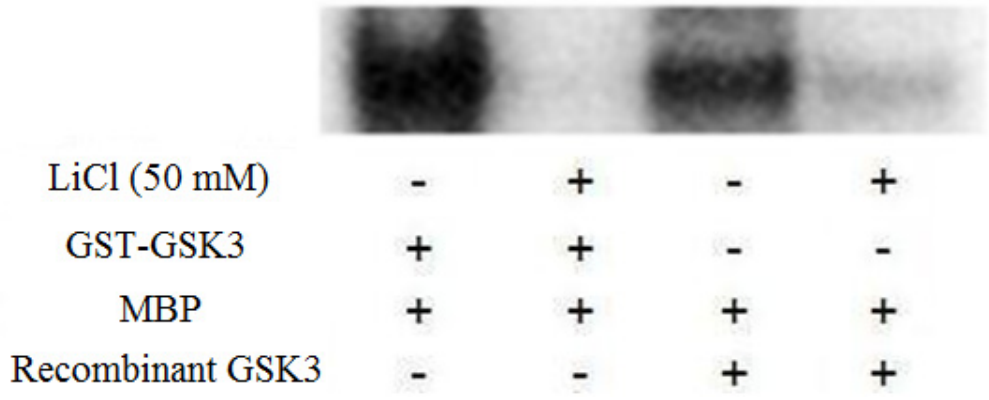

Fig 5.14 Kinase activity of *E.coli* expressed GST-GSK3. Compared to positive control, IPTG induced GST-GSK3 was able to phosphorylation MBP. Data are representative of at least three independent experiments.

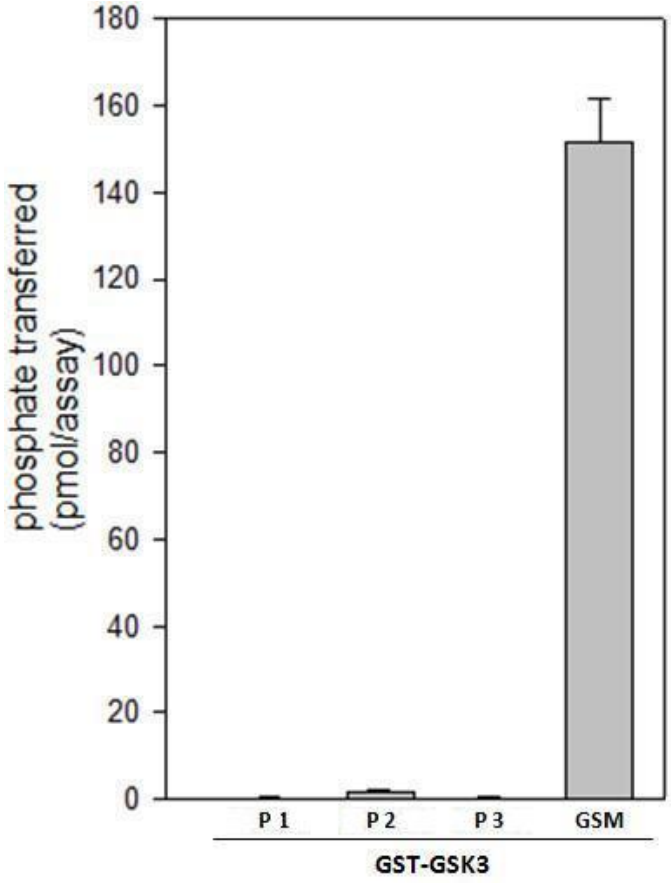

Fig 5.15 *In vitro* peptide kinase assay using *E.coli* expressed GST-GSK3. Three primed artificially synthesized peptides were not substrates of GST-GSK3 while positive control using GSM peptide worked fine. Data are representative of at least three independent experiments. Error bars represent standard deviations.

5.2.5 Recombinant GSK3 could only phosphorylate one of the artificially synthesized peptides

I also performed *in vitro* peptide kinase assay mentioned above using recombinant GSK3. In this case, only P2 peptide was shown to be a substrate of recombinant GSK3 compared to GSM positive control (Figure 5.16).

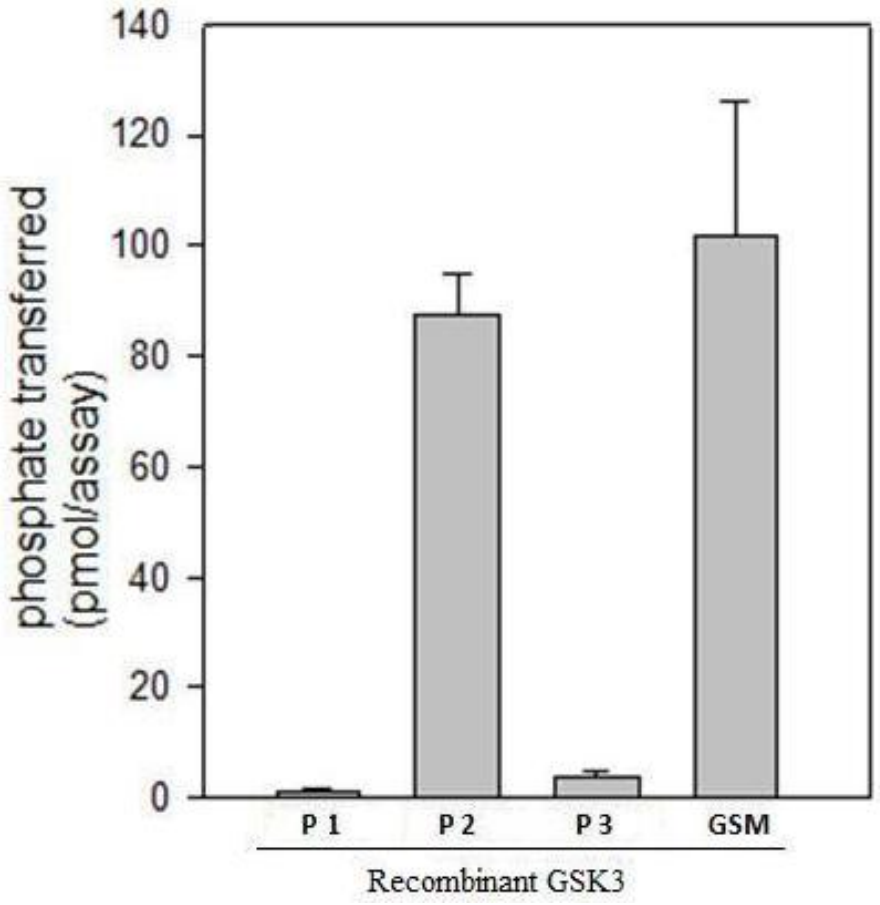

Fig 5.16 *In vitro* peptide kinase assay using recombinant GSK3. Compared to positive control, only the second artificially synthesized primed peptide could be phosphorylated by GSK3. Data are representative of at least three independent experiments. Error bars represent standard deviations.

5.2.6 Peptide Kinase assay using whole cell lysate of wild type cells indicated all artificially synthesized peptides were GSK3 substrates

When I performed *in vitro* peptide kinase assay using whole cell lysate, all three peptides were revealed to be substrates of GSK3 compared to the positive control (Ryves et al., 1998). No significant kinase activity toward GSM was detected using whole cell lysate of *gsk3*$^{-}$ cells. Same set of experiments were performed in the presence of lithium chloride, a GSK3 inhibitor, to determine the nonspecific kinase activities. The GSK3 specific activities were calculated by subtracting nonspecific activities from the raw values (Figure 5.17).

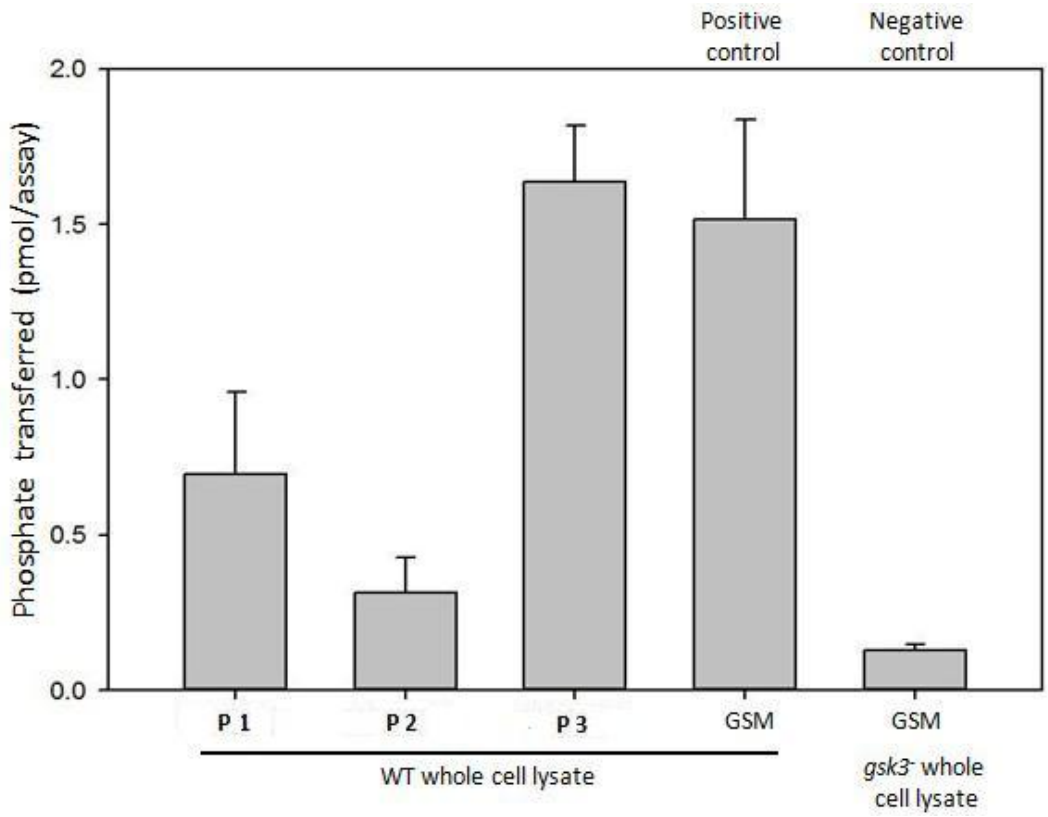

Fig 5.17 *In vitro* peptide kinase assay using whole cell lysate. Data are representative of at least three independent experiments. Error bars represent standard deviations.

5.3 Discussion

Given that PI3K1-LD is significantly less phosphorylated in *gsk3*$^-$ cells, it is likely that the serine phosphorylation of PI3K1-LD serves as a prerequisite signal for chemoattractant induced regulation of PI3K1. *In vitro* peptide kinase assay support the possibility that GSK3 is able to directly phosphorylate these sites upon primed by another kinase. Furthermore, biochemical fractionation assay indicated that GSK3 regulated serine phosphorylation of PI3K1 membrane localization domain served as a permissive signal for chemoattractant induced plasma membrane localization of PI3K1. Thus, it is possible that chemoattractant signal modifies PI3K1 localization by modulating binding partners of PI3K1 either in the cytosol or on the plasma membrane. I hypothesize that a cytosolic PI3K1 retention factor and a membrane component would both associate with PI3K1-LD and are susceptible to chemoattractant signaling mediated modification. It is also possible that the chemoattractant signal may modify PI3K1-LD in addition to the GSK3 dependent serine phosphorylation.

CHAPTER VI

CONCLUSIONS AND FUTURE DIRECTIONS

In this dissertation, I reported that *gsk3*$^-$ cells generated from JH10 parental cells showed severe defectives in motility and direction sensing ability towards cAMP gradient. The main goal was to determine the mechanism of GSK3 mediated PI3K regulation.

Loss of GSK3 caused a biased membrane localization of PI3K and an elevated basal PIP3 level on the plasma membrane. Upon cAMP stimulation, unlike wild type cells, which experienced a transient PIP3 increase on the membrane, the membrane PIP3 level in *gsk3*$^-$ cells showed no such increase in the PIP3 level even during the course of the stimulation. Consistently, PI3K also exhibited no further membrane localization in *gsk3*$^-$ cells in response to cAMP stimulation. Given that PI3K generates PIP3, I reasoned that the loss of GSK3 could facilitate PI3K plasma membrane localization and thus increase basal PIP3 level. I also showed both *in vivo* and *in vitro* that PI3K1 was phosphorylated on its membrane localization domain in a GSK3 dependent manner. Furthermore, I identified several serine residues are likely the targets of GSK3 phosphorylation and play a critical role in the subcellular localization of PI3K1. It was likely that PI3K1-LD was phosphorylated upon primed by a yet to be identified priming kinase. I proposed that phosphorylated PI3K1 is likely the target of chemoattractant mediated signaling since that sextuple phosphomimetic substitution mutant displayed transient membrane localization in response to chemoattractant stimulation similarly to the wild type PI3K1. It is thus plausible that phosphorylated PI3K1 interacted with a putative cytosolic retention factor, of which interaction with PI3K will be weakened upon receiving

chemoattractant signaling. It is also possible that a chemoattractant signal may augment interactions between phospho-PI3K1 and a membrane component that interacts with PI3K1. In both scenarios, it is possible that the chemoattractant signal regulated interactions by modifying either PI3K1 or its binding targets (the cytosolic retention factor or a plasma membrane-associated component). Further studies will be necessary to determine the molecular mechanism of chemoattractant mediated regulation of PI3K subcellular shuttling besides the GSK3 mediated phosphorylation of PI3K.

One of the puzzling observations from *gsk3*$^-$ cells is that there was no further increase in the level of PIP3 in response to chemoattractant stimulation. A previous study of Teo et al. (2010), demonstrated that an increase in the level of PIP2 by altering phosphoinositide metabolism restored transient increase in the PIP3 level in response to chemoatteractant stimulation, suggesting that PI3K1 may not have sufficient PIP2 to generate PIP3. Furthermore, it was suggested that there are two pools of PIP2 – one smaller pool which is mainly responsible for PIP3 synthesis and one much larger pool that is slowly metabolized and bound to cytoskeleton regulating proteins (King et al., 2009). This may explain the previous finding that both wild type and *gsk3*$^-$ cells contain similar total levels of PIP2, which might make the difference of the smaller PIP2 pools for PI3K invisible.

The other possibility is that *gsk3*$^-$ cells may not be able to properly activate PI3K in response to cAMP stimulation. Upon stimulation with cAMP, *gsk3*$^-$ cells displayed a persistent Ras activation, detected by GST-Raf1-RBD. However, normal Ras activation pattern was observed with GST-Byr2-RBD. Given that Byr2-RBD binds RasC and RasG and Raf1-RBD binds RasB, RasD, and RasG, it is likely that GSK3 was essential for

regulating RasB or RasD, but not RasC and RasG. It is thus likely that RasC or RasG were properly activated in *gsk3*$^-$ cells by chemoattractant stimulation, and the lack of transient increase in the levels of PIP3 were not caused by a misregulation of RasC or RasG but likely caused by the lack of sufficient PI3K substrate PIP2. It will be interesting and significant to determine the nature of misregulated Ras species in *gsk3*$^-$ cells, which may be a cause for their developmental abnormalities.

It is worthy to mention that GSK3 affects motility and chemotaxis through regulating expression of key regulators of chemotaxis and motility. It was reported that GSK3 is able to reduce the transcription level of *sodC,* which encodes a superoxide dismutase, *pdsA* which encodes a cAMP phosphodiesterase, and *acaA* which encodes the adenylyl cyclase (Strmecki et al., 2007; Teo et al., 2010; Veeranki et al., 2008).

Studies shown in this dissertation demonstrated that GSK3 played multiple roles in orchestrating cell motility and chemotaxis by regulating pre-stimulus membrane localization of PI3K as well as regulating expression of *sodC*.

The PI3K-mediated PIP3 signaling pathway is also prevalent in mammalian systems. In mammalian systems, PI3Ks are classified into three different groups: class I, class II and class III (Weiger and Parent, 2012). Among all these classes of PI3Ks, class I PI3Ks act through similar mechanisms compared to *Dictyostelium*. Upon activation of class IA PI3Ks through receptor tyrosine kinases (RTKs), class IA PI3Ks display a trans-location from the cytosol to the plasma membrane by binding to the Src-homology (SH2) domains on the RTKs, which further turns on the PIP3 signaling pathway (Weiger and Parent, 2012). Unlike class IA PI3Ks, class IB PI3Ks are mainly activated through G-protein-coupled receptors and Ras (Weiger and Parent, 2012). In mouse macrophages, PI3K has

crucial role in regulating macrophage-colony stimulating factor (M-CSF) stimulated chemotaxis through further activation of Rac GEF, Vav (Vedham et al., 2005). Also, neutrophils and macrophages with disrupted PI3Kγ in mouse system exhibit reduced chemotaxis *in vitro*. *In vivo*, less accumulation of neutrophils and macrophages at the sites of inflammation were observed (Hirsch et al., 2000; Sasaki et al., 2000). In fibroblasts, platelet derived growth factor (PDGF) triggers the activation of class IA PI3K through RTKs, and the activation of class IA PI3K is important for the chemotaxis (Hawkins et al., 1992; Wennstrom et al., 1994). It has been well established before that in mammalian systems, PI3K lies upstream of GSK3 and PI3K could indirectly inactivate GSK3 by activating PKB (Grimes and Jope, 2001). Based on the evidence obtained in this dissertation, it would be worthy and interesting to test whether GSK3 is able to influence class I PI3Ks in mammalian system, which may contribute to the study of certain inflammatory diseases and the wound healing process.

REFERENCES

Adler, J. (1987). How motile bacteria are attracted and repelled by chemicals: an approach to neurobiology. Lecture held on the occasion of the receipt of the Otto-Warburg-Medaille 1986. *Biol Chem Hoppe Seyler* 368, 163-73.

Baluch, D. P. and Capco, D. G. (2008). GSK3 beta mediates acentromeric spindle stabilization by activated PKC zeta. *Dev Biol* 317, 46-58.

Behrens, J., Jerchow, B. A., Wurtele, M., Grimm, J., Asbrand, C., Wirtz, R., Kuhl, M., Wedlich, D. and Birchmeier, W. (1998). Functional interaction of an axin homolog, conductin, with beta-catenin, APC, and GSK3beta. *Science* 280, 596-9.

Bijur, G. N. and Jope, R. S. (2000). Opposing actions of phosphatidylinositol 3-kinase and glycogen synthase kinase-3beta in the regulation of HSF-1 activity. *J Neurochem* 75, 2401-8.

Bonner, J. T. (1947). Evidence for the formation of cell aggregates by chemotaxis in the development of the slime mold *Dictyostelium discoideum*. *J Exp Zool* 106, 1-26.

Bonner, J. T. and Eldredge, D., Jr. (1945). A note on the rate of morphogenetic movement in the slime mold, *Dictyostelium discoideum*. *Growth* 9, 287-97.

Bosgraaf, L. and Van Haastert, P. J. (2009). Navigation of chemotactic cells by parallel signaling to pseudopod persistence and orientation. *PLoS ONE* 4, e6842.

Boyle, W. J., Smeal, T., Defize, L. H., Angel, P., Woodgett, J. R., Karin, M. and Hunter, T. (1991). Activation of protein kinase C decreases phosphorylation of c-Jun at sites that negatively regulate its DNA-binding activity. *Cell* 64, 573-84.

Brouns, M. R., Matheson, S. F., Hu, K. Q., Delalle, I., Caviness, V. S., Silver, J., Bronson, R. T. and Settleman, J. (2000). The adhesion signaling molecule p190 RhoGAP is required for morphogenetic processes in neural development. *Development* 127, 4891-903.

Brouns, M. R., Matheson, S. F. and Settleman, J. (2001). p190 RhoGAP is the principal Src substrate in brain and regulates axon outgrowth, guidance and fasciculation. *Nat Cell Biol* 3, 361-7.

Cai, H., Das, S., Kamimura, Y., Long, Y., Parent, C. A. and Devreotes, P. N. (2010). Ras-mediated activation of the TORC2-PKB pathway is critical for chemotaxis. *J Cell Biol* 190, 233-45.

Chang, M. T. and Raper, K. B. (1981). Mating types and macrocyst formation in *Dictyostelium*. *J Bacteriol* 147, 1049-53.

Charest, P. G., Shen, Z., Lakoduk, A., Sasaki, A. T., Briggs, S. P. and Firtel, R. A. (2010). A Ras signaling complex controls the RasC-TORC2 pathway and directed cell migration. *Dev Cell* 18, 737-49.

Chen, L., Iijima, M., Tang, M., Landree, M. A., Huang, Y. E., Xiong, Y., Iglesias, P. A. and Devreotes, P. N. (2007). PLA2 and PI3K/PTEN pathways act in parallel to mediate chemotaxis. *Dev Cell* 12, 603-14.

Chen, Y., Rodrick, V., Yan, Y. and Brazill, D. (2005). PldB, a putative phospholipase D homolog in *Dictyostelium discoideum* mediates quorum sensing during development. *Eukaryot Cell* 4, 694-702.

Cho, J. H. and Johnson, G. V. (2003). Glycogen synthase kinase 3beta phosphorylates tau at both primed and unprimed sites. Differential impact on microtubule binding. *J Biol Chem* 278, 187-93.

Cho, J. H. and Johnson, G. V. (2004). Primed phosphorylation of tau at Thr231 by glycogen synthase kinase 3beta (GSK3beta) plays a critical role in regulating tau's ability to bind and stabilize microtubules. *J Neurochem* 88, 349-58.

Ciani, L., Krylova, O., Smalley, M. J., Dale, T. C. and Salinas, P. C. (2004). A divergent canonical WNT-signaling pathway regulates microtubule dynamics: dishevelled signals locally to stabilize microtubules. *J Cell Biol* 164, 243-53.

Cook, D., Fry, M. J., Hughes, K., Sumathipala, R., Woodgett, J. R. and Dale, T. C. (1996). Wingless inactivates glycogen synthase kinase-3 via an intracellular signalling pathway which involves a protein kinase C. *Embo J* 15, 4526-36.

Cross, D. A., Alessi, D. R., Cohen, P., Andjelkovich, M. and Hemmings, B. A. (1995). Inhibition of glycogen synthase kinase-3 by insulin mediated by protein kinase B. *Nature* 378, 785-9.

Cross, D. A., Watt, P. W., Shaw, M., van der Kaay, J., Downes, C. P., Holder, J. C. and Cohen, P. (1997). Insulin activates protein kinase B, inhibits glycogen synthase kinase-3 and activates glycogen synthase by rapamycin-insensitive pathways in skeletal muscle and adipose tissue. *FEBS Lett* 406, 211-5.

Cui, H., Meng, Y. and Bulleit, R. F. (1998). Inhibition of glycogen synthase kinase 3beta activity regulates proliferation of cultured cerebellar granule cells. *Brain Res Dev Brain Res* 111, 177-88.

Davidoff, F. F. (1964). The Metabolism of 9(10)-Hydroxystearic Acid by the Cellular Slime Mold, *Dictyostelium discoideum*. *Biochim Biophys Acta* 90, 414-6.

de Groot, R. P., Auwerx, J., Bourouis, M. and Sassone-Corsi, P. (1993). Negative regulation of Jun/AP-1: conserved function of glycogen synthase kinase 3 and the *Drosophila* kinase shaggy. *Oncogene* 8, 841-7.

Delcommenne, M., Tan, C., Gray, V., Rue, L., Woodgett, J. and Dedhar, S. (1998). Phosphoinositide-3-OH kinase-dependent regulation of glycogen synthase kinase 3 and protein kinase B/AKT by the integrin-linked kinase. *Proc Natl Acad Sci U S A* 95, 11211-6.

DePaoli-Roach, A. A. (1984). Synergistic phosphorylation and activation of ATP-Mg-dependent phosphoprotein phosphatase by F A/GSK-3 and casein kinase II (PC0.7). *J Biol Chem* 259, 12144-52.

Devreotes, P. (1989). *Dictyostelium discoideum*: a model system for cell-cell interactions in development. *Science* 245, 1054-8.

Ding, V. W., Chen, R. H. and McCormick, F. (2000). Differential regulation of glycogen synthase kinase 3beta by insulin and Wnt signaling. *J Biol Chem* 275, 32475-81.

Dominguez, I., Itoh, K. and Sokol, S. Y. (1995). Role of glycogen synthase kinase 3 beta as a negative regulator of dorsoventral axis formation in *Xenopus* embryos. *Proc Natl Acad Sci U S A* 92, 8498-502.

Eichinger, L., Pachebat, J. A., Glockner, G., Rajandream, M. A., Sucgang, R., Berriman, M., Song, J., Olsen, R., Szafranski, K., Xu, Q. et al. (2005). The genome of the social amoeba *Dictyostelium discoideum*. *Nature* 435, 43-57.

Embi, N., Rylatt, D. B. and Cohen, P. (1980). Glycogen synthase kinase-3 from rabbit skeletal muscle. Separation from cyclic-AMP-dependent protein kinase and phosphorylase kinase. *Eur J Biochem* 107, 519-27.

Etienne-Manneville, S. and Hall, A. (2003). Cdc42 regulates GSK-3beta and adenomatous polyposis coli to control cell polarity. *Nature* 421, 753-6.

Farr, G. H., 3rd, Ferkey, D. M., Yost, C., Pierce, S. B., Weaver, C. and Kimelman, D. (2000). Interaction among GSK-3, GBP, axin, and APC in *Xenopus* axis specification. *J Cell Biol* 148, 691-702.

Fiol, C. J., Haseman, J. H., Wang, Y. H., Roach, P. J., Roeske, R. W., Kowalczuk, M. and DePaoli-Roach, A. A. (1988). Phosphoserine as a recognition determinant for glycogen synthase kinase-3: phosphorylation of a synthetic peptide based on the G-component of protein phosphatase-1. *Arch Biochem Biophys* 267, 797-802.

Fiol, C. J., Wang, A., Roeske, R. W. and Roach, P. J. (1990). Ordered multisite protein phosphorylation. Analysis of glycogen synthase kinase 3 action using model peptide substrates. *J Biol Chem* 265, 6061-5.

Fiol, C. J., Williams, J. S., Chou, C. H., Wang, Q. M., Roach, P. J. and Andrisani, O. M. (1994). A secondary phosphorylation of CREB341 at Ser129 is required for the cAMP-mediated control of gene expression. A role for glycogen synthase kinase-3 in the control of gene expression. *J Biol Chem* 269, 32187-93.

Funamoto, S., Meili, R., Lee, S., Parry, L. and Firtel, R. A. (2002). Spatial and temporal regulation of 3-phosphoinositides by PI 3-kinase and PTEN mediates chemotaxis. *Cell* 109, 611-23.

Funamoto, S., Milan, K., Meili, R. and Firtel, R. A. (2001). Role of phosphatidylinositol 3' kinase and a downstream pleckstrin homology domain-containing protein in controlling chemotaxis in *Dictyostelium*. *J Cell Biol* 153, 795-810.

Galletti, M., Riccardo, S., Parisi, F., Lora, C., Saqcena, M. K., Rivas, L., Wong, B., Serra, A., Serras, F., Grifoni, D. et al. (2009). Identification of domains responsible for ubiquitin-dependent degradation of dMyc by glycogen synthase kinase 3beta and casein kinase 1 kinases. *Mol Cell Biol* 29, 3424-34.

Gerisch, G. (1982). Chemotaxis in *Dictyostelium*. *Annu Rev Physiol* 44, 535-52.

Gerisch, G. and Huesgen, A. (1976). Cell aggregation and sexual differentiation in pairs of aggregation-deficient mutants of *Dictyostelium discoideum*. *J Embryol Exp Morphol* 36, 431-42.

Grebe, T. W. and Stock, J. (1998). Bacterial chemotaxis: the five sensors of a bacterium. *Curr Biol* 8, R154-7.

Gregory, M. A., Qi, Y. and Hann, S. R. (2003). Phosphorylation by glycogen synthase kinase-3 controls c-myc proteolysis and subnuclear localization. *J Biol Chem* 278, 51606-12.

Grimes, C. A. and Jope, R. S. (2001a). CREB DNA binding activity is inhibited by glycogen synthase kinase-3 beta and facilitated by lithium. *J Neurochem* 78, 1219-32.

Grimes, C. A. and Jope, R. S. (2001b). The multifaceted roles of glycogen synthase kinase 3beta in cellular signaling. *Prog Neurobiol* 65, 391-426.

Halse, R., Rochford, J. J., McCormack, J. G., Vandenheede, J. R., Hemmings, B. A. and Yeaman, S. J. (1999). Control of glycogen synthesis in cultured human muscle cells. *J Biol Chem* 274, 776-80.

Han, J. W., Leeper, L., Rivero, F. and Chung, C. Y. (2006). Role of RacC for the regulation of WASP and phosphatidylinositol 3-kinase during chemotaxis of *Dictyostelium*. *J Biol Chem* 281, 35224-34.

Hart, M. J., de los Santos, R., Albert, I. N., Rubinfeld, B. and Polakis, P. (1998). Downregulation of beta-catenin by human Axin and its association with the APC tumor suppressor, beta-catenin and GSK3 beta. *Curr Biol* 8, 573-81.

Hartigan, J. A. and Johnson, G. V. (1999). Transient increases in intracellular calcium result in prolonged site-selective increases in Tau phosphorylation through a glycogen synthase kinase 3beta-dependent pathway. *J Biol Chem* 274, 21395-401.

Harwood, A. J., Plyte, S. E., Woodgett, J., Strutt, H. and Kay, R. R. (1995). Glycogen synthase kinase 3 regulates cell fate in *Dictyostelium*. *Cell* 80, 139-48.

Hawkins, P.T., T.R. Jackson, and L.R. Stephens. 1992. Platelet-derived growth factor stimulates synthesis of PtdIns(3,4,5)P3 by activating a PtdIns(4,5)P2 3-OH kinase. *Nature*. 358:157-9.

Hedgepeth, C. M., Deardorff, M. A., Rankin, K. and Klein, P. S. (1999). Regulation of glycogen synthase kinase 3beta and downstream Wnt signaling by axin. *Mol Cell Biol* 19, 7147-57.

Hemmings, B. A., Aitken, A., Cohen, P., Rymond, M. and Hofmann, F. (1982a). Phosphorylation of the type-II regulatory subunit of cyclic-AMP-dependent protein kinase by glycogen synthase kinase 3 and glycogen synthase kinase 5. *Eur J Biochem* 127, 473-81.

Hemmings, B. A. and Cohen, P. (1983). Glycogen synthase kinase-3 from rabbit skeletal muscle. *Methods Enzymol* 99, 337-45.

Hemmings, B. A., Resink, T. J. and Cohen, P. (1982b). Reconstitution of a Mg-ATP-dependent protein phosphatase and its activation through a phosphorylation mechanism. *FEBS Lett* 150, 319-24.

Hemmings, B. A., Yellowlees, D., Kernohan, J. C. and Cohen, P. (1981). Purification of glycogen synthase kinase 3 from rabbit skeletal muscle. Copurification with the activating factor (FA) of the (Mg-ATP) dependent protein phosphatase. *Eur J Biochem* 119, 443-51.

Henry, S. P. and Killilea, S. D. (1993). Hierarchical regulation by casein kinases I and II of the activation of protein phosphatase-1i by glycogen synthase kinase-3 is ionic strength dependent. *Arch Biochem Biophys* 301, 53-7.

Hirsch, E., V.L. Katanaev, C. Garlanda, O. Azzolino, L. Pirola, L. Silengo, S. Sozzani, A. Mantovani, F. Altruda, and M.P. Wymann. 2000. Central role for G protein-coupled phosphoinositide 3-kinase gamma in inflammation. *Science*. 287:1049-53.

Hoeller, O. and Kay, R. R. (2007). Chemotaxis in the absence of PIP3 gradients. *Curr Biol* 17, 813-7.

Hughes, K., Nikolakaki, E., Plyte, S. E., Totty, N. F. and Woodgett, J. R. (1993). Modulation of the glycogen synthase kinase-3 family by tyrosine phosphorylation. *Embo J* 12, 803-8.

Hughes, K., Ramakrishna, S., Benjamin, W. B. and Woodgett, J. R. (1992). Identification of multifunctional ATP-citrate lyase kinase as the alpha-isoform of glycogen synthase kinase-3. *Biochem J* 288 (Pt 1), 309-14.

Iijima, M. and Devreotes, P. (2002). Tumor suppressor PTEN mediates sensing of chemoattractant gradients. *Cell* 109, 599-610.

Iijima, M., Huang, Y. E. and Devreotes, P. (2002). Temporal and spatial regulation of chemotaxis. *Dev Cell* 3, 469-78.

Iijima, M., Huang, Y. E., Luo, H. R., Vazquez, F. and Devreotes, P. N. (2004). Novel mechanism of PTEN regulation by its phosphatidylinositol 4,5-bisphosphate binding motif is critical for chemotaxis. *J Biol Chem* 279, 16606-13.

Insall, R. (1995). Glycogen synthase kinase and *Dictyostelium* development: old pathways pointing in new directions? *Trends Genet* 11, 37-9.

Itoh, K., Krupnik, V. E. and Sokol, S. Y. (1998). Axis determination in *Xenopus* involves biochemical interactions of axin, glycogen synthase kinase 3 and beta-catenin. *Curr Biol* 8, 591-4.

Jiang, H., Guo, W., Liang, X. and Rao, Y. (2005). Both the establishment and the maintenance of neuronal polarity require active mechanisms: critical roles of GSK-3beta and its upstream regulators. *Cell* 120, 123-35.

Jiang, W., Betson, M., Mulloy, R., Foster, R., Levay, M., Ligeti, E. and Settleman, J. (2008). p190A RhoGAP is a glycogen synthase kinase-3-beta substrate required for polarized cell migration. *J Biol Chem* 283, 20978-88.

Kae, H., Lim, C. J., Spiegelman, G. B. and Weeks, G. (2004). Chemoattractant-induced Ras activation during *Dictyostelium* aggregation. *EMBO Rep* 5, 602-6.

Kamimura, Y. and Devreotes, P. N. (2010). Phosphoinositide-dependent protein kinase (PDK) activity regulates phosphatidylinositol 3,4,5-trisphosphate-dependent and –independent protein kinase B activation and chemotaxis. *J Biol Chem* 285, 7938-46.

Kamimura, Y., Xiong, Y., Iglesias, P. A., Hoeller, O., Bolourani, P. and Devreotes, P. N. (2008). PIP3-independent activation of TorC2 and PKB at the cell's leading edge mediates chemotaxis. *Curr Biol* 18, 1034-43.

Kim, B. J., Choi, C. H., Lee, C. H., Jeong, S. Y., Kim, J. S., Kim, B. Y., Yim, H. S. and Kang, S. O. (2005). Glutathione is required for growth and prespore cell differentiation in *Dictyostelium*. *Dev Biol* 284, 387-98.

Kim, L., Brzostowski, J., Majithia, A., Lee, N. S., McMains, V. and Kimmel, A. R. (2011). Combinatorial cell-specific regulation of GSK3 directs cell differentiation and polarity in *Dictyostelium*. *Development* 138, 421-30.

Kim, L., Harwood, A. and Kimmel, A. R. (2002). Receptor-dependent and tyrosine phosphatase-mediated inhibition of GSK3 regulates cell fate choice. *Dev Cell* 3, 523-32.

Kim, L. and Kimmel, A. R. (2000). GSK3, a master switch regulating cell-fate specification and tumorigenesis. *Curr Opin Genet Dev* 10, 508-14.

Kim, L. and Kimmel, A. R. (2006). GSK3 at the edge: regulation of developmental specification and cell polarization. *Curr Drug Targets* 7, 1411-9.

Kim, L., Liu, J. and Kimmel, A. R. (1999). The novel tyrosine kinase ZAK1 activates GSK3 to direct cell fate specification. *Cell* 99, 399-408.

King, J. S. and Insall, R. H. (2009). Chemotaxis: finding the way forward with *Dictyostelium*. *Trends Cell Biol* 19, 523-30.

King, J. S., Teo, R., Ryves, J., Reddy, J. V., Peters, O., Orabi, B., Hoeller, O., Williams, R. S. and Harwood, A. J. (2009). The mood stabiliser lithium suppresses PIP3 signalling in *Dictyostelium* and human cells. *Dis Model Mech* 2, 306-12.

Kishida, S., Yamamoto, H., Ikeda, S., Kishida, M., Sakamoto, I., Koyama, S. and Kikuchi, A. (1998). Axin, a negative regulator of the Wnt signaling pathway, directly interacts with adenomatous polyposis coli and regulates the stabilization of beta-catenin. *J Biol Chem* 273, 10823-6.

Kolsch, V., Shen, Z., Lee, S., Plak, K., Lotfi, P., Chang, J., Charest, P. G., Romero, J. L., Jeon, T. J., Kortholt, A. et al. (2012). Daydreamer, a Ras effector and GSK-3 substrate, is important for directional sensing and cell motility. *Mol Biol Cell*.

Konijn, T. M. and Van Haastert, P. J. (1987). Measurement of chemotaxis in *Dictyostelium*. *Methods Cell Biol* 28, 283-98.

Kortholt, A., Kataria, R., Keizer-Gunnink, I., Van Egmond, W. N., Khanna, A. and Van Haastert, P. J. (2011). *Dictyostelium* chemotaxis: essential Ras activation and accessory signalling pathways for amplification. *EMBO Rep* 12, 1273-9.

Lardy, B., Bof, M., Aubry, L., Paclet, M. H., Morel, F., Satre, M. and Klein, G. (2005). NADPH oxidase homologs are required for normal cell differentiation and

morphogenesis in *Dictyostelium discoideum*. *Biochim Biophys Acta* 1744, 199-212.

Lee, S., Comer, F. I., Sasaki, A., McLeod, I. X., Duong, Y., Okumura, K., Yates, J. R., 3rd, Parent, C. A. and Firtel, R. A. (2005). TOR complex 2 integrates cell movement during chemotaxis and signal relay in *Dictyostelium*. *Mol Biol Cell* 16, 4572-83.

Lesort, M., Jope, R. S. and Johnson, G. V. (1999). Insulin transiently increases tau phosphorylation: involvement of glycogen synthase kinase-3beta and Fyn tyrosine kinase. *J Neurochem* 72, 576-84.

Liao, X. H., Majithia, A., Huang, X. and Kimmel, A. R. (2008). Growth control via TOR kinase signaling, an intracellular sensor of amino acid and energy availability, with crosstalk potential to proline metabolism. *Amino Acids* 35, 761-70.

Loovers, H. M., Kortholt, A., de Groote, H., Whitty, L., Nussbaum, R. L. and van Haastert, P. J. (2007). Regulation of phagocytosis in *Dictyostelium* by the inositol 5-phosphatase OCRL homolog Dd5P4. *Traffic* 8, 618-28.

Loovers, H. M., Postma, M., Keizer-Gunnink, I., Huang, Y. E., Devreotes, P. N. and van Haastert, P. J. (2006). Distinct roles of PI(3,4,5)P3 during chemoattractant signaling in *Dictyostelium*: a quantitative in vivo analysis by inhibition of PI3-kinase. *Mol Biol Cell* 17, 1503-13.

Louis, J. M., Ginsburg, G. T. and Kimmel, A. R. (1994). The cAMP receptor CAR4 regulates axial patterning and cellular differentiation during late development of *Dictyostelium*. *Genes Dev* 8, 2086-96.

Louis, S.A., G.B. Spiegelman, and G. Weeks. 1997. Expression of an activated *rasD* gene changes cell fate decisions during Dictyostelium development. *Mol Biol Cell*. 8:303-12.

Mondal, S., Subramanian, K. K., Sakai, J., Bajrami, B. and Luo, H. R. (2012). Phosphoinositide lipid phosphatase SHIP1 and PTEN coordinate to regulate cell migration and adhesion. *Mol Biol Cell* 23, 1219-30.

Morisco, C., Zebrowski, D., Condorelli, G., Tsichlis, P., Vatner, S. F. and Sadoshima, J. (2000). The Akt-glycogen synthase kinase 3beta pathway regulates transcription of atrial natriuretic factor induced by beta-adrenergic receptor stimulation in cardiac myocytes. *J Biol Chem* 275, 14466-75.

Moule, S. K., Welsh, G. I., Edgell, N. J., Foulstone, E. J., Proud, C. G. and Denton, R. M. (1997). Regulation of protein kinase B and glycogen synthase kinase-3 by insulin and beta-adrenergic agonists in rat epididymal fat cells. Activation of protein

kinase B by wortmannin-sensitive and -insensitive mechanisms. *J Biol Chem* 272, 7713-9.

Murai, H., Okazaki, M. and Kikuchi, A. (1996). Tyrosine dephosphorylation of glycogen synthase kinase-3 is involved in its extracellular signal-dependent inactivation. *FEBS Lett* 392, 153-60.

Nagano, S. (2000). Modeling the model organism *Dictyostelium discoideum*. *Dev Growth Differ* 42, 541-50.

Neal, J. W. and Clipstone, N. A. (2001). Glycogen synthase kinase-3 inhibits the DNA binding activity of NFATc. *J Biol Chem* 276, 3666-73.

Newell, P. C., Europe-Finner, G. N. and Small, N. V. (1987). Signal transduction during amoebal chemotaxis of *Dictyostelium discoideum*. *Microbiol Sci* 4, 5-11.

Nikolakaki, E., Coffer, P. J., Hemelsoet, R., Woodgett, J. R. and Defize, L. H. (1993). Glycogen synthase kinase 3 phosphorylates Jun family members *in vitro* and negatively regulates their transactivating potential in intact cells. *Oncogene* 8, 833-40.

Nishio, M., Watanabe, K., Sasaki, J., Taya, C., Takasuga, S., Iizuka, R., Balla, T., Yamazaki, M., Watanabe, H., Itoh, R. et al. (2007). Control of cell polarity and motility by the PtdIns(3,4,5)P3 phosphatase SHIP1. *Nat Cell Biol* 9, 36-44.

Palanivelu, R. and Preuss, D. (2000). Pollen tube targeting and axon guidance: parallels in tip growth mechanisms. *Trends Cell Biol* 10, 517-24.

Pap, M. and Cooper, G. M. (1998). Role of glycogen synthase kinase-3 in the phosphatidylinositol 3-Kinase/Akt cell survival pathway. *J Biol Chem* 273, 19929-32.

Papkoff, J. and Aikawa, M. (1998). WNT-1 and HGF regulate GSK3 beta activity and beta-catenin signaling in mammary epithelial cells. *Biochem Biophys Res Commun* 247, 851-8.

Parent, C. A. (2004). Making all the right moves: chemotaxis in neutrophils and *Dictyostelium*. *Curr Opin Cell Biol* 16, 4-13.

Parent, C. A., Blacklock, B. J., Froehlich, W. M., Murphy, D. B. and Devreotes, P. N. (1998). G protein signaling events are activated at the leading edge of chemotactic cells. *Cell* 95, 81-91.

Parent, C. A. and Devreotes, P. N. (1999). A cell's sense of direction. *Science* 284, 765-70.

Peifer, M., Sweeton, D., Casey, M. and Wieschaus, E. (1994). wingless signal and Zeste-white 3 kinase trigger opposing changes in the intracellular distribution of Armadillo. *Development* 120, 369-80.

Plyte, S. E., O'Donovan, E., Woodgett, J. R. and Harwood, A. J. (1999). Glycogen synthase kinase-3 (GSK-3) is regulated during *Dictyostelium* development via the serpentine receptor cAR3. *Development* 126, 325-33.

Raper, K. B. and Smith, N. R. (1939). The growth of *Dictyostelium discoideum* upon pathogenic bacteria. *J Bacteriol* 38, 431-45.

Rappel, W. J. and Loomis, W. F. (2009). Eukaryotic chemotaxis. *Wiley Interdiscip Rev Syst Biol Med* 1, 141-9.

Ross, S. E., Erickson, R. L., Hemati, N. and MacDougald, O. A. (1999). Glycogen synthase kinase 3 is an insulin-regulated C/EBPalpha kinase. *Mol Cell Biol* 19, 8433-41.

Rubinfeld, B., Albert, I., Porfiri, E., Fiol, C., Munemitsu, S. and Polakis, P. (1996). Binding of GSK3beta to the APC-beta-catenin complex and regulation of complex assembly. *Science* 272, 1023-6.

Ruel, L., Stambolic, V., Ali, A., Manoukian, A. S. and Woodgett, J. R. (1999). Regulation of the protein kinase activity of Shaggy(Zeste-white3) by components of the wingless pathway in *Drosophila* cells and embryos. *J Biol Chem* 274, 21790-6.

Ryves, W. J., Fryer, L., Dale, T. and Harwood, A. J. (1998). An assay for glycogen synthase kinase 3 (GSK-3) for use in crude cell extracts. *Anal Biochem* 264, 124-7.

Sagi, Y., Khan, S. and Eisenbach, M. (2003). Binding of the chemotaxis response regulator CheY to the isolated, intact switch complex of the bacterial flagellar motor: lack of cooperativity. *J Biol Chem* 278, 25867-71.

Sasaki, T., J. Irie-Sasaki, R.G. Jones, A.J. Oliveira-dos-Santos, W.L. Stanford, B. Bolon, A. Wakeham, A. Itie, D. Bouchard, I. Kozieradzki, N. Joza, T.W. Mak, P.S. Ohashi, A. Suzuki, and J.M. Penninger. 2000. Function of PI3Kgamma in thymocyte development, T cell activation, and neutrophil migration. *Science*. 287:1040-6.

Sasaki, A. T., Chun, C., Takeda, K. and Firtel, R. A. (2004). Localized Ras signaling at the leading edge regulates PI3K, cell polarity, and directional cell movement. *J Cell Biol* 167, 505-18.

Sasaki, A. T. and Firtel, R. A. (2005). Finding the way: directional sensing and cell polarization through Ras signalling. *Novartis Found Symp* 269, 73-87; discussion 87-91, 223-30.

Sasaki, A. T. and Firtel, R. A. (2006). Regulation of chemotaxis by the orchestrated activation of Ras, PI3K, and TOR. *Eur J Cell Biol* 85, 873-95.

Sasaki, A. T., Janetopoulos, C., Lee, S., Charest, P. G., Takeda, K., Sundheimer, L. W., Meili, R., Devreotes, P. N. and Firtel, R. A. (2007). G protein-independent Ras/PI3K/F-actin circuit regulates basic cell motility. *J Cell Biol* 178, 185-91.

Scharf, B. E., Fahrner, K. A., Turner, L. and Berg, H. C. (1998). Control of direction of flagellar rotation in bacterial chemotaxis. *Proc Natl Acad Sci U S A* 95, 201-6.

Schlesinger, A., Shelton, C. A., Maloof, J. N., Meneghini, M. and Bowerman, B. (1999). Wnt pathway components orient a mitotic spindle in the early *Caenorhabditis elegans* embryo without requiring gene transcription in the responding cell. *Genes Dev* 13, 2028-38.

Schwartz, R., Brooks, W. and Zinsser, H. H. (1958). Evidence of chemotaxis as a factor in sperm motility. *Fertil Steril* 9, 300-8.

Sheridan, C. M., Heist, E. K., Beals, C. R., Crabtree, G. R. and Gardner, P. (2002). Protein kinase A negatively modulates the nuclear accumulation of NF-ATc1 by priming for subsequent phosphorylation by glycogen synthase kinase-3. *J Biol Chem* 277, 48664-76.

Spohn, G. and Scarlato, V. (2001). Motility, Chemotaxis, and Flagella. In *Helicobacter pylori: Physiology and Genetics*, (eds H. L. T. Mobley G. L. Mendz and S. L. Hazell). Washington (DC).

Strmecki, L., Bloomfield, G., Araki, T., Dalton, E., Skelton, J., Schilde, C., Harwood, A., Williams, J. G., Ivens, A. and Pears, C. (2007). Proteomic and microarray analyses of the *Dictyostelium* Zak1-GSK-3 signaling pathway reveal a role in early development. *Eukaryot Cell* 6, 245-52.

Sun, T., Rodriguez, M. and Kim, L. (2009). Glycogen synthase kinase 3 in the world of cell migration. *Dev Growth Differ* 51, 735-42.

Sun, W., Qureshi, H. Y., Cafferty, P. W., Sobue, K., Agarwal-Mawal, A., Neufield, K. D. and Paudel, H. K. (2002). Glycogen synthase kinase-3beta is complexed with tau protein in brain microtubules. *J Biol Chem* 277, 11933-40.

Sutherland, C., Leighton, I. A. and Cohen, P. (1993). Inactivation of glycogen synthase kinase-3 beta by phosphorylation: new kinase connections in insulin and growth-factor signalling. *Biochem J* 296 (Pt 1), 15-9.

Takahashi-Yanaga, F., Shiraishi, F., Hirata, M., Miwa, Y., Morimoto, S. and Sasaguri, T. (2004). Glycogen synthase kinase-3beta is tyrosine-phosphorylated by MEK1 in human skin fibroblasts. *Biochem Biophys Res Commun* 316, 411-5.

Teo, R., Lewis, K. J., Forde, J. E., Ryves, W. J., Reddy, J. V., Rogers, B. J. and Harwood, A. J. (2010). Glycogen synthase kinase-3 is required for efficient *Dictyostelium* chemotaxis. *Mol Biol Cell* 21, 2788-96.

Trivedi, N., Marsh, P., Goold, R. G., Wood-Kaczmar, A. and Gordon-Weeks, P. R. (2005). Glycogen synthase kinase-3beta phosphorylation of MAP1B at Ser1260 and Thr1265 is spatially restricted to growing axons. *J Cell Sci* 118, 993-1005.

Tsujio, I., Tanaka, T., Kudo, T., Nishikawa, T., Shinozaki, K., Grundke-Iqbal, I., Iqbal, K. and Takeda, M. (2000). Inactivation of glycogen synthase kinase-3 by protein kinase C delta: implications for regulation of tau phosphorylation. *FEBS Lett* 469, 111-7.

Tullai, J. W., Chen, J., Schaffer, M. E., Kamenetsky, E., Kasif, S. and Cooper, G. M. (2007). Glycogen synthase kinase-3 represses cyclic AMP response element-binding protein (CREB)-targeted immediate early genes in quiescent cells. *J Biol Chem* 282, 9482-91.

van der Velden, J. L., Schols, A. M., Willems, J., Kelders, M. C. and Langen, R. C. (2008). Glycogen synthase kinase 3 suppresses myogenic differentiation through negative regulation of NFATc3. *J Biol Chem* 283, 358-66.

van Haastert, P. J., Keizer-Gunnink, I. and Kortholt, A. (2007). Essential role of PI3-kinase and phospholipase A2 in *Dictyostelium discoideum* chemotaxis. *J Cell Biol* 177, 809-16.

Vedham, V., H. Phee, and K.M. Coggeshall. 2005. Vav activation and function as a rac guanine nucleotide exchange factor in macrophage colony-stimulating factor-induced macrophage chemotaxis. *Mol Cell Biol*. 25:4211-20.

Veeranki, S., Kim, B. and Kim, L. (2008). The GPI-anchored superoxide dismutase SodC is essential for regulating basal Ras activity and for chemotaxis of *Dictyostelium discoideum*. *J Cell Sci* 121, 3099-108.

Veltman, D. M., Roelofs, J., Engel, R., Visser, A. J. and Van Haastert, P. J. (2005). Activation of soluble guanylyl cyclase at the leading edge during *Dictyostelium* chemotaxis. *Mol Biol Cell* 16, 976-83.

Veltman, D. M. and Van Haastert, P. J. (2006). Guanylyl cyclase protein and cGMP product independently control front and back of chemotaxing *Dictyostelium* cells. *Mol Biol Cell* 17, 3921-9.

Vlahou, G. and Rivero, F. (2006). Rho GTPase signaling in *Dictyostelium discoideum*: insights from the genome. *Eur J Cell Biol* 85, 947-59.

Walston, T. D. and Hardin, J. (2006). Wnt-dependent spindle polarization in the early C. elegans embryo. *Semin Cell Dev Biol* 17, 204-13.

Wang, Q. M., Fiol, C. J., DePaoli-Roach, A. A. and Roach, P. J. (1994). Glycogen synthase kinase-3 beta is a dual specificity kinase differentially regulated by tyrosine and serine/threonine phosphorylation. *J Biol Chem* 269, 14566-74.

Weiger, M.C., and C.A. Parent. 2012. Phosphoinositides in chemotaxis. *Subcell Biochem*. 59:217-54.

Wennstrom, S., A. Siegbahn, K. Yokote, A.K. Arvidsson, C.H. Heldin, S. Mori, and L. Claesson-Welsh. 1994. Membrane ruffling and chemotaxis transduced by the PDGF beta-receptor require the binding site for phosphatidylinositol 3' kinase. *Oncogene*. 9:651-60.

Woodgett, J. R. (1990). Molecular cloning and expression of glycogen synthase kinase-3/factor A. *Embo J* 9, 2431-8.

Woodgett, J. R. and Cohen, P. (1984). Multisite phosphorylation of glycogen synthase. Molecular basis for the substrate specificity of glycogen synthase kinase-3 and casein kinase-II (glycogen synthase kinase-5). *Biochim Biophys Acta* 788, 339-47.

Xavier, I. J., Mercier, P. A., McLoughlin, C. M., Ali, A., Woodgett, J. R. and Ovsenek, N. (2000). Glycogen synthase kinase 3beta negatively regulates both DNA-binding and transcriptional activities of heat shock factor 1. *J Biol Chem* 275, 29147-52.

Yamamoto, H., Kishida, S., Kishida, M., Ikeda, S., Takada, S. and Kikuchi, A. (1999). Phosphorylation of axin, a Wnt signal negative regulator, by glycogen synthase kinase-3beta regulates its stability. *J Biol Chem* 274, 10681-4.

Yoshimura, T., Kawano, Y., Arimura, N., Kawabata, S. and Kaibuchi, K. (2005a). [Molecular mechanisms of neuronal polarity]. *Nihon Shinkei Seishin Yakurigaku Zasshi* 25, 169-74.

Yoshimura, T., Kawano, Y., Arimura, N., Kawabata, S., Kikuchi, A. and Kaibuchi, K. (2005b). GSK-3beta regulates phosphorylation of CRMP-2 and neuronal polarity. *Cell* 120, 137-49.

Yost, C., Farr, G. H., Pierce, S. B., Ferkey, D. M., Chen, M. M. and Kimelman, D. (1998). GBP, an inhibitor of GSK-3, is implicated in *Xenopus* development and oncogenesis. *Cell* 93, 1031-41.

Yost, C., Torres, M., Miller, J. R., Huang, E., Kimelman, D. and Moon, R. T. (1996). The axis-inducing activity, stability, and subcellular distribution of beta-catenin is regulated in *Xenopus* embryos by glycogen synthase kinase 3. *Genes Dev* 10, 1443-54.

Zouwail, S., Pettitt, T. R., Dove, S. K., Chibalina, M. V., Powner, D. J., Haynes, L., Wakelam, M. J. and Insall, R. H. (2005). Phospholipase D activity is essential for actin localization and actin-based motility in *Dictyostelium*. *Biochem J* 389, 207-14.

APPENDICES

Figure A1 DNA sequence of PI3K1-LD (1476 bp).

```
1       ATGAATAGTA TTGAAAGTTC TTCTAATGAT AGCAATGAGA TAAATAAAAA
51      TTCAAACAAA AATAATACAC ACTTAAACTC CAACTATAAT AATATTTATA
101     AAAATAATAG CACTAGTAGT AATAATAATA ATAATCATAA TAATATTGAA
151     ATTATTGGGA TAGATAATAA TAAAAATAAT AATAAAAATA ATAACGATAA
201     TAATAATAAT AATAATAATA TAGATAAAAA AAGAAAGGAT AGTAAAAATA
251     AACAAAACCA AGAAATAAAT CAAGAAATGT CAGAAAATAA AAAAATTTAT
301     AATAGTAATG ATAGTAATTG TAGTAGTGGT AGTAGTAGTG GAGGACATGT
351     AAATAATGGT CATCATATAT TAATTGAAGA GAATGAAAGA TTAGAACATG
401     AAAATCAAGA GATTCAAGAA ATTTATAAAC AAAAGGGTAT GGAATTTCAA
451     AAAAAAGATT TAAGATTTGG ATATGATGTT AATAGTAATA ATAATAATAA
501     TAATGGTGGT GGTAGTAGCA GTGGTAGTAG CAGTGGTGGT AGTGATGAAT
551     CTGCTTCAAA TCAACCTATA ATTAGAACTA GAAATAGAGA AGGTTCAATT
601     TTAAATTTAA AGAAACAAGG TCTTGTAAAA GAAATTAGTC AAAGATTTCA
651     AACACCAGAT ACAGCATCAT ATACAAGACC AAATGCAAAT AATATTTCAA
701     TTAAAGATAA AATTTCTATA TTAAAAAAGG AGCAAGAAAG AAGAAAACAA
751     GATTCAGAAG TACAACAACG AGAAAAGGTT ATAGTATTAT CAGCAGATAG
801     TTCAAATATT CAAATTTATC ATCCCTCTGT TTTAATAGAA AAAATGAATA
851     GTAAATTGGA TACCGAAGAA AAGCCAGCAA CAACGACAAC AACTACTACT
901     ACAACATCAA CATCAATATC AACATCAACA CCAACAACTA CTACTACTAC
951     TACAACTAAT ACTTCTACTA CTAATGATAT TACAATTAAA CCAAAAACAT
1001    CACCAACAAA AAATAATGAA GAAAGATCAC AATCACCAAT TACAACACCA
1051    AAACAACCAG TTGAAGAAAT TGTTAAAAAA GTATCAACAC CAAAATCAAA
1101    TAATACTTCT AAAAAGACAT CATCCGATAC AACACCAACA GGAAAAACAA
1151    CTAAAAAAGA TAAAAAAGAT AAAAAAGATA AATCAAGAGA TAGTGGTAAT
1201    TTAGTAATTG TTAATAATAC TAATAATACT AGTAGTAATA ATAACAATAA
1251    TAATAATAAT AATAATAATA ATGAAACAAT TATAAAACGT AGAGGTAGAG
1301    TTTTAGTTAC ACCATCAAGT GATTTAAAAA AGAATATTCA AATTTATTTT
1351    ACAATTCCAA TAAATCCACC AGTAAATAAA ACCAATAAAC CAAATCAATT
1401    ATTATCAAAT ACATCACAAC AATTTTTAAA AACATTAATT TCAAATGAAA
1451    TTCCAATCGA TTGTAAAATC AATGAT
```

Figure A2 Protein sequence of PI3K1-LD (492 amino acids) with potential GSK3 phosphorylation sites underlined.

```
1       MNSIESSSND SNEINKNSNK NNTHLNSNYN NIYKNNSTSS NNNNNHNNIE
51      IIGIDNNKNN NKNNNDNNNN NNNIDKKRKD SKNKQNQEIN QEMSENKKIY
101     NSNDSNCSSG SSSGGHVNNG HHILIEENER LEHENQEIQE IYKQKGMEFQ
151     KKDLRFGYDV NSNNNNNNGG GSSSGSSSGG SDESASNQPI IRTRNREGSI
201     LNLKKQGLVK EISQRFQTPD TASYTRPNAN NISIKDKISI LKKEQERRKQ
251     DSEVQQREKV IVLSADSSNI QIYHPSVLIE KMNSKLDTEE KPATTTTTTT
301     TTSTSISTST PTTTTTTTTN TSTTNDITIK PKTSPTKNNE ERSQSPITTP
351     KQPVEEIVKK VSTPKSNNTS KKTSSDTTPT GKTTKKDKKD KKDKSRDSGN
401     LVIVNNTNNT SSNNNNNNNN NNNNETIIKR RGRVLVTPSS DLKKNIQIYF
451     TIPINPPVNK TNKPNQLLSN TSQQFLKTLI SNEIPIDCKI ND
```

Figure A3 Map of PGEX-4T-1 IPTG inducible vector.

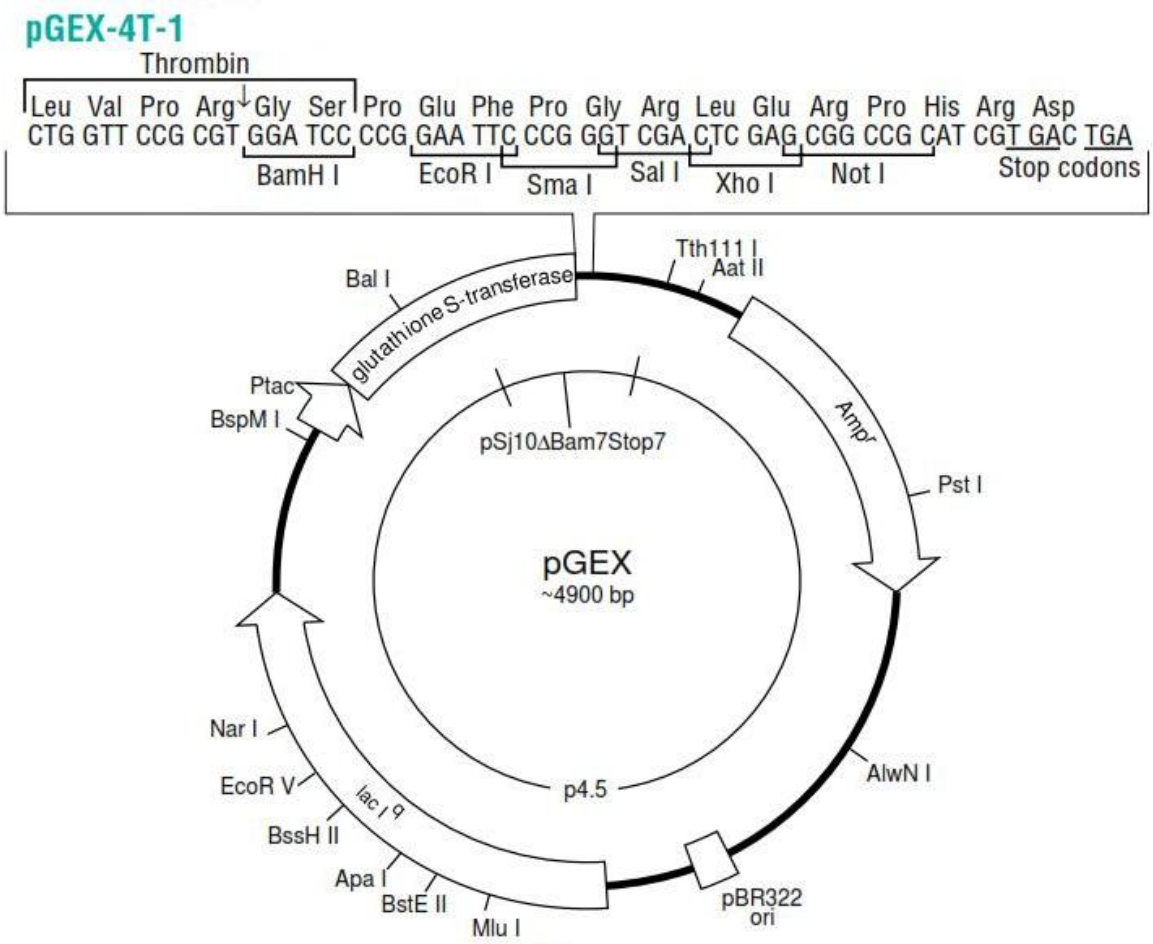

Figure A4 Map of expression vector EXP-4 (+).

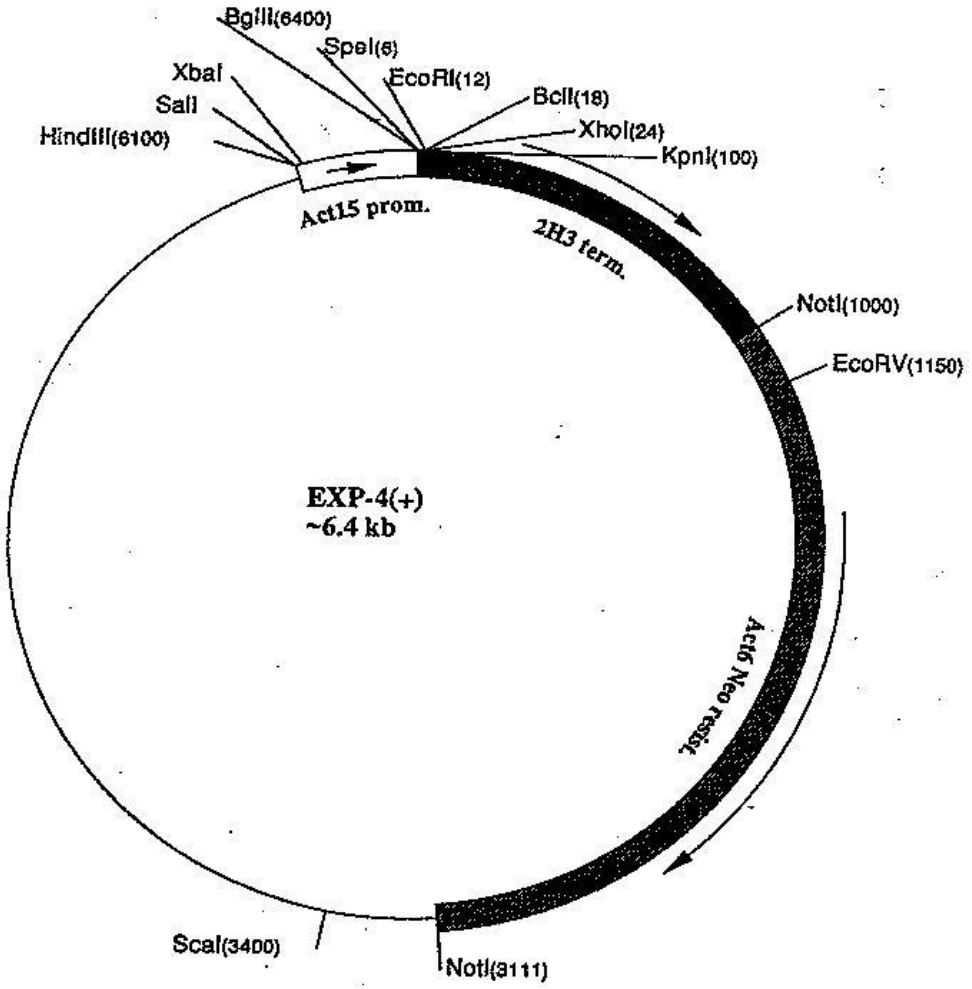

Figure A5 Map of expression vector EXP-4 (+)-GST-PI3K1-LD. which is generated from EXP-4(+) in figure A4. PI3K1-LD contains no intro and has a stop codon at its C-terminal. A thrombin cutting site lies immediate downstream of GST.

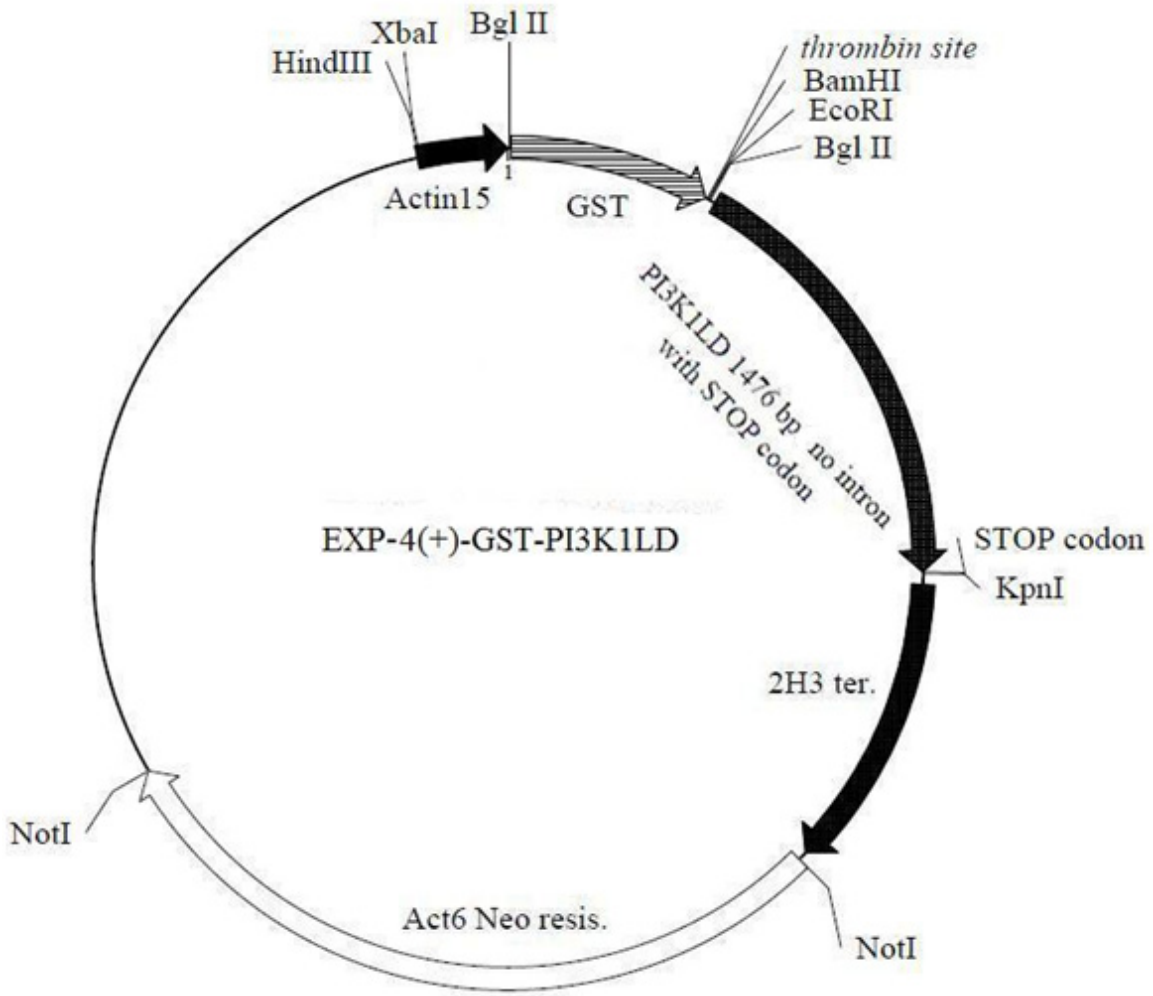

VITA

TONG SUN

Born, Nanjing, Jiangsu, P.R.China

2001-2005	Bachelor of Bioengineering Nanjing University of Technology Nanjing, Jiangsu, P.R.China
2005-2006	Master of Business Administration Salem International University Salem, West Virginia, USA
2007-2013	Doctoral Candidate Florida International University Miami, Florida, USA
	Teaching Assistant Florida International University Miami, Florida, USA

PUBLICATIONS AND PRESENTATIONS

Sun T., Rodriguez M., and Kim L. GSK3 in the world of cell migration. Development, Growth, and Differentiation. 2009. 9:735-742.

Sun T., and Kim L. Tyrosine Phosphorylation mediated Signaling Pathways in *Dictyostelium*. Journal of Signal Transduction. 2011. 2011:894351.

Veeranki S., Hwang S., Sun T., Kim B., Kim L. LKB1 regulates development and the stress response in *Dictyostelium*. Developmental Biology. 2011. 360:351-357.

Tong Sun, Bohye Kim and Lou Kim. (January, 2011) The Regulation of Cell Motility by GSK3 in *Dictyostelium discoideum.* Biology Research Symposium, Department of Biological Sciences, Biscayne Bay Campus, FIU, Miami, FL.

Tong Sun, Bohye Kim and Lou Kim. (March, 2012) The Role of GSK3 in Eukaryotic Cell Movement. 14th Annual Biomedical & Comparative Immunology Symposium, Modesto Maidique Campus, FIU, Miami, FL.